LOW TEMPERATURE STUDIES OF CHANNEL COMPOUNDS.

A thesis submitted for the Degree of Doctor of Philosophy of the University of London.

by

David John Gannon
B.Sc. A.R.C.S.

Department of Chemistry,
Imperial College,
London, S.W.7.

July 1970.

ABSTRACT

The heat capacities of three urea-1-alkene adducts have been measured from 12-300K. The 1-tetradecene and 1-octadecene adducts exhibit co-operative type anomalies but the major anomaly in the 1-dodecene adduct occurs over a large temperature range. The excess entropies involved were calculated and found to be comparable with the entropies determined for other urea-1-alkene adducts by earlier workers. Two small anomalies, at 16K and at 190-240K, also found in previous heat capacity measurements of urea adducts, were observed for the three 1-alkene adducts.

The possible effect of vibration or translation of the guest molecules in the urea channels on the adduct heat capacity has been estimated by Monte Carlo sampling technique and by considering the guest molecules as Born-von-Kármán and Einstein oscillators.

A miniaturised Joule Thomson cryostat system has been constructed and used as a cold stage with a polarising microscope. This has been used to study the optical birefringence of urea adduct crystal sections at low temperatures, in order to gain further information about guest molecule ordering.

The heat capacities of the thiourea adducts of cycloheptane and cyclooctane have been measured from 12 to 300K. To explain the complex series of anomalies

found for both adducts the possibility of both host lattice and guest molecule contributions have been considered. For a very large broad anomaly for the cyclooctane adduct the possibility of conformational interconversion has been discussed.

The heat capacities of three tungsten bronzes, $(NH_4)_{0.26}WO_3$, $K_{0.26}WO_3$ and $H_{0.40}WO_3$ have been measured from 12-300K. Ammonium and potassium tungsten bronzes exhibit no heat capacity anomalies and the heat capacity contribution from the NH_4^+ ion is consistent with this ion behaving as a restricted rotator. An anomalously high heat capacity region is observed in $H_{0.40}WO_3$. A model of the H^+ ions behaving as a 'proton gas' moving in a periodic potential has been considered as a possible explanation for this anomaly.

ACKNOWLEDGMENTS.

I wish to thank Dr. N. G. Parsonage, who, by his enthusiastic and thoughtful supervision, has made my work towards this thesis most exciting throughout.

I would like to acknowledge gratefully the work of Dr. P. G. Dickens and Dennis Murphy of the Inorganic Chemistry Department, Oxford who prepared and analysed all the tungsten bronzes studied in this thesis.

I thank all members of the academic and technical staff and research students of Imperial College who have assisted in various aspects of my work. In particular I must mention Dr. Henry Stroud whose participation in practical workand in many interesting discussions has been invaluable, and Peter Reucroft who investigated the purity of some of the compounds used. Thanks are also due to Misses Elizabeth Green and Eugenie Gee for typing the manuscript.

Finally I acknowledge a Research Studentship from the Science Research Council from October 1967 to September 1970.

INDEX.

Page No.

CHAPTER 1 INTRODUCTION

A. The Adducts of Urea and Thiourea 1

(i) Composition and structure 1

(ii) Stability. 9

(iii) Molecular freedom of the guest. 11

(a) N.M.R. Studies. 11

(b) Dielectric measurements. 16

(c) Heat capacity measurements. 16

B. The Tungsten Bronzes 27

(i) Composition and structure. 27

(ii) Stability 32

(iii) Electrical and magnetic susceptibility studies 32

(iv) N.M.R. 33

C. This Thesis 35

CHAPTER 2 THE ADIABATIC CALORIMETER SYSTEM 37

(i) Introduction. 37

(ii) The cryostat and calorimeter vessel 38

(iii) The calorimeter heater and heater circuit 40

(iv) The thermometer and thermometer circuit 45

(v) The adiabatic shield assembly 48

(vi) The differential thermocouple system 50

(vii) The automatic shield control 51

CHAPTER 3 EXPERIMENTAL DETERMINATION OF HEAT CAPACITIES 58

(i) Assembly of the calorimeter system 58

(ii) The heat capacity measurements 61

Page No.

CHAPTER 4 THE PREPARATION AND ANALYSIS OF THE CHANNEL COMPOUNDS STUDIED 63

(i) Urea adducts.

(A) Preparation 63

(B) Analysis 65

(C) X-ray Analysis 66

(ii) Thiourea adducts

(A) Preparation 70

(B) Analysis 71

(C) X-ray Analysis 72

(iii) Tungsten Bronzes

(A) Preparation 73

(B) Analysis 76

(C) Structural Analysis 76

CHAPTER 5 OPTICAL BIREFRINGENCE MEASUREMENTS 78

(i) Introduction 78

(ii) The Apparatus

(a) The Joule-Thompson Cryostat. 81

(b) The Optical System. 83

(iii) Birefringence measurements of ammonium sulphate crystal sections 86

(iv) Preparation of adducts crystal sections 88

(v) Birefringence studies on urea adduct crystal sections 90

CHAPTER 6 THERMODYNAMIC PROPERTIES OF SOME UREA-HYDROCARBON ADDUCTS 92

(i) Differential thermal analysis measurements on some urea-n-alkane adducts 92

(ii) Experimental determination of the heat capacities of some urea-1-alkene adducts 96

(iii) Discussion of the heat capacity anomalies of the urea-1-alkenes studied 119

(a) The low temperature and high temperature anomalies 119

(1) Monte-Carlo study of translation of guest molecules 120

Page No.

(2) Born-von Karman and Einstein Oscillators 125

(b) The major anomalies 129

(iv) Proposals for further work 130

CHAPTER 7 THERMODYNAMIC PROPERTIES OF THIOUREA-CYCLOHEPTANE AND THIOUREA-CYCLOOCTANE ADDUCTS 134

(i) Experimental determination of the heat capacities 134

(ii) Ferroelectric measurements 152

(iii) Discussion of the heat capacity anomalies of the thiourea cycloalkane adducts 156

(a) The thiourea lattice 156

(b) The guest molecules 158

(1) Conformational interconversions 160

(2) Rotation and translation 165

(c) X-ray studies 166

(iv) Proposals for further work 168

CHAPTER 8 THERMODYNAMIC PROPERTIES OF SOME TUNGSTEN BRONZES 169

(i) Experimental determination of the heat capacities 169

(ii) Discussion of the heat capacities of the tungsten bronzes 182

(a) Ammonium and potassium tungsten bronzes 182

(b) Hydrogen tungsten bronze 189

Proton gas models 191

(1) Energy gap model 195

(2) The Kronig-Penney Model 199

(3) $D^{\frac{1}{2}}$ energy distribution model 204

(iii) Proposals for further work 206

REFERENCES 209

CHAPTER 1

Introduction

A channel compound is so named because its crystal structure contains infinitely long channels in which molecules or ions are held by dispersion forces or by ionic attraction. The molecules or ions in the channels often retain a high degree of vibrational, rotational and even translational freedom down to very low temperatures. There are many experimental techniques by which the position and movement of the molecules or ions in the channels may be studied. The most important of these are X-ray and neutron diffraction studies, nuclear magnetic resonance, dielectric studies and heat capacity measurements.

In this thesis three types of channel compounds are studied. These are:

(a) Adducts of urea with straightchain hydrocarbons;

(b) Adducts of thiourea with cycloalkanes;

(c) Ammonium, potassium and hydrogen tungsten bronzes.

In the section below the crystal structures, compositions and stabilities and molecular freedom in the channels of these compounds are considered.

A. THE ADDUCTS OF UREA AND THIOUREA

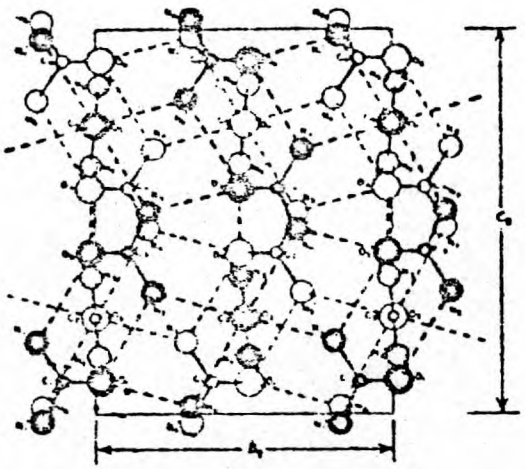
(i) The Compositions and Structure of Urea and Thiourea Adducts

Urea adducts were first prepared by Bengen (1940) and thiourea adducts were independently discovered by Fetterly

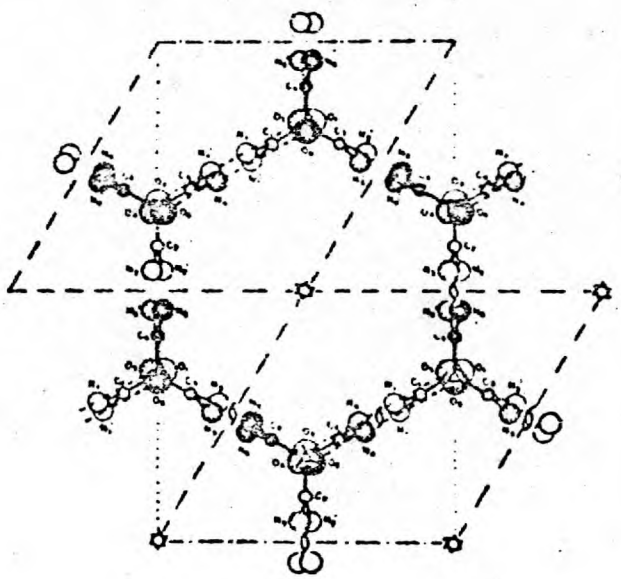
(1947) and Angla (1947). The major difference between the urea and thiourea adducts lies in the dimension of the channel in the 'host' lattice. These dimensions may be explained in terms of the diameter of the approximately circular region whose perimeter is where the attractive and repulsive forces between the host lattice and the guest molecules balance out. In the urea lattice the 'guest' molecules are situated in channels 5.3 Å in diameter whereas in the thiourea lattice the channels are 6.1 Å in diameter, divided into zones by the large sulphur atoms. For this reason urea forms its most stable adducts with straight-chain unsubstituted or terminally substituted hydrocarbons and thiourea with branch-chained or cyclic hydrocarbons.

X-ray investigation of various adducts of urea with straight-chain compounds were made by Smith (1952), Hermann and Lenné (1952) and Lenné (1954). Smith examined powder patterns of n-paraffins and straight chain acids, alcohols and esters from C_{10} to C_{50} and found that they were essentially identical. From more detailed single crystal studies on the n-hexadecane adduct he found that the unit cell was of the hexagonal space group $P6_12$ or $P6_52$ and consisted of six urea molecules with a = 3.230 $\pm$ 0.004 Å and c = 11.005 $\pm$ 0.005 Å. The urea molecules are hydrogen - bonded together in three interpenetrating spirals to form the walls of the hexagonal channel lattice in the unit cell (see Figure 1.1). Each oxygen is hydrogen -bonded to four nitrogens and each nitrogen is hydrogen - bonded to

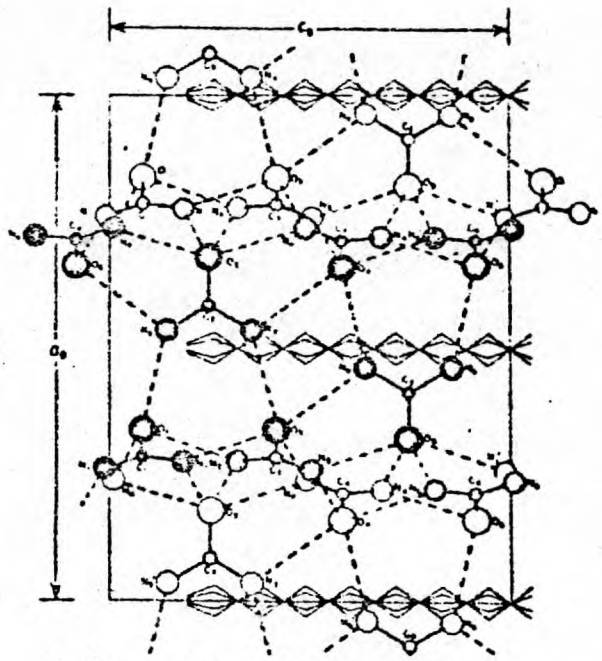
FIG.1.1. The n-hexadecane - hexagonal urea structure. (After Smith 1952).



(a). Projection along the "a" axis.



(b). Projection along the "c" axis.



(c). Projection along the "b" axis.

two oxygens. The spirals are by chance in either the left hand or right hand direction.

From a-axis Weissenberg patterns and c-axis rotation photographs Smith found that the hydrocarbon molecules were in their extended zig-zag form parallel to the crystal c-axis. The diffuse bands found in the rotation photograph of the dibromodecane-urea adduct suggest that in general the repeat distance of the adducted molecule is not rationally related to the repeat distance of the urea host lattice.

The electron density projection and implication diagram indicated that at room temperature the time average of the positions of the plane of the hydrocarbon molecule ~~are~~ is randomly dispersed over positions perpendicular to the a-axis and at multiples of 60° to this position. However X-ray analysis is unable to distinguish between rotation and random distribution amongst the energetically favourable sites. Smith assumed a distance of 4.0 Å between terminal methyl groups in the same channel (the sum of their van der Waals packing radii). However more recently Laves, Nicolaides and Peng (1965) have found the value 3.74 Å in agreement with the potential energy calculations of Parsonage and Pemberton (1967). The increased interaction between the hydrocarbon and the urea lattice makes this close approach of terminal groups energetically favourable.

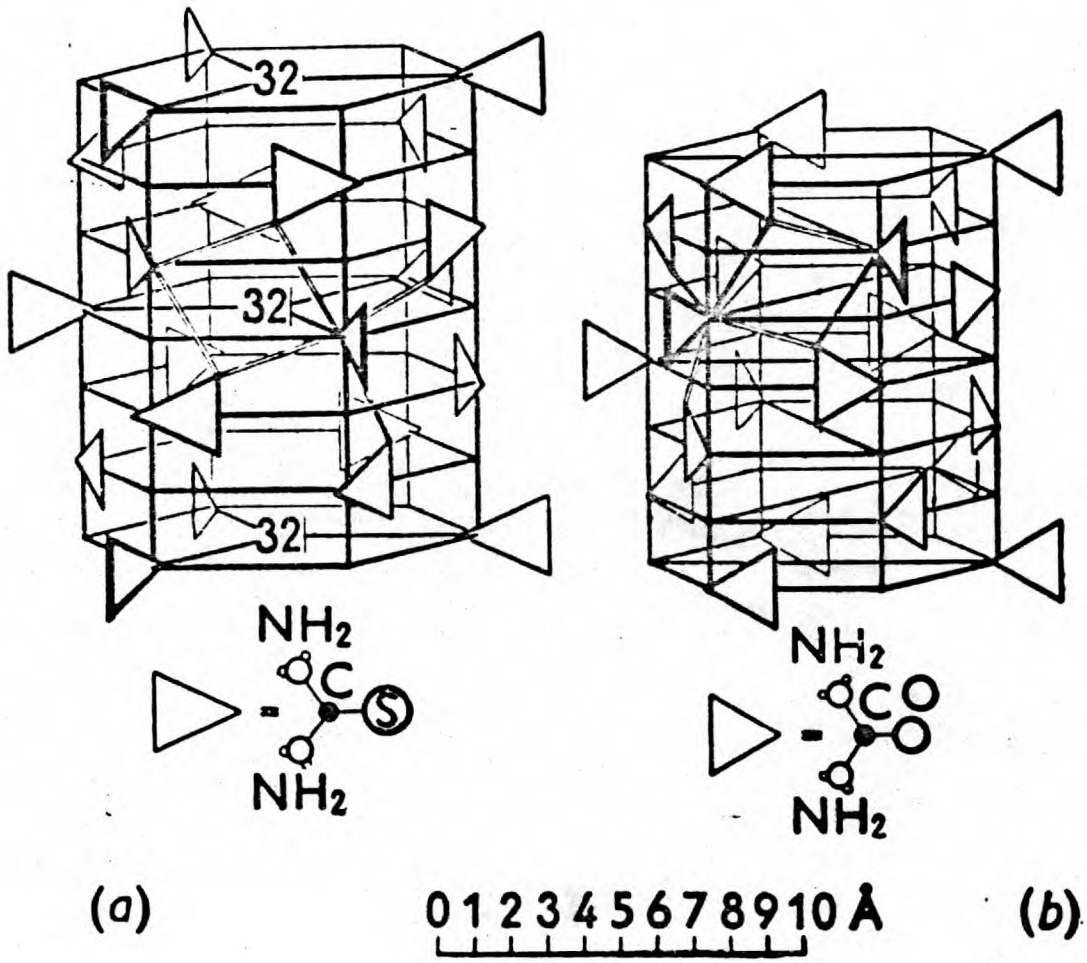
Lenné (1954) has studied the crystal structures of

various thiourea adducts extensively. From single crystal rotation photographs about the main axis he found that the host lattice belongs to the rhombohedral space group $R\bar{3}2/C$ with a = 15.8 Å and c = 12.5 Å. The pseudohexagonal unit cell comprises six thiourea molecules and as with urea the host lattice contains hexagonal channels (but larger than in urea adducts as mentioned above). The different size of channels in the two types of adduct and the differing arrangement of the urea and thiourea molecules are illustrated in Figure 1.2. It can be seen from Figure 1.2 a) that in every third plane of thiourea molecules the large sulphur atoms point towards the centre of the channel. The strong van der Waals interaction available in this plane effects the position of the guest molecules.

Urea forms adducts with most non-substituted and terminally substituted straight-chain alkanes. Chains of less than six carbon atoms however form adducts not stable at room temperature. e.g. Schlief (1955) has even prepared the urea adducts of n-propane and n-butane at lower temperatures and under pressure. Non-terminally substituted alkanes will form urea adducts only if the main carbon chain is sufficiently long to offset the unfavourable interaction of the substituent with the host lattice.

With thiourea however only n-alkanes of sixteen carbon atoms or more will form adducts. X-ray evidence (Laves, Nicolaides and Peng, 1965) suggests that the alkanes in

FIGURE 1.2 THE CHANNELS IN UREA AND THIOUREA ADDUCTS.



these adducts coil around the walls of thiourea. Schiessler and Flitter (1952) concluded from the study of Fisher-Hirschfelder models of molecules that adduct with thiourea that the cross section of the guest molecule should be 5.8 ± 0.5 Å by 6.8 ± 0.3 Å.

In general the urea adducts are non-stoichiometric. For instance the ratio of urea molecules to n-alkane molecules is given by

mole ratio urea/n-alkane = 0.65n + 1.51

where n is the number of carbon atoms in the alkane. Similar relationships hold for n-acids and n-alcohols. Smith (1952) has suggested that in the case of n-hexadecane, whose length is just greater than twice the host lattice c repeat distance, the alkane is slightly shortened by twisting and stoichiometry is obtained. He proposes this on the basis of discrete spots in the rotation photograph of the n-hexadecane adduct which may be due to the guest molecule stoichiometry. However Lenné (1954, 1963a) and Laves, Nicolaides and Peng (1965) disagree with Smith's interpretation of the X-ray data and assert that the hydrocarbon molecules are in their fully extended configuration.

Lenné (1963b) has reported stoichiometric urea adducts but with a rhombohedral (not hexagonal) host lattice. This lattice contains larger channels and can include guest molecules such as trioxane (unit cell/

trioxane ratio 1:2) and hexadecylcyclohexane (5:2). The channel field is non-uniform and the guest molecules attain maximum van der Waals interaction by being located near to the oxygen atom plane of the host lattice. This leads to a rational relationship between guest molecules and host lattice and to stoichiometry.

Similarly in the rhombohedral thiourea lattice the guest molecules may attain maximum interaction with the plane of sulphur atoms. Lenné (1954) has shown from X-ray data that cyclohexane molecules are situated near this plane leading to a molar ratio thiourea:cyclohexane 3:1. Other examples of this stoichiometry are carbon tetrachloride and w.w' bridged dicyclohexyls (Schlenk W. Jr). In the second case the methylene bridges coil to accommodate the cyclohexyl group in the plane of sulphur atoms.

Lenné (1963b) has also reported urea adducts in which the urea host lattice is disordered in two dimensions. The urea spirals are not in the left or right hand direction as with the hexagonal urea lattice (see Figure 2.1.b) to give (++++++) or (------) or as in rhombohedral urea (+-+-+-). Instead they have arrangements such as (+++---) or (++-+--) which will also give a closed canal whose axes will no longer possess any rotation symmetry. Lenné also suggests that the guest molecules in these adducts will exhibit two dimensional disorder. As one of the adducts possessing a disordered urea lattice (according to Lenné)

is that of n-tetracosane (the n-alkane with twenty-four carbon atoms) this is very relevant to the work in this thesis and will be discussed further in Chapter 4.

(ii) Stability of urea and thiourea adducts

Urea and thiourea adducts form clear hexagonal needles whose stability depends on the guest component. In general the urea adducts are more stable than those of thiourea. Neither type has a true melting point because the guest molecules usually escape from the channels before the adduct appears to melt.

The stability of the urea adduct lattice can only be understood by comparing the nature of the binding forces in the adduct with those in the tetragonal urea and guest molecule lattices. From infrared studies of urea (Stewart, 1957) and the urea adducts (Fischer and McDowell, 1960) it was determined that both lattices contain strong hydrogen bonding. The length of the hydrogen bonds and other bond lengths in the two lattices (Wyckoff and Corey 1932a), (Smith, 1952) are listed in Table 1.1.

TABLE 1.1 Atomic Distances in Urea Crystal Lattices

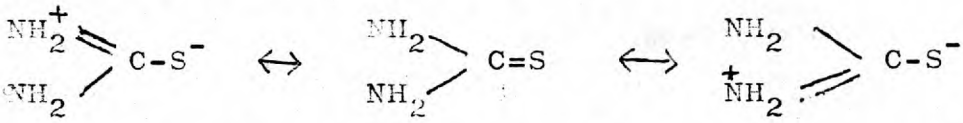
Urea-hydrocarbon complex		Tetragonal urea	
C-O	1.28 Å	C-O	1.26 Å
C-N	1.33 Å	C-N	1.33 Å
N-N	2.30 Å	N-H...O	2.99 Å
N-H...O	2.93 Å	N-H...O	3.03 Å
N-H...O	3.04 Å		

In tetragonal urea hydrogen bonding between neighbouring atoms results in a rather open framework rather like the situation occurring in the formation of ice. In the hexagonal adduct lattice the net shortening of the hydrogen bonds suggests that the empty lattice would be stable at room temperature. However although Kyrieau (1959) reported preparing small quantities of the empty lattice it is generally thought to be unstable. Thus although the hydrogen bonding is possibly stronger in the hexagonal lattice than in the tetragonal lattice, the hexagonal lattice has a higher energy than the tetragonal lattice and will be unstable with respect to it unless guest molecules are present. Then the increased guest molecules-host lattice interaction possible with the hexagonal lattice makes it the most stable form.

Unlike urea adducts the thiourea adducts are not stabilised by stronger hydrogen bonding. This is because the electronic configuration of sulphur allows donation of electronic density and thus impedes the formation of hydrogen bonds. In fact the nitrogen-nitrogen distances

in orthorhombic thiourea (Wyckoff and Corey 1932b) and in the thiourea adducts (Lenné, 1954) are greater than the limiting N-H...N bond distance (Pimental and McClellan 1960). Also infra-red studies of thiourea and thiourea adducts (Mecke and Kutzelnigg 1959) showed negligible difference between the respective N-H stretching frequencies.

However the data of Wyckoff and Corey (1932b) and Lenné (1954) shows that the C=S bond is lengthened and the C-N bond shortened in going from orthorhombic to rhombohedral thiourea suggesting that tautomeric forms play a more important role in the adduct.



This accumulation of electron density on the sulphur atom may be an additional incentive for the guest molecules to be located near the planes of sulphur atoms.

(iii) Molecular freedom of the guest in urea and thiourea adducts

(a) Nuclear Magnetic Resonance Studies

Urea adducts have been studied by N.M.R. methods by Gilson and McDowell (1959,1961), Umemoto and Danyluk (1967) and Bell and Richards (1969).

Gilson and McDowell (1961) investigated the wide-line proton magnetic resonance spectra of the urea-n-tridecane and n-hexadecane adducts from 77K to 298K. The second

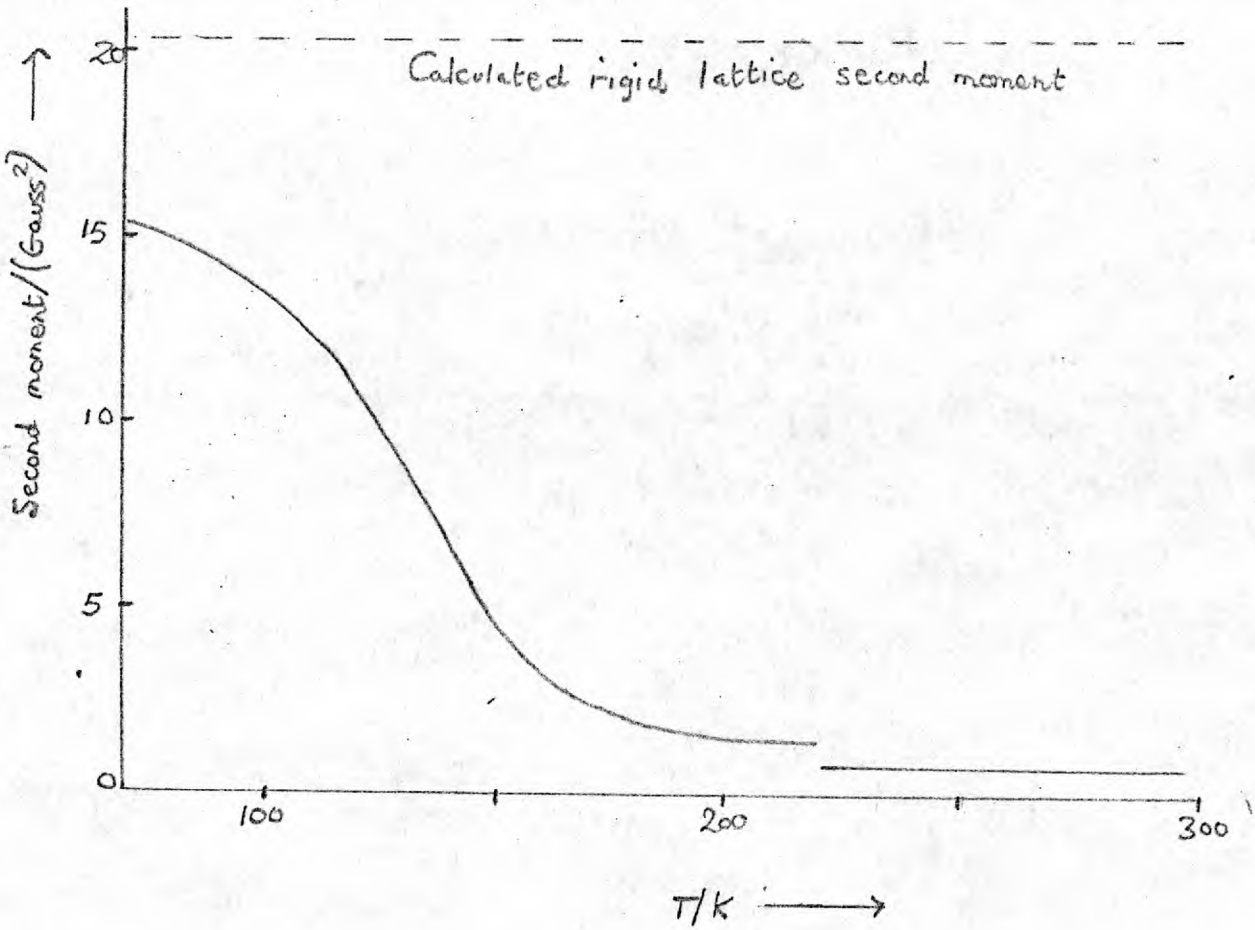
moments of these two urea-d_4 adducts were below the calculated rigid lattice value at 77K and decreased rapidly in both cases reaching a fairly constant value at 160K for both adducts. At 220-230K there was a sharp discontinuity in the second moments of both adducts. The second moment for urea-d_4- n-hexadecane is shown in Figure 1.3. Umemoto and Danyluk studied the urea-d_4 adducts of n-dodecane, n-tetradecane, n-hexadecane and n-octadecane from 80 to 300K using the same technique. They found that the second moments all decreased with temperature but that the decrease was displaced to higher temperatures in a regular manner with increasing chain length. They also observed further small but measurable discontinuities in the second moments at temperatures ranging from 134 to 236K.

Gibson and McDowell (1961) concluded from their results that the hydrocarbon molecules were able to rotate more or less freely about their longitudinal axis at temperatures well below those for the pure n-alkanes. Umemoto and Danyluk confirmed these conclusions and estimated from second moment measurements temperatures for the onset of this hydrocarbon molecule rotation. The temperatures are listed in Table 1.2.

TABLE 1.2 'Transition' Temperatures for Urea-n-alkane Adducts

Adduct	T_t (second moments)
$n\text{-}C_{12}H_{26}$	114
$n\text{-}C_{14}H_{30}$	126
$n\text{-}C_{16}H_{34}$	132
$n\text{-}C_{18}H_{38}$	144

FIGURE 1.3 VARIATION OF THE SECOND MOMENT WITH TEMPERATURE FOR THE RESONANCE LINE FROM UREA-D_4-N-HEXADECANE



Gilson and McDowell (1961) suggested that the discontinuity occuring at 220-230K in the urea adduct second moments resulted from an expansion of the urea lattice allowing the hydrocarbon greater freedom of motion.

Bell and Richards studied four urea-n-alkane adducts and two terminally substituted alkanes using nuclear spin relaxation methods from -150°C to the decomposition temperature of the adduct. All the adducts studied exhibited at 'T_1' minimum at 35MHz. The value of T_1 and the temperature at which the minimum occurred was found to vary considerably with the nature of the guest molecule.

For these results Bell and Richards suggested two possible explanations. First that the guest molecule can make torsional oscillations of fairly large amplitude about a mean position. In this case as the temperature was increased the torsional oscillations would be expected to increase until complete rotation is achieved. The second explanation is that the guest molecule reorientates between two potential minima of very unequal depth as suggested by the calculations of Parsonage and Pemberton (1967). The experimental activation energies obtained from T_1 measurements are compared with the potential barriers calculated by Parsonage and Pemberton in Table 1.3.

TABLE 1.3

chain length of n-alkane	10	12	16	20
potential barrier/(kJ mol^{-1}) (Parsonage and Pemberton)	7.1	8.2	8.7	10.8
experimental activation energy/(kJ mol^{-1})	3.8	5.3	9.7	6.7

Excepting the n-hexadecane adduct the calculated values are close to the experimental activation energies provided that the potential barrier due to interactions between guest molecules in the same channel which was calculated to be 3.0 kJ for a separation of 3.74 Å is included. Bell and Richards suggest that the n-hexadecane discrepancy is due to shortening of the guest molecule in the channel to obtain stoichiometry as postulated by Smith (1952).

Gilson and McDowell also studied some thiourea adducts containing cyclic hydrocarbons. For the thiourea -d_4 - cyclohexane adduct they reported that the second moment diminished from 2.7 $gauss^2$ at 77K to 1.6 $gauss^2$ at 298K. As 3.6 $gauss^2$ is the calculated second moment for a cyclohexane molecule reorientating about its triad axis the low experimental values suggest some translational motion of the cyclohexane molecules in the channel. The narrow line of modulation width found for the thiourea-d_4-cyclopentane adduct suggest that this smaller ring has greater translational freedom along the channel.

(b) Dielectric Measurements

Meakins (1953) found large dielectric absorption at microwave frequences for the urea adducts of various long chain compounds with polar groups. He showed that the absorption was due to the orientation of the long chain dipoles in the urea crystal lattice. The presence of dielectric absorption in the 1:10 dibromodecane adduct, which should possess a resultant zero dipole moment as X-ray data shows that the guest molecules are fully extended, suggests that the C-Br dipoles are capable of orientation independently of the main carbon chain. Further evidence for the independent orientation of polar groups is given by the similarity of the dielectric loss factors of several ketones of vastly different chain lengths (C_{17}, C_{31}, C_{35}).

These findings to not contradict the N.M.R. studies and heat capacity measurements discussed in this chapter as Meakins studied guest molecules with bulky substituent groups and long carbon chains and both these factors hinder rotation of the molecule about its long axis.

Lauritsen (1958) was able to calculate the relaxation times for re-orientation of a polar group from one position of minimum potential energy in the urea field to another and hence calculate the dielectric properties of urea adducts. His calculated values are in good agreement with Meakins experimental values.

(c) Heat capacity measurements

Pemberton and Parsonage (1965, 1966) have measured

the heat capacities of the urea adducts of five n-alkanes (C_{10}, C_{12}, C_{15}, C_{16}, C_{20}) and the 2-methylpentadecane urea adduct from 12 to 300K. Gradual transitions were observed in all the n-alkane adducts but not in the 2-methylpentadecane adduct. The transition temperatures for the 'even' n-alkane adducts increase regularly with chain length and the n-pentadecane adduct has a transition temperature rather higher than the even n-alkane curve. Cope and Parsonage (1969) have studied the urea adduct of another 'odd' n-alkane, n-undecane. This adduct also exhibits a transition at a temperature rather higher than that expected from the even n-alkane adduct relationship. These results indicate that the transitions are due to the onset of rotation or re-orientation of the guest molecules about their long axes. The absence of a transition in the 2-methylpentadecane adduct may be explained by the greater interactions of the substituted methyl group with the urea lattice hindering any rotation or re-orientation of the guest molecule.

To understand the nature of these transitions more fully Parsonage and Pemberton (1967) calculated the potential energy as a function of the orientation of the n-alkane molecules in the urea channels.

Hrst they considered the urea-alkane interactions for various orientations of the alkane molecules and in various positions along the channels relative to the urea molecules.

Molecules with different chain lengths were considered. As the length of the n-alkanes is not rationally related to the host lattice c-axis repeat distance the CH_2 units are in different environments, differing interactions are experienced by them and hence the urea-alkane interactions vary irregularly with chain length.

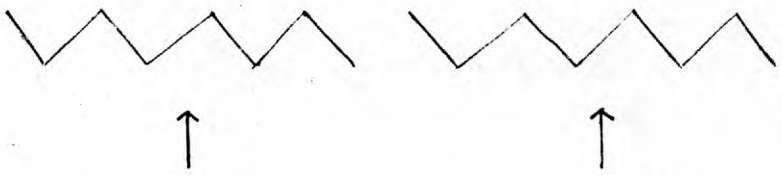
Next the 'longitudinal' interactions between terminal methyl groups of guest molecules in the same adduct channel were estimated for a series of relative orientations of the two groups. This distance between the terminal groups was calculated by balancing the added interactions available to the alkanes and the urea lattice by close ap roach with the repulsive force experienced by the terminal groups. With this data thepotential energy barrier to rotation was determined. This barrier is independent of chain length.

Finally the interaction between alkane molecules in different channels (lateral interactions) were determined. Various orientation of two alkane molecules and various relative staggerings in the channels were considered. These interactions are very small but were found to be most important.

Considering all three types of interaction together showed that there were six minima in the graph of potential energy versus orientation. However in order to simply the mathematical treatment it was postulated that the guest molecule could re-orientate about its long axis between only two

potential minima one of lower energy than the other. The orientating effect of the urea lattice was represented by the term $2V \cos\phi$ where 2V is the difference between the greatest and least minimum of the urea lattice-alkane potential energy graphs and ϕ is the phase angle which is a function of the position of the alkane molecule in the channel.

The restriction of the alkane molecule to two possible minima enabled the Ising model (first used to study ferromagnetism and antiferromagnetism) to be employed. Parsonage and Pemberton considered alkane molecules in the same channel as a system of dipoles. At low temperatures all the molecules will be in the low energy potential minima.



This is probably the 'ferromagnetic' arrangement shown above for the even n-alkanes and the antiferromagnetic arrangement for the odd n-alkanes.

The Ising model considers only nearest neighbour interactions and the potential energy of interaction is then $-J\mu_1\mu_2$ where J is a parameter depending upon the nature of the longitudinal interactions and μ_1 and μ_2 are either +1 or -1 depending on whether the molecule is in the low or high energy orientation. However as Ising showed

a one dimensional array is incapable of exhibiting a co-operative transition and hence the weaker lateral hydrocarbon interactions must be important. The urea lattice can be considered to be the analogue of an external field in a magnetic Ising model. This gives then a three dimensional array with an external field. As neither the simpler three dimensional array without external field or the two dimensional array with external field have been solved exactly Parsonage and Pemberton were compelled to use an approximate solution. They did this by using a Weiss or Bragg-Williams model for the lateral interactions whilst retaining the exact Ising model for the longitudinal interactions. The interaction in the Weiss model for the ith molecule in a channel is given by $J\langle\mu_i\rangle\mu_i$ where $\langle\mu_i\rangle$ is the average value of μ taken over all guest molecules in the same plane (perpendicular to the urea host lattice c-axis).

The partition function for this model was then calculated using a matrix method due to ter Haar (1954). $\langle\mu_i\rangle$ was determined for various temperatures (by iterative solution of the derived equations relating $\langle\mu_i\rangle$ with the partition function) and the temperature at which $\langle\mu_i\rangle \approx 1$ goes to $\langle\mu_i\rangle \approx 0$ was determined. This transition temperature was largely unaffected by variation of V, was very dependant on the value chosen for J, and varied in a linear fashion with J^1. As J^1 is approximately

proportional to chain length the model correctly predicted that the transition temperature is proportional to chain length. The model also predicted that the transition temperature of the odd adducts would be higher than those of the even series.

The use of the Ising model restricts the entropy of transition to R ln 2 whereas the experimental values in all cases were larger than this - perhaps because the guest molecules have more than two potential minima to re-orientate between or perhaps because they flex on re-orientation (i.e. behave like springs rather than rigid rods). Nevertheless Parsonage's and Pemberton's model is successful at predicting the temperature of transition and gives a good indication of the nature of the transition.

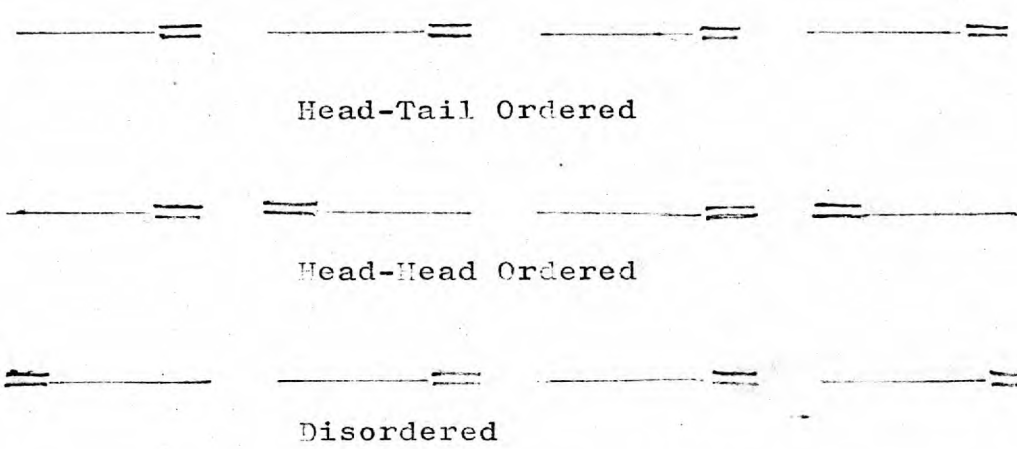
Cope and Parsonage (1969) measured the heat capacities of three urea 1-alkene adducts. Two of the adducts (those of 1-hexadecene and 1-eicosene) showed co-operative-type anomalies but the third, the 1-decene adduct, contained several anomalous regions in which there were smooth shallow humps in the heat capacity versus temperature curve. The transition temperaturesof the urea-1-hexadecene and 1-eicosene adducts were slightly lower than the corresponding urea-n-alkane adduct transition temperatures. Cope and Parsonage were able to show that the smooth humps in the urea-1-decene adduct heat capacity curve had an excess

heat and excess

entropy similar to the co-operative anomaly of the urea-n-decane adduct (their treatment is given in Chapter 6 part (ii) of this thesis).

The theoretical treatment of the urea-1-alkene adducts is more complex than that of the n-alkane adducts. This is because whereas the n-alkane molecules have only one possible ordering along the channels the 1-alkenes may be ordered in three different ways (see Figure 1.4).

FIGURE 1.4 SCHEMATIC DIAGRAM OF ORDERING OF 1-ALKENE MOLECULES ALONG THE UREA CHANNELS



Cope (1967) determined the barrier to rotation for the 1-alkene molecules in the channels using a treatment similar to that of Parsonage and Pemberton. The adaptation of the Ising-Weiss model employed for the urea-n-alkane adducts to the 1-alkene adducts with head-tail order is simple requiring only alteration of the longitudinal interaction parameter. However if the 1-alkenes are head-tail disordered along thechannel this model can no longer be used.

Cope (1967) therefore used an Ising-Monte Carlo method

to study the urea-1-alkene adduct transitions. He chose a cube of 512 molecules as his model and considered both the head-tail ordered and head-tail disordered arrangements. Allowance was made for the fact that in the crystal each hydrocarbon has at least six neighbours whereas in the model it has only four. The energy of the cube was determined from the sum of the Ising interactions. The change in energy, ΔE, of re-orientating one of the guest molecules (μ_i goes from +1 to -1 or -1 to +1) is determined. If the ΔE is negative (the energy of the cube is lowered) the change is automatically accepted. If ΔE is positive $e^{-\Delta E/k_B T}$ is compared with a random number between 0 and 1. If the exponential is greater the change is accepted, if less it is rejected. Two sets of molecules were considered one initially completely rotationally ordered and the other initially completely rotationally disordered. Each molecule of the two sets was given the chance to re-orientate repeatedly until the properties of the two sets of molecules converged. Then the average of the energy for many cycles of the cube of molecules $\langle E \rangle$ and the average of the energy squared for the same number of cycles of the cube of molecules $\langle E^2 \rangle$ were determined. From these quantities the heat capacity (Cp) could be evaluated from the relationship:

$$Cp/R = \frac{\langle E^2 \rangle - \langle E \rangle^2}{512 \cdot (RT)^2}$$

where R is the gas constant, T is the temperature.

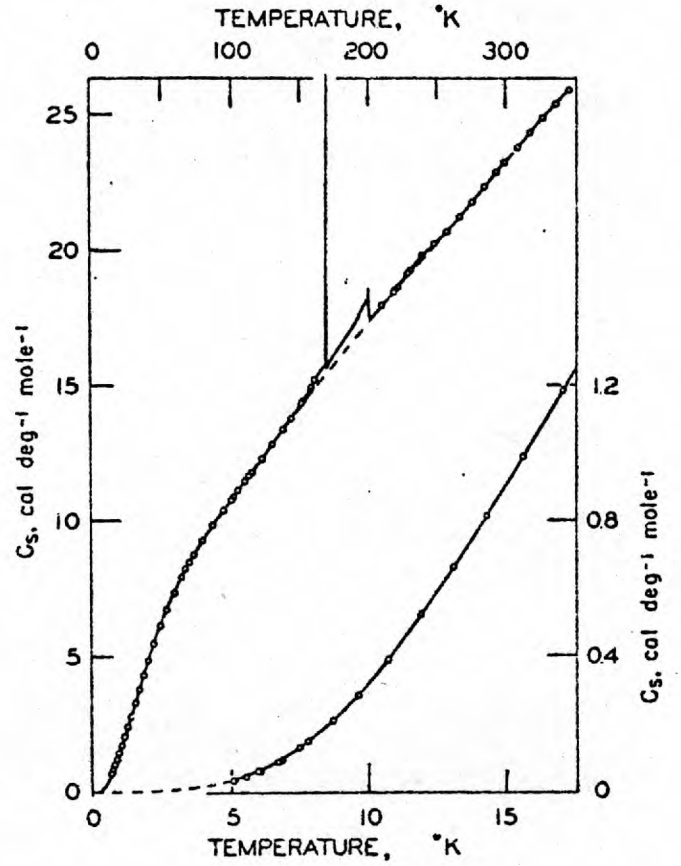
Thecalculations were carried out for various temperatures with head-tail order and disorder for the three urea-1-alkene adducts. It was found that the head-tail ordered and disordered arrangements both predicted co-operative-type heat capacity anomalies. Thus it was impossible to explain the non-co-operative anomaly of the urea-1-decene adduct from these calculations.

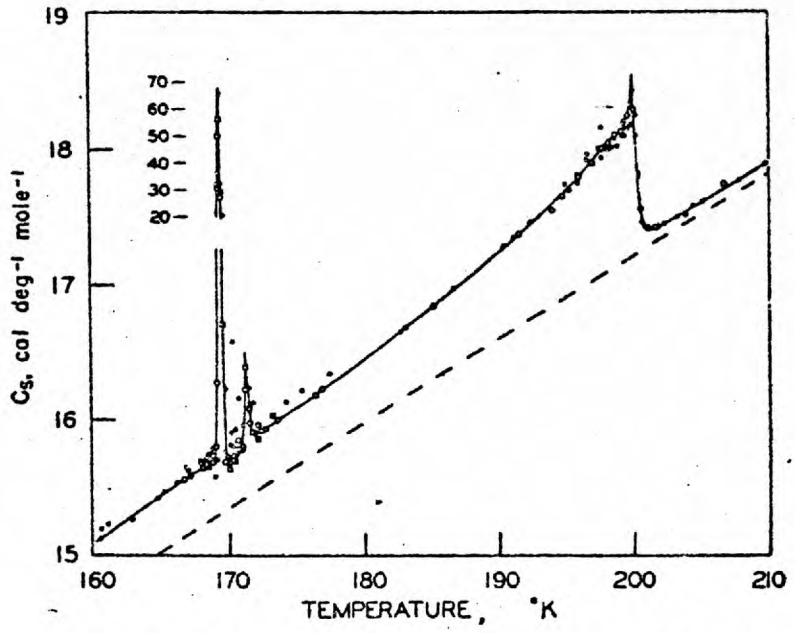
Cope (1967) also measured the heat capacity of the thiourea adducts of cyclohexane and 2,2-dimethylbutane. Both adducts exhibited a rather complex series of anomalies in their heat capacity versus temperature curves. The heat capacity of the thiourea cyclohexane adduct is shown in Chapter 7, Figure 7.1.

The anomalies in thiourea adducts have two possible sources: the host lattice and the guest molecules. The orthorhombic thiourea lattice is ferroelectric at low temperatures, Solomon (1956), Goldsmith and White (1959) and undergoes ferroelectric-antiferrelectric transitions in the 160-200K temperature range. The heat capacity has been measured by Chang and Westrum (1961) (Figure 1.5). The ferroelectricity in thiourea is unique in that it is associated with the displacement of complete molecules rather than with the motion of ions within the crystal.

The rhombohedral thiourea adduct lattice may also exhibit ferroelectric-antiferroelectric transitions at low

Fig. 1.5 The Heat Capacity of Thiourea





Heat capacity of thiourea in the region of the dielectric anomalies

temperatures although the different arrangement of molecules might alter the size of the transitions and the temperatures at which they occur. The two adducts studied by Cope showed heat capacity anomalies at similar temperatures (170K) to those in the orthorhombic thiourea lattice. In thiourea the heat capacity anomalies have an excess entropy of 0.9 JK^{-1} $mole^{-1}$ compared with ~ 6.3 JK^{-1} $mole^{-1}$ for the thiourea cyclohexane and 2,2 dimethylbutane adducts. Obviously the host lattice transitions cannot account for all the heat capacity anomalies in the thiourea adducts.

The guest molecules may begin to rotate or re-orientate themselves at sufficiently high temperatures and the onset of this movement could account for the other anomalies observed in the heat capacities of the thiourea adducts.

Parsonage (Cope 1967) devised a model to attempt to predict the major (130K) transition in thiourea cyclohexane adduct. The intermolecular interactions were determined to find the most favourable positions of the cyclohexane molecules relative to themselves and to the thiourea lattice. From these calculations he decided that there were six favoured configurations. The longitudinal interactions were treated by the exact Ising model and the lateral interaction by the Ising-Weiss model as used by Parsonage and Pemberton (1967). The configurational partition function was determined using the matrix method of ter Haar (1954).

However this model predicted a rather broad transition

between 50K and 90K and variation of the coupling parameters although increasing the temperature of the transition did not sharpen it at all.

B. THE TUNGSTEN BRONZES

(i) Composition and structure

Wöhler (1824) observed the formation of golden yellow metallic crystals while passing dry hydrogen over heated acid sodium tungstate. This was the first account of the formation of a tungsten bronze (so named on account of its metal-like appearance).

Tungsten bronzes are non-stoichiometric compounds with the general formula M_xWO_3 where M is a metal (most commonly an alkali) or H or NH_4. Similar compounds of the type M_xZO_3 may also be prepared where Z may be molybdenum, vanadium, niobium and titanium. In all these compounds x is a variable falling in the range $0 < x < 1$.

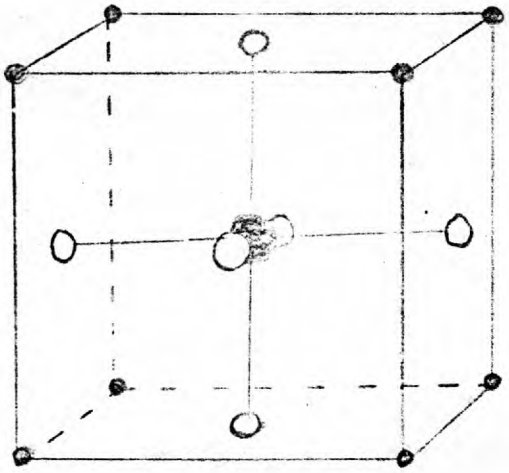
The crystal structures of the tungsten bronzes were first investigated by Hägg and Magneli (1954). There are three general factors which determine the structure of the compound M_xWO_3. First as x decreases so does the symmetry of the crystal structure. Secondly the particular structure adopted by a bronze is governed to a considerable extent by the ionic radius of M. Finally all bronzes structures are formed by the linking together of WO_6 octahedra at their corners. The two limiting structures of Na_xWO_3

with x = 1 and x = 0 are shown in Figure 1.6. '$NaWO_3$' has the perovskite type structure. Each unit cell consists of a WO_6 octahedra, the six O atoms being placed at the centres of the faces of a cube. Eight sodiums are located at the corners of this cube. Figure 1.6 b) shows the WO_3 structure which is a distorted ReO_3 structure with the tungsten atoms slightly displaced from the centre of the cube leading to W-W distances in the crystal which are alternatively short and long.

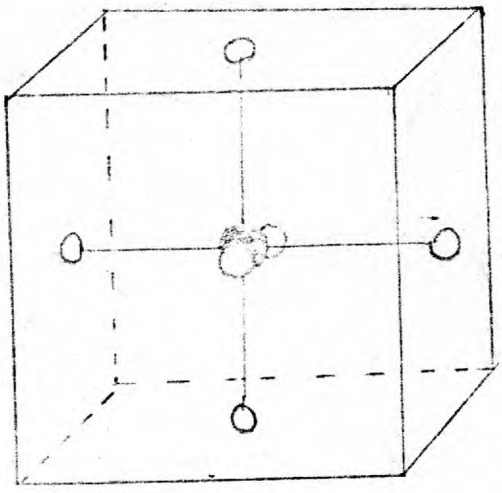
In fact for Na_xWO_3 with $0.30 < x < 0.95$ a cubic structure is found which is intermediate between the hypothetical $NaWO_3$ and undistorted WO_3 i.e. 1-x sodium atoms are missing from the cube corners of the Na_xWO_3 unit cell. For lower sodium contents than 0.30 the structure symmetry is lowered in several stages down to monoclinic at very low x. The phase diagram for Na_xWO_3 (Ribnick, Post and Banks, 1963) and the relationship between the crystals phases formed is shown in Fig 1.7.

Other metals with small ionic radii and hydrogen form tungsten bronzes with similar phase diagrams. However with alkali metals of larger ionic radii (K, Rb, Cs and NH_4) a further crystal structure is formed in which the WO_6 octahedra are joined in six membered rings to give a hexagonal symmetry, (Magneli, 1953) The hexagonal structure is shown in Fig 1.8. The maxiumum value of x in $MxWO_3$ is $\frac{1}{3}$ for the hexagonal structure. The radii of

FIGURE 1.6 STRUCTURES OF $NaWO_3$ and WO_3.



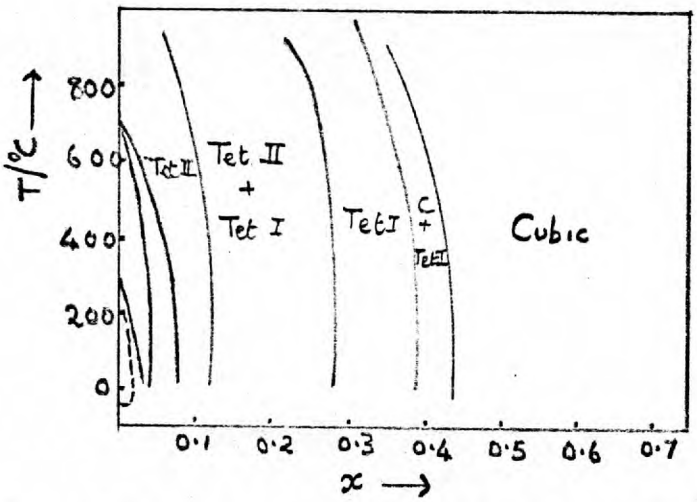
a) '$NaWO_3$'



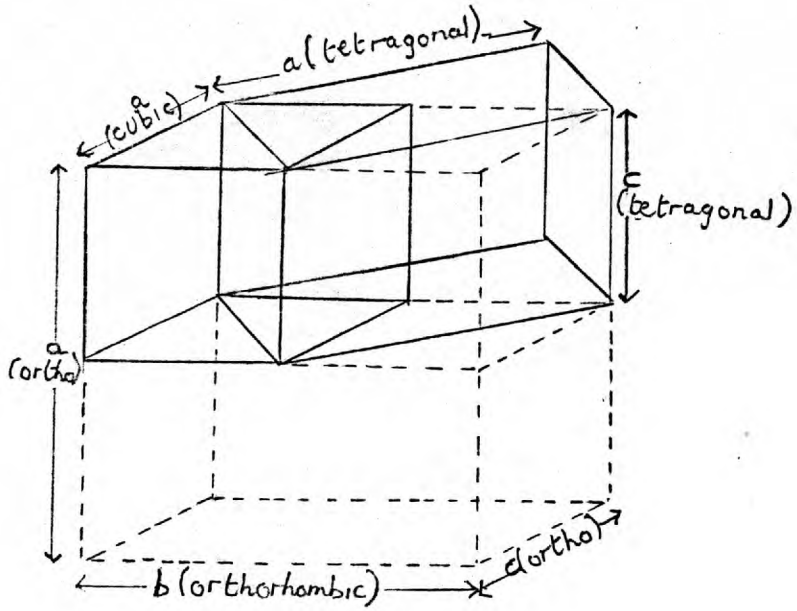
b) WO_3

• = Sodium, O = Oxygen, ⊗ = Tungsten.

FIGURE 1.7

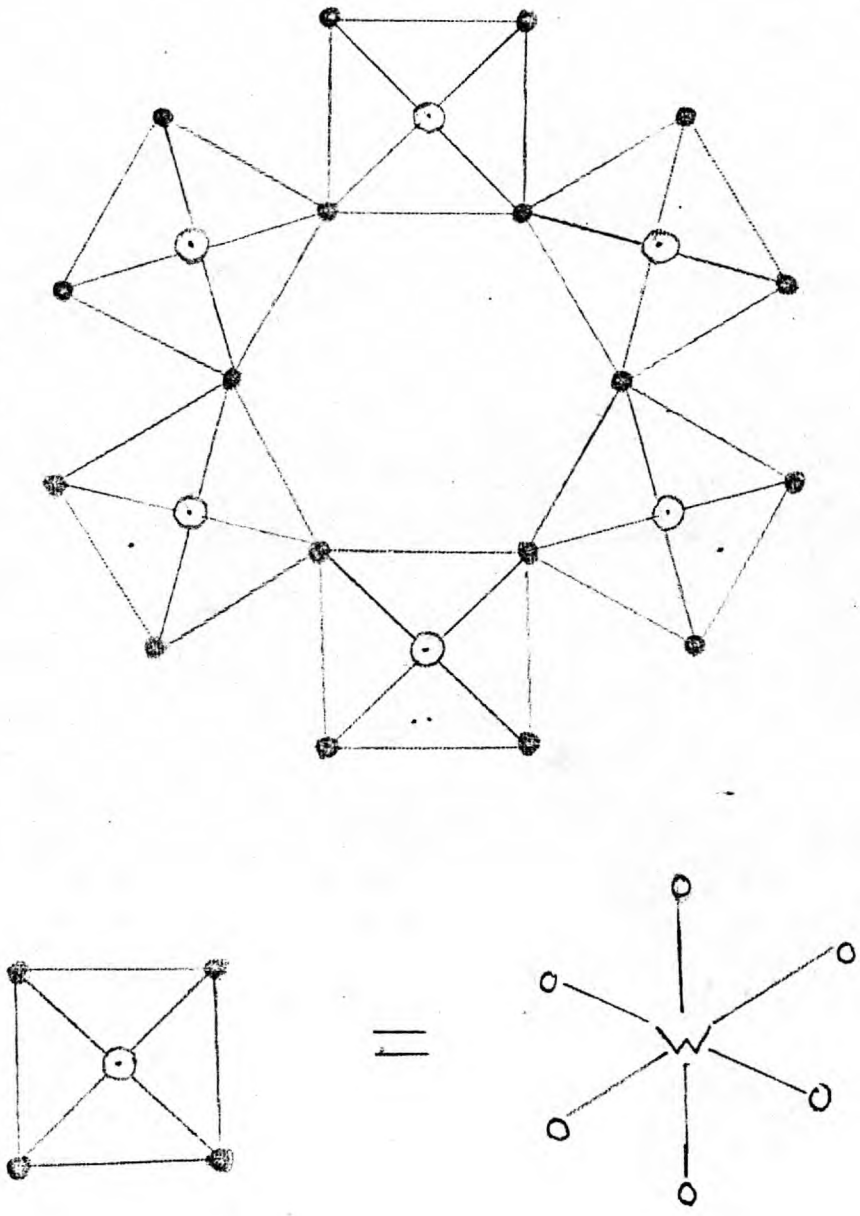


Phase Diagram For Na_xWO_3



Relationship between the cubic, tetragonal II and orthorhombic phases

FIGURE 1.8. SCHEMATIC DIAGRAM OF HEXAGONAL BRONZE STRUCTURE.



the inscribed spheres in this structure is 1.63 Å compared with 0.96 Å for the cubic and 0.96 and 1.29 Å for the tetragonal structures.

X-ray studies of the tungsten bronzes are dominated by the scattering of the heavy tungsten atoms and hence do not show the oxygen and sodium positions. However Atoji and Rundle (1960) studied $Na_{0.75}WO_3$ by neutron diffraction methods and found that the sodium atoms were at the cubic cell corners as predicted and formed an ordered sub-lattice. Neutron diffraction studies of $H_{0.23}WO_3$ by Dickens and Hurditch (1967) confirmed that the crystal structure was identical to that of $Na_{0.1}WO_3$ (Tetragonal II phase). However here no evidence for ordering of the hydrogen atoms was found.

(ii) Stability

The alkali metal tungsten bronzes are very unreactive. They are stable in air, insoluble in water and very resistant towards acids. In the presence of alkalis the tungsten bronzes are readily oxidised to tungstates. In contrast the hydrogen tungsten bronzes are very reactive being slowly attacked by air and quantitively oxidised by hot dichromate solution.

(iii) Electrical and magnetic susceptibility measurements

Single crystals of alkali metal bronzes with $x > 0.25$ exhibit electrical conductivity. Hall

effect and Seebeck effect measurements together with the observed constancy of thermal coefficient of resistance for different alkali metal bronzes suggest that the charge carriers are free electrons in the common WO_3 matrix.

Below x= 0.25 a different mechanism of conduction is operative. McNeill and Conroy (1962) found that for a single crystal of $Na_{0.025}WO_3$ the resistivity decreased with increasing temperature according to the relationship $\log\rho \propto \frac{1}{T}$. This semi-conductor behaviour has since been noted for $Li_{0.097}WO_3$ and in both cases an activation energy of 0.02eV was found for the conduction process.

Greiner and Shanks (1962) have measured the magnetic susceptibilities of the cubic tungsten bronzes and found weak, temperature independent, paramagnetism. They found that the magnetic susceptibility, χ, varied as $\chi \propto x^{1/3}$ and not as predicted by the band theory $\chi \propto x$.

(iv) Nuclear Magnetic resonance

With the metallic-type electrical conductance and magnetic susceptibilities of the tungsten bronzes it might be expected that the n.m.r. signal for the sodium or tungstennuclei would be shifted to lower magnetic fields relative to the signal of their nuclei in non-metallic environment. This shift which is observed for many metals is known as the Knight shift and is proportional to the density of conduction electrons at the nucleus. Electrons in s-type

orbitals or bands can contribute to the shift whereas those in p or d orbitals cannot. Studies by Barnes, Hultsch and Jones (1959) and other workers show very small or zero Knight shifts for tungsten bronze suggesting that the 5d orbitals of tungsten rather than the s orbitals of the alkali metals must contribute to the conduction band.

C. THIS THESIS

The work in this thesis falls into two main parts.

The first is an extension of the work of Parsonage and Cope (see section A (iv) of this Chapter). Of the three urea-1-alkene adducts whose heat capacities they measured that of 1-decene was unique in having no co-operative type anomaly in its heat capacity but instead exhibiting smooth anomalous humps over a large range of temperature. Ising Monte Carlo calculations were unable to predict this non-cooperative anomaly. In this thesis the heat capacities of three further urea-1-alkene adducts, 1-dodecene ($C_{12}H_{24}$), 1-tetradene ($C_{14}H_{28}$) and 1-octadecene ($C_{18}H_{36}$) have been measured from 12-300K to give more information about the guest molecule transitions. It was also thought possible thatoptical birefringence measurements on urea crystal sections at low temperatures might clarify the nature of the guest molecule transitions. To this end a low temperature microscope stage was constructed and used in conjunction with a polarising microscope to investigate the birefringence of various urea adducts at low temperatures.

Cope (1967) measured the heat capacities of the thiourea adducts of cyclohexane and 2,2 dimethylbutane. In view of the very complex nature of the anomalies found in the heat capacities of these adducts it was decided to study the heat capacities of two further cycloalkane adducts, those of cycloheptane (C_7H_{14}) and cyclooctane (C_8H_{16}).

It was hoped that these measurements might show which anomalies were due to the host lattice and which were due to the guest molecules.

The second part of the thesis is concerned with measuring the heat capacities of some tungsten bronzes. The N.M.R. spectrum of ammonium tungsten bronze has recently been studied by Dr. P. G. Dickens and co-workers of the Inorganic Chemistry Department, Oxford University. Narrowing of the second moment of the bronze suggests increasing rotational freedom of the NH_4^+ ions with increasing temperature. To study the thermodynamic properties of the NH_4^+ ions the heat capacities of $(NH_4)_{0.26}WO_3$ and $K_{0.26}WO_3$ were measured from 12 to 300K.

N.M.R. measurements of Boudard (1970) on hydrogen tungsten bronze suggests that the H^+ ions possess a significant amount of molecular freedom at low temperatures. As the hydrogen ions cannot have any rotational freedom they most probably acquire vibration or translational motion along the channels at temperatures above zero degrees Kelvin. The heat capacity of $H_{0.40}WO_3$ was measured from 12 to 300K to give more information about the nature of this motion.

CHAPTER 2

The Adiabatic Calorimeter System

(i) Introduction

The most accurate and convenient way of measuring the heat capacity of solids at low temperatures is the method of electrical heating. In this method the temperature rise of the sample of solid and its container (of known heat capacity) is determined when a measured quantity of electrical energy is supplied. An adiabatic calorimeter system is one in which no heat is interchanged between the calorimeter and its surroundings during heat capacity measurements. Perfect adiabatic conditions can never be realised in practice but heat interchange between the calorimeter and surroundings may be minimised by suspending the calorimeter in a vacuum and surrounding it by metal shields which are kept at the same temperature as the calorimeter.

The first adiabatic calorimeter was employed by Lange (1924). The calorimeter system used in this research used Southard and Brickwedde's (1933) refinement of the Lange calorimeter as the basis for its design. The cryostat was constructed by Kington and Edwards (1962) and the sample container, thermometer and thermocouple system by Pemberton and Parsonage (1966). Cope (1967) used this calorimeter system with certain modifications to study adducts of urea and thiourea.

In this research the apparatus which Cope describes was used to study three urea and two thiourea adducts and the tungsten bronzes. The control of the temperature of the adiabatic shields was automated by Stroud (1969) and this system was used for all the compounds studied.

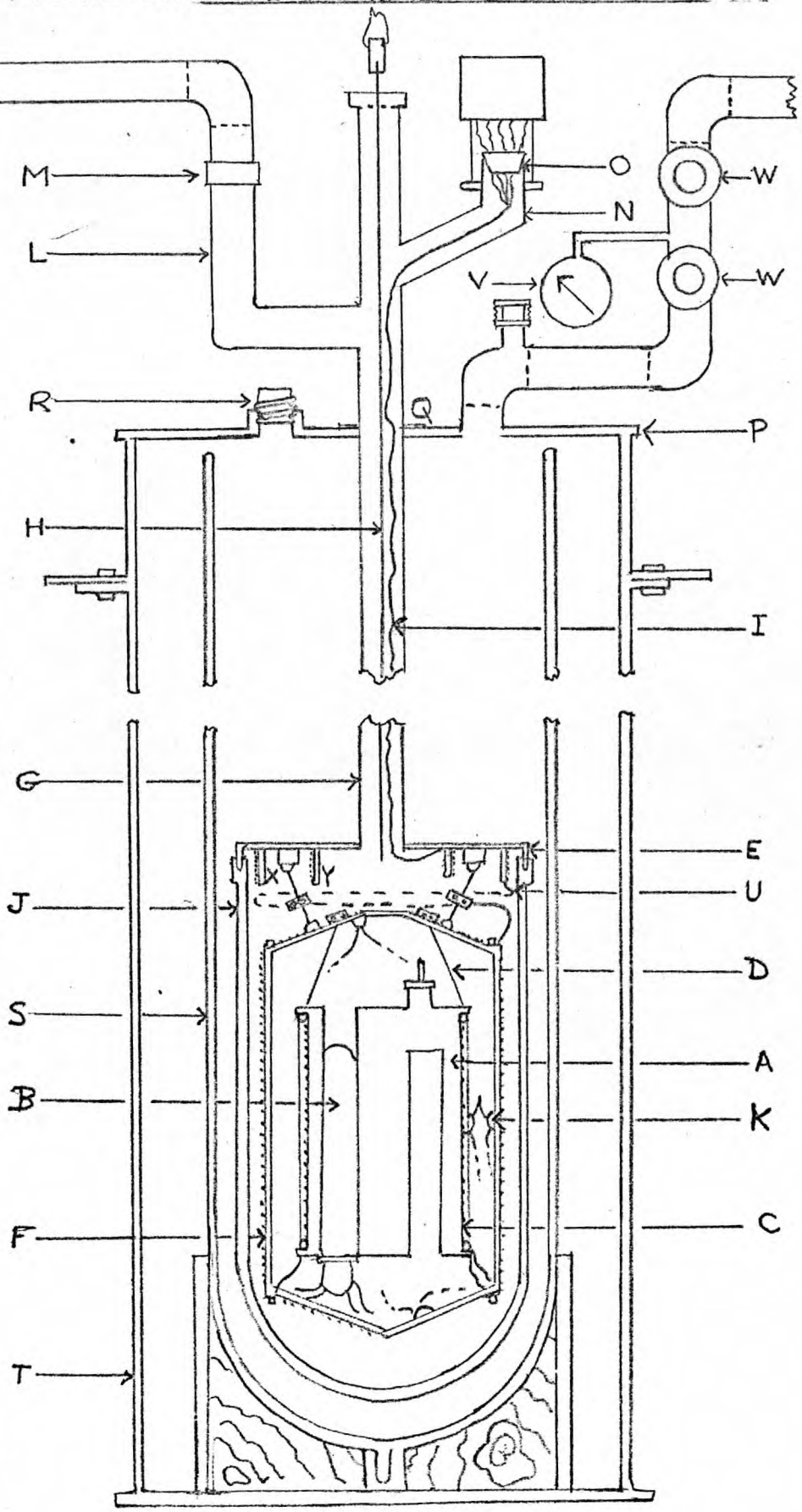
(ii) The cryostat and calorimeter vessel

The adiabatic calorimeter system is shown in Figure 2.1. The calorimeter vessel and shields are suspended from a brass plate (F) by nylon threads. Before starting on a series of heat capacity measurements the copper submarine (J) was soldered to the brass plate using iridium/tin eutectic solder (Johnson Matthey Ltd.). The brass plate was connected to the main frame (P) by a one inch diameter monel metal tube (G) which led to a glass line.

The submarine was immersed in a large glass Dewar vessel (S) which contained the refrigerant. This Dewar was mounted inside a large iron can (T) which was raised on runners to make a vacuum tight seal when bolted to the main frame. The can (T) could be evacuated by a Kinney high capacity pump or vented to the roof by two inch connecting pipes.

The refrigerant used for measurements in the temperature range 77-300K was liquid nitrogen; between 50 and 90K liquid nitrogen was cooled by evaporation (nitrogen is solid below its triple point at 64K). For measurements in the range 12-50K liquid hydrogen was the refrigerant. The

FIGURE 2.1. THE CALORIMETRIC APPARATUS.



system was precooled with liquid nitrogen which was then forced from the Dewar with nitrogen gas and liquid hydrogen was introduced through (R) by means of a glass syphon with an evacuated glass jacket. As the heat capacity of materials falls rapidly below 80K precooling saves a considerable amount of hydrogen otherwise lost by evaporation. When the system had cooled to 30K the liquid hydrogen was pumped on and the temperature eventually reached was below 12K (triple point of hydrogen is 14K).

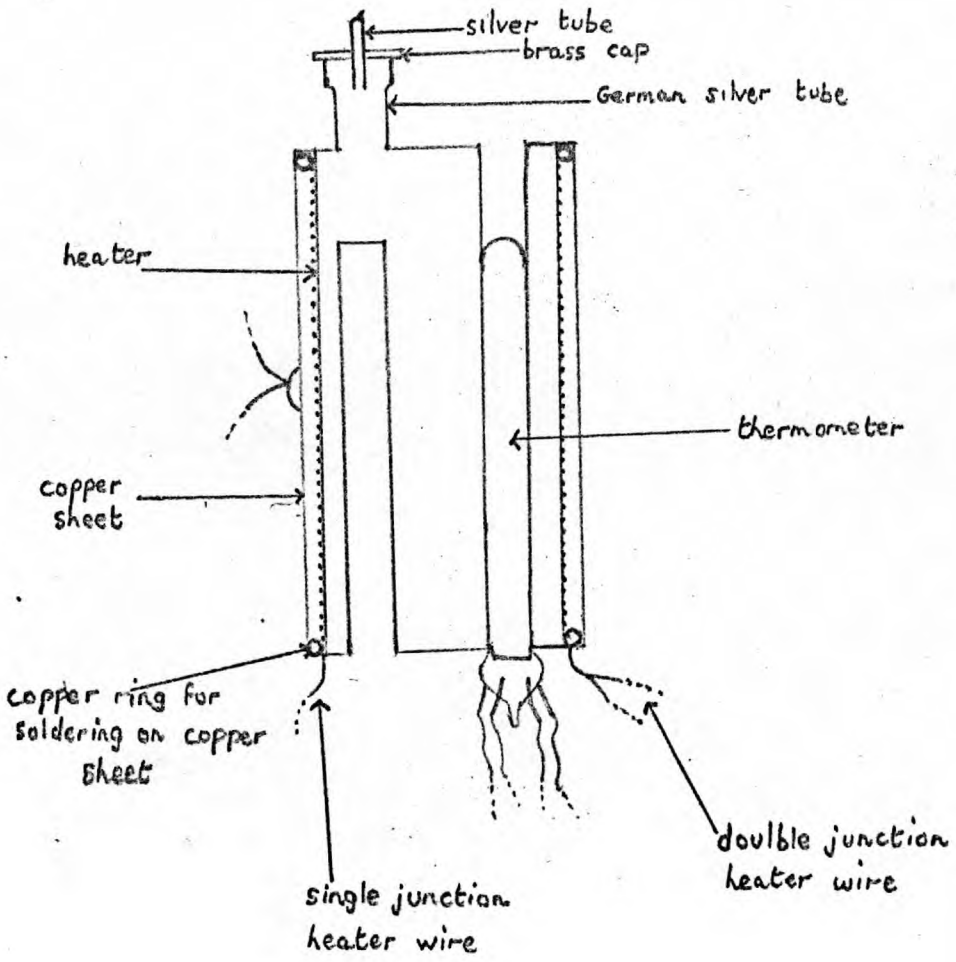
The calorimeter vessel (Figure 2.2 was manufactured from a platinum -10% iridium alloy by Johnson Matthey Ltd. and weighed 115g. with a capacity of 41cm^3. The cylindrical body of the calorimeter (3.1cm diameter, 6.5cm long and 0.04cm wall thickness) was gold soldered to circular top and bottom plates (3.7cm diameter). The bottom plate contained two re-entrant tubes (0.8cm diameter), one to hold the thermometer and one originally intended for the calorimeter heater. A short German silver tube 1 cm long, 0.8cm diameter) was soldered to the top plate and was used for loading the calorimeter.

(iii) <u>The calorimeter heater and heater circuit</u>

The calorimeter heater used by Pemberton was housed in a second re-entrant tube in the bottom plate of the calorimeter vessel described above. However Finke (1965) reported that this form of heating leads to an appreciable

FIGURE 2.2

THE CALORIMETER VESSEL.



temperature gradient along the outside surface of the vessel. To minimise this effect Cope wound the heater wires around the outside of the vessel.

A coil of cotton covered manganin resistance wire (s.w.g. 40, resistance 410 ohms) was wound uniformly and non-inductively around the varnished outside surface of the calorimeter. Copper wires (s.w.g. 34) which were soldered to the manganin coil were lead through separate holes drilled in the flanges of the bottom plate and fixed in the holes with varnish (cryogenic insulating varnish, Oxford Instrument Co. Ltd.). These wires were cut shortly after the holes and bent to form hooks. To one of these hooks was joined a single lead of s.w.g. 38 copper wire and to the other hook was joined a double lead of the same wire. The reason for this choice of leads is explained later.

The manganin wires were then covered with a layer of cigarette paper stuck down with varnish and a thin copper sheet (thickness 4 thou) was soldered to copper rings soldered to the top and bottom flanges, so as to completely surround the manganin wires without making contact with them.

The calorimeter heater current was supplied by two six volt accumulators and controlled by a decade box (1 ohm - 10,000 ohms). When not in use the accumulators were discharged through a dummy heater maintained at a similar resistance to the calorimeter heater. A switch

ganged to switch A, the heater current on-off switch (see Figure 2.3), activated a "decatron timer" (Labgear type D.4108), which together with a ten second "add on register" (type D 4109) gave a value for the time of heating accurate to 0.003%.

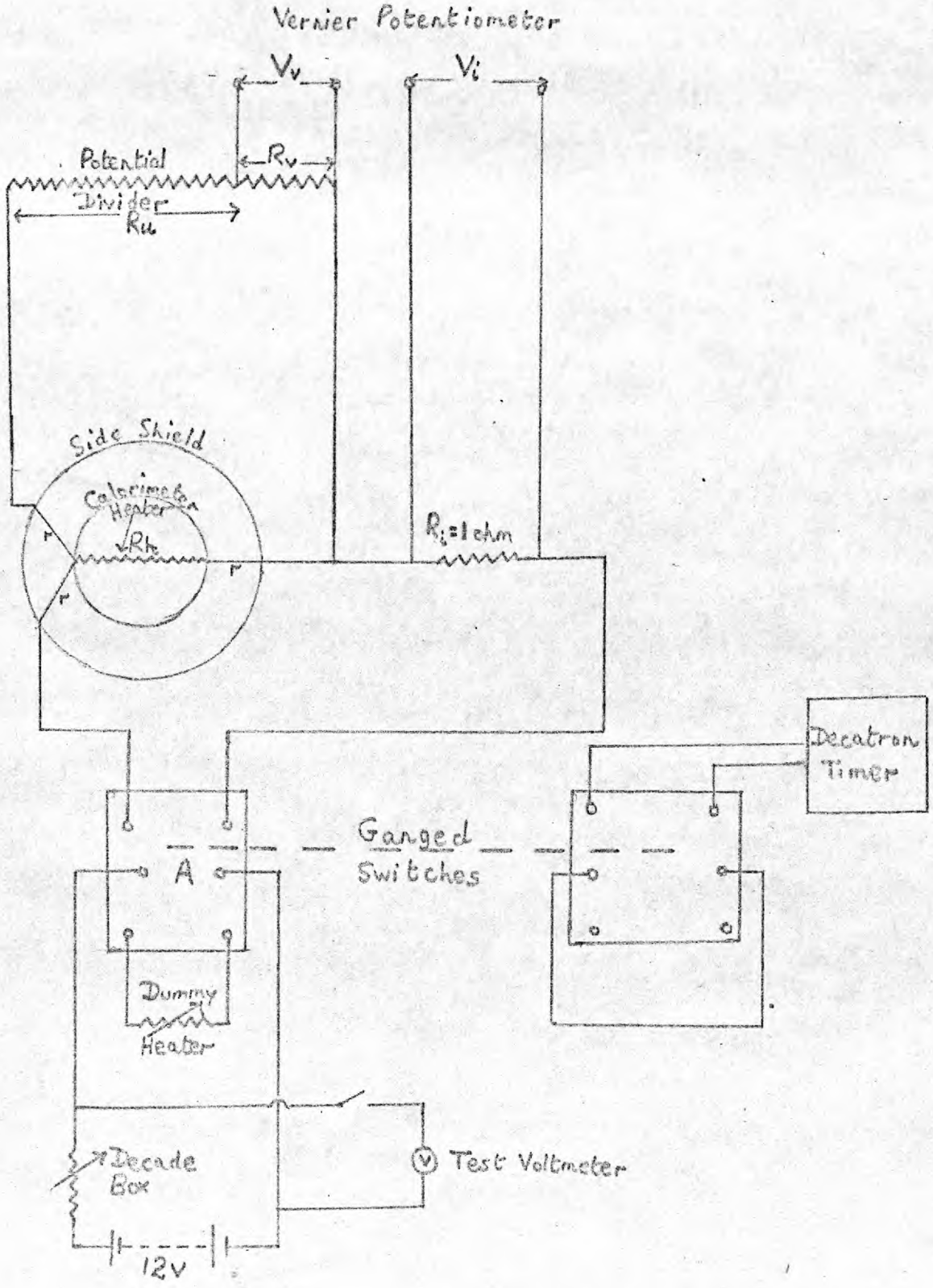
To measure the energy supplied to the calorimeter in a heating period the potentials Vi and Vr across the resistances Ri and Rv (Figure 2.3) were measured using a Tinsley vernier potentiometer (type 5590B) reading to 0.1 microvolts in conjunction with a Tinsley galvanometer (type 4500L). The resistance of Ri was 1.0001(3) absolute ohms at 20°C and Rx was 100.015 absolute ohms at 20°C.

A major difficulty in the measurement of energy input in high precision calorimetry has been to determine the heat supplied to the calorimeter by the calorimeter heater leads (Ginnings and West, 1964). These leads must not be too thick (or heat will be conducted along them and will cause serious errors particularly at temperatures below 40K) and not too thin (as their resistance should be negligible compared with the heater resistance). With the compromise chosen the heat developed in the leads cannot be ignored. It is then a question of deciding how much of this heat finds its way to the sample container.

To overcome this problem one single junction and one double junction both of 38 s.w.g. copper wire were used

FIGURE 2.3

CALORIMETER HEATER CIRCUIT.



for the heater leads. By this choice of heater leads the heat supplied to the calorimeter could be determined to an accuracy of better than 0.1% by measuring the current and voltage between the heater leads at the base of the side shield (Cope 1967).

(iv) The thermometer and thermometer circuit

The thermometer used in this research was a coiled filament platinum resistance thermometer (called "C") of the type described by Mayers (1932). It was constructed by Pemberton (1966) and calibrated from 12-300K by comparison with thermometer "A". Thermometer "A" was calibrated by Edwards (1959) against a thermometer made available by Dr J. A. Morrison (then of the National Research Council of Canada). This thermometer was calibrated using the Provisional Temperature Scale of the National Bureau of Standards below 90K and from 90K to 0°C the resistance of the thermometer was defined by the Callendar-Van Dusen equation

$$t = \frac{100\,(R_t - R_0)}{(R_{100} - R_0)} + \frac{\delta t}{100}\left[\frac{t}{100} - 1\right] + \beta\left[\frac{t}{100}\right]^3\left[\frac{t}{100} - 1\right]$$

and above 0°C by the Callendar equation

$$t = \frac{100\,(R_t - R_0)}{(R_{100} - R_0)} + \frac{\delta t}{100}\left[\frac{t}{100} - 1\right]$$

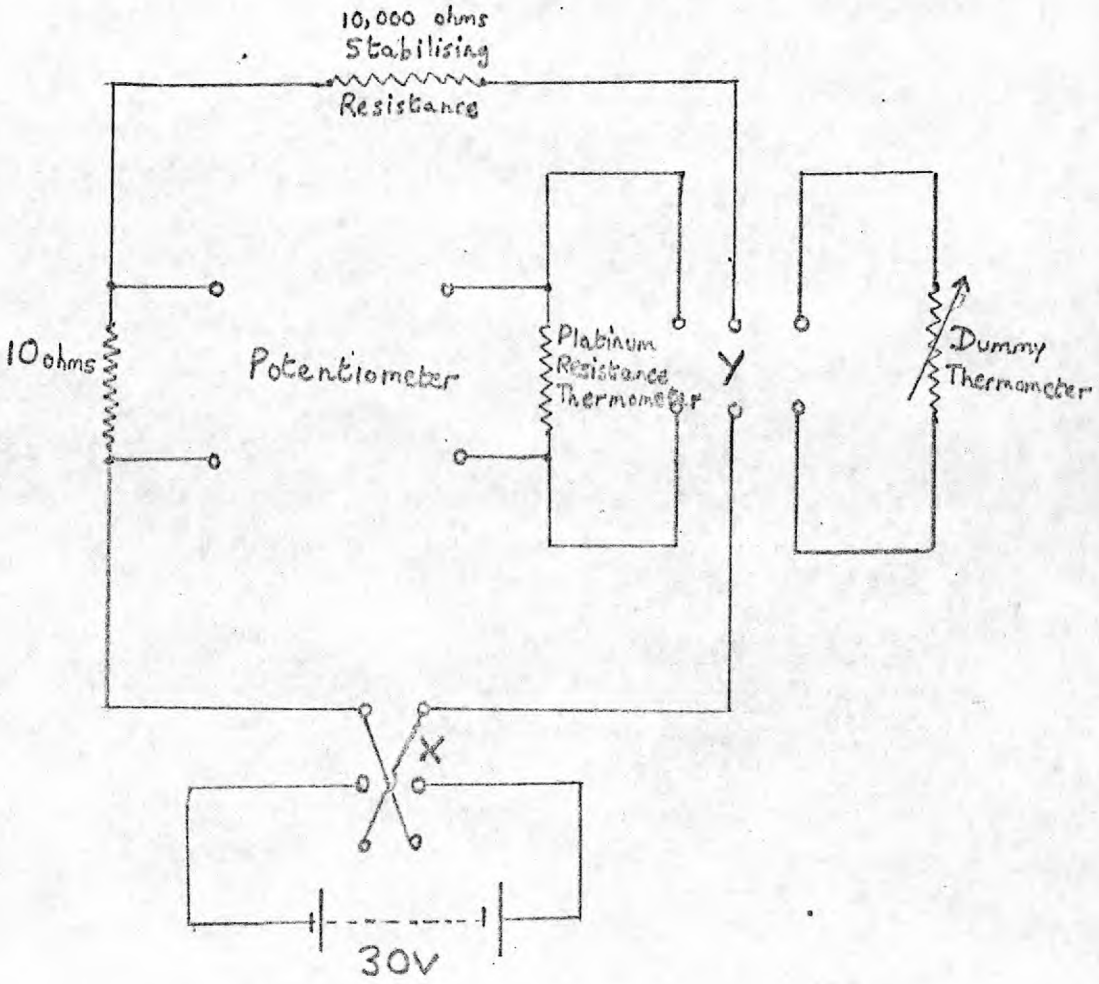
where t is the temperature in °C, Rt is the resistance at temperature t°C and β and δ are constants characteristic of the thermometer.

The resistances of both "A" and Morrison's thermometer were quoted in international ohms but for the thermometer "C" the resistances were converted into absolute ohms to be consistent with the units of the standards of the measuring circuit.

The thermometer fitted into the re entrant hole in the bottom plate of the calorimeter vessel (see Figure 2.2) A snug fit and good thermal contact were ensured by wrapping the thermometer with a piece of aluminium foil and coating the thermometer with a little Apiezon T grease.

The thermometer current was supplied by five six volt accumulators. The measuring circuit is shown in Figure 2.4. A 10,000 ohms resistance in circuit kept the thermometer current virtually constant at approximately three milliamps despite the change in the resistance of the thermometer. The potential across the thermometer was measured, on the vernier potentiometer, and the current passing through the thermometer was determined by measuring the potential across a calibrated ten ohm resistance (Pemberton 1965) in series with the thermometer. The direction of the current passing through the thermometer was reversed by the switch X. An average value of thermometer current and potential for the two current directions was used to eliminate switch contacts and other parasitic potentials.

FIGURE 2.4 THERMOMETER CIRCUIT.



X was a nine-pole, four-way selection switch (Pye type 6001) and was of the make-before-break variety with a thermal e.m.f. specified as less than 0.2 μV for 1°C across the switch contacts. The switch was housed in a metal box to prevent contamination by dust.

When the thermometer was not in use the current was switched through the dummy thermometer (a decade box adjusted to a resistance similar to that of the thermometer) to keep the batteries under constant load conditions.

(v) The adiabatic shield assembly (For letters in brackets see Figure 2.1.)

In an adiabatic system convection, conduction and radiation of heat must be minimised. The adiabatic shield assembly was constructed to ensure this.

The calorimeter vessel was suspended from and completely surrounded by three brass shields (F) which were kept at the same temperature as the vessel. This assembly was enclosed in a vacuum can (J) and the pressure inside this can was maintained at 10^{-6} mm of mercury while heat capacity measurements were taken (minimising convective heat transfer).

Transfer of heat along the calorimeter and thermometer leads was minimised as follows. The leads were chosen to be as thin as practically possible and on entering the system by the monel metal tube (G) were wrapped around two rings (X and Y) attached to the brass plate (E).

This plate and hence the wires are in direct thermal contact with the refrigerant. The wires were then wound around the side shield so that they attained thermal equilibrium with it and therefore also with the calorimeter. Non-conducting nylon threads suspended the top shield from the brass plate (E) and the calorimeter from the top shield.

The calorimeter vessel was polished and the outside of the shields were plated with rhodium to reduce heat transfer by radiation. The exterior surfaces of the shields were covered with aluminium foil to reduce heat transfer with the vacuum can (J) which was in contact with the refrigerant.

The shield system was completely rewired after completing the urea adduct measurements. No alterations were made to the system. 22 wires (16 copper, s.w.g. 40, and 6 constantan, s.w.g. 34) were wound around the side shield, one wire being placed in each of the 20 helical grooves. The wires were insulated from (and fixed to) the side shield with varnish. At the base of the shield the constantan wires were passed straight into holes situated in the grooves and fixed there by filling the holes with varnish.

However the copper wires being thinner tended to break more easily and so before the base of the shield they were soldered to short lengths of thicker (s.w.g. 26) copper

wire which were then passed through the holes. To prevent the soldered junctions causing short circuits between the wires and the shields small pieces of silk ribbon were stuck under the junctions.

The wires around the shield were then covered with a layer of cigarette papers and a coil of manganin resistance wire (440 ohms, s.w.g. 36) was wound uniformly and non-inductively over the papers forming the side-shield heater. This heater was then covered with a layer of cigarette paper which was stuck down with varnish. The top and bottom shields were as used by Cope. Their resistances were 70 and 65 ohms respectively.

From the top of the side shield the 22 wires were led as one cable for about three feet and then were individually wound around and stuck down by varnish to the rings (X) and (Y). From the inner ring the wires were led as one cable up the monel tube and out of the vacuum space at O to a tag board, where they were soldered to screened cables leading to the measuring circuits. O was a brass socket with grooves through which the wires passed. The socket made a tight fit with a brass socket and to ensure a perfect vacuum the wires were waxed and the grooves were filled with Apiezon W. wax.

(vi) The differential thermocouple system

The system described by Cope (1967) was used for all the heat capacity measurements in this research. It is

shown diagrammatically in Figure 2.5. As can be seen the side shield temperature was compared with that of the calorimeter and the top and bottom shields were then compared with the side shield.

The constantan wires were joined to copper leads inside the equal temperature junction (a massive brass block surrounded by polystyrene) to ensure that no thermal gradients were set up between these junctions.

It was possible that inductive effects might have occurred in the thermocouple wires when controlling the shields automatically due to the changing of currents in the various heater wires. However no such effects were found presumably because each pair of thermocouple wires had an environment sufficiently similar for no net current to be induced.

(vii) The automatic shield control

A completely automatic adiabatic shield control has been constructed by Stroud (1969) and this system was used from 12-300K for all heat capacity measurements made in this research. A brief description of this control system is given here.

A block diagram of the component parts of the control system is shown in Figure 2.6. The differential thermocouple potential is amplified by a ~~microvoltmeter~~ galvanometer-amplifier (Pye-type 11340/5) and is displayed on a chart recorder

FIGURE 2.5 DIFFERENTIAL THERMOCOUPLES SYSTEM

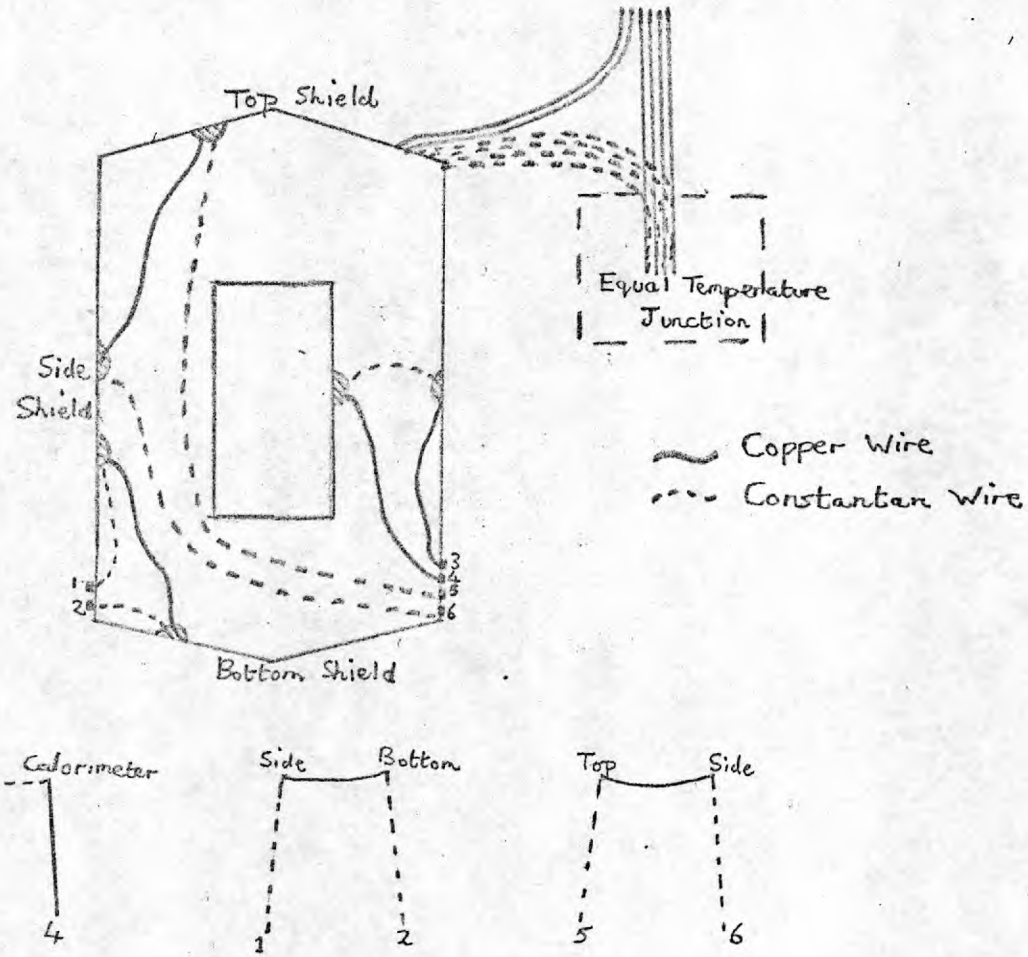
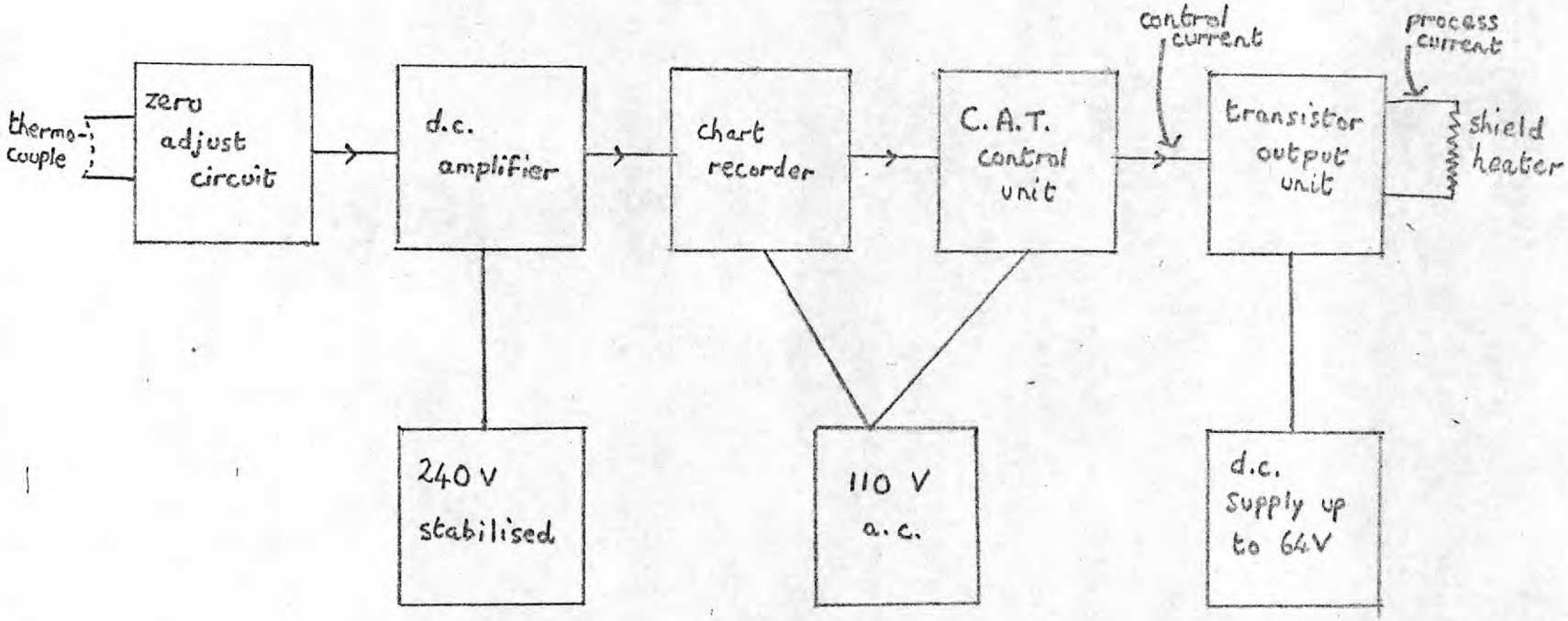


FIGURE 2.6 BLOCK DIAGRAM OF AUTOMATIC CONTROL SYSTEM.

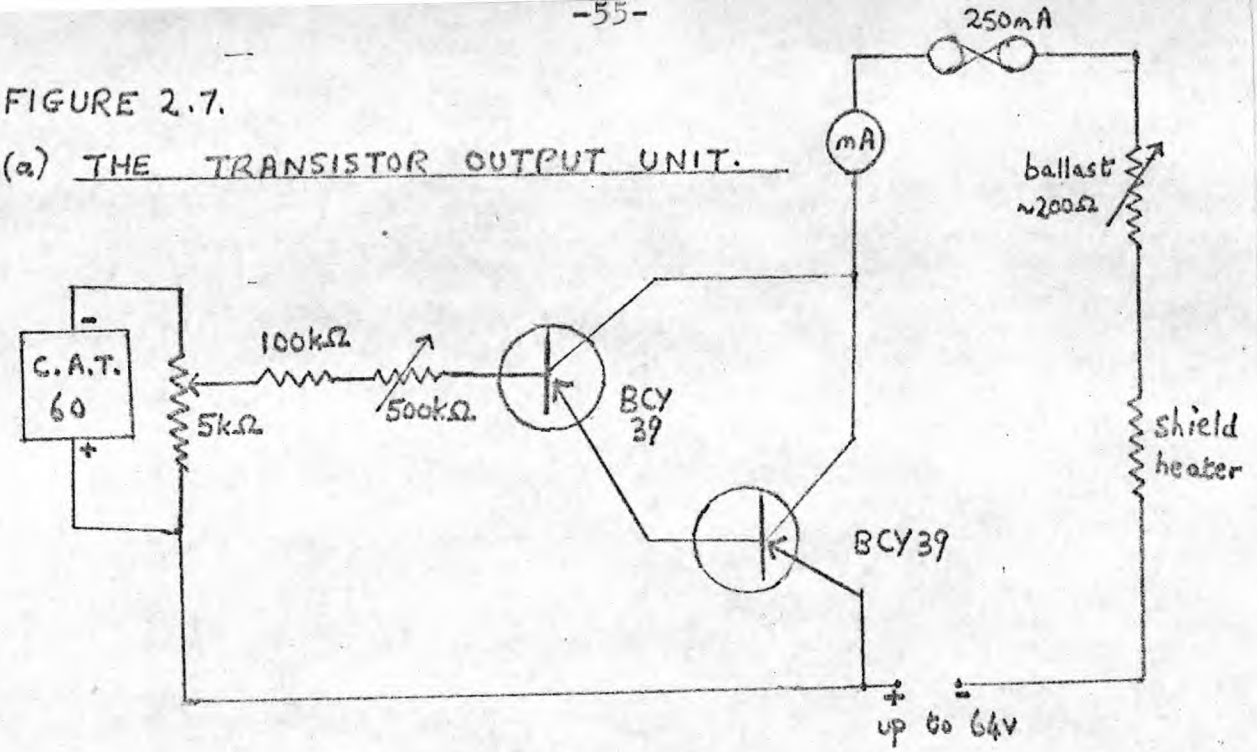


(Leeds and Northrup Speedomax H recorder). A current adjusting type (C.A.T.) control unit (Leeds and Northrup 3 action C.A.T. control unit) which is integrally built with this recorder responds to the deflection of the recorder pen from zero producing a 'control' current which is made up of three components. First the 'proportional band' current which is proportional to the displacement of the recorder pen from the null position. Second the 'reset' current which is a function of the time the pen has been displaced from the null position and third the 'rate' current which depends on the rate of change of recorder pen displacement. The relative importance of these three currents is adjusted to give the best shield control using the 'Proportional', 'Automatic Reset' and 'Rate' controls.

The resultant control current is then fed into the transistor output unit (see Figure 2.7 (a)) and this supplies the 'process' current which energises the shield heater. All three heaters are powered by a single 60 volt d.c. voltage supply. When more than one shield is controlled automatically the fluctuations in current demand of one shield cause variations in the current supplied to the others making control for the C.A.T. unit more difficult. This effect was minimised by incorporating ballast resistances in the top and bottom circuits which greatly reduced the fractional change in total current supplied

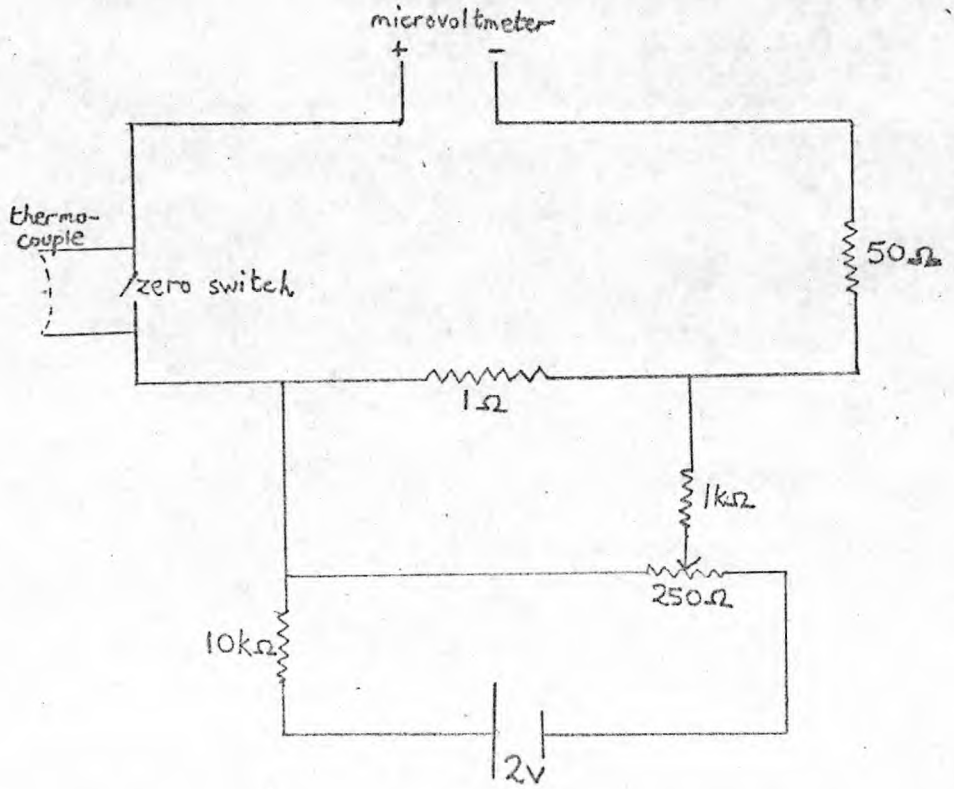
FIGURE 2.7.

(a) THE TRANSISTOR OUTPUT UNIT.



There is no ballast resistor in the side shield circuit.

(b) D.C. AMPLIFIER INPUT CIRCUIT.

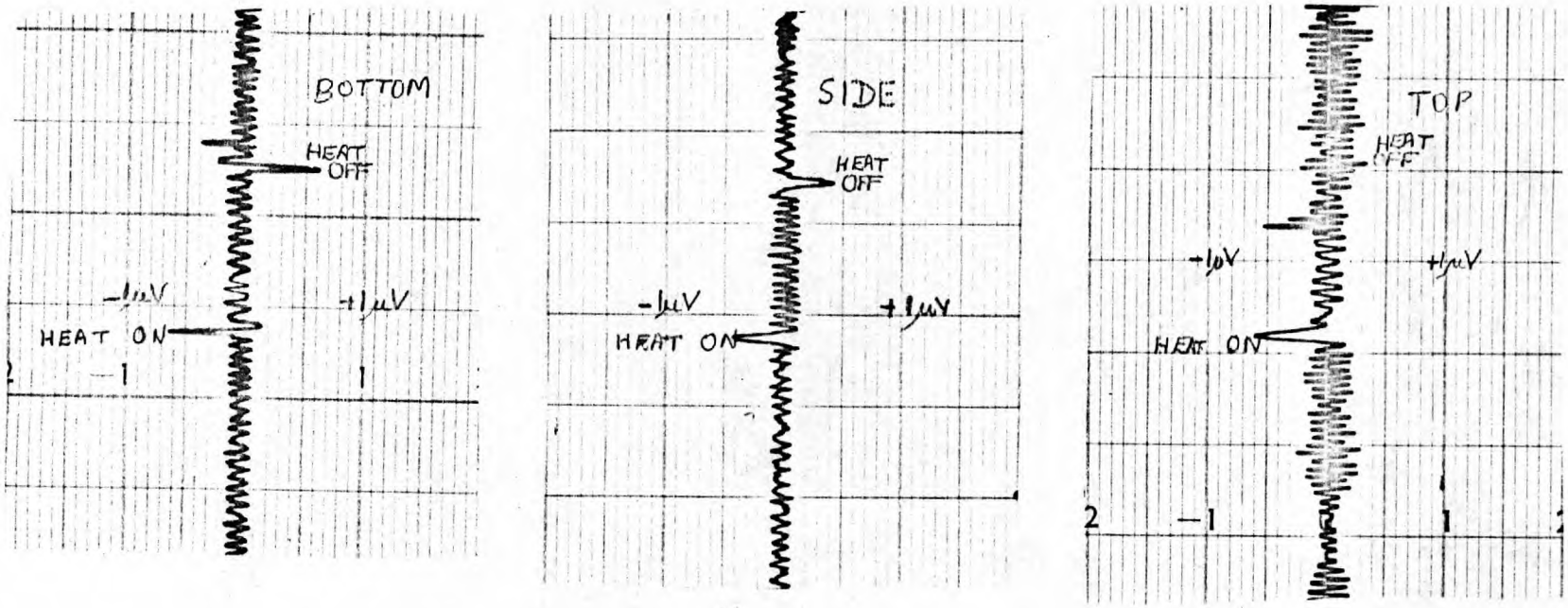


with varying demands of the heaters.

The zero of the D.C. amplifier circuits was adjusted manually. The control of the C.A.T. unit was set on manual and the thermocouple was shorted out by switching to the 'zero position' on a rotary thermal - e.m.f. - free switch (Croydon Instrument Co. Ltd.). Coarse adjustment of the zero was then made using the control on the microvoltmeter. Fine adjustment was effected by changing the potential drop across a one ohm resistor by varying X (see Figure 2.7 (b)).

An example of the charts of the three shields controlled automatically during a heat capacity run is shown in Figure 2.8.

FIGURE 2.8. AUTOMATIC SHIELD CONTROL FOR A HYDROGEN TUNGSTEN BRONZE HEAT CAPACITY POINT (RUN No. 3)



In this temperature range (~90K) thermocouple sensitivity is ~ 20μV/K.

CHAPTER 3

Experimental Determination of Heat Capacities

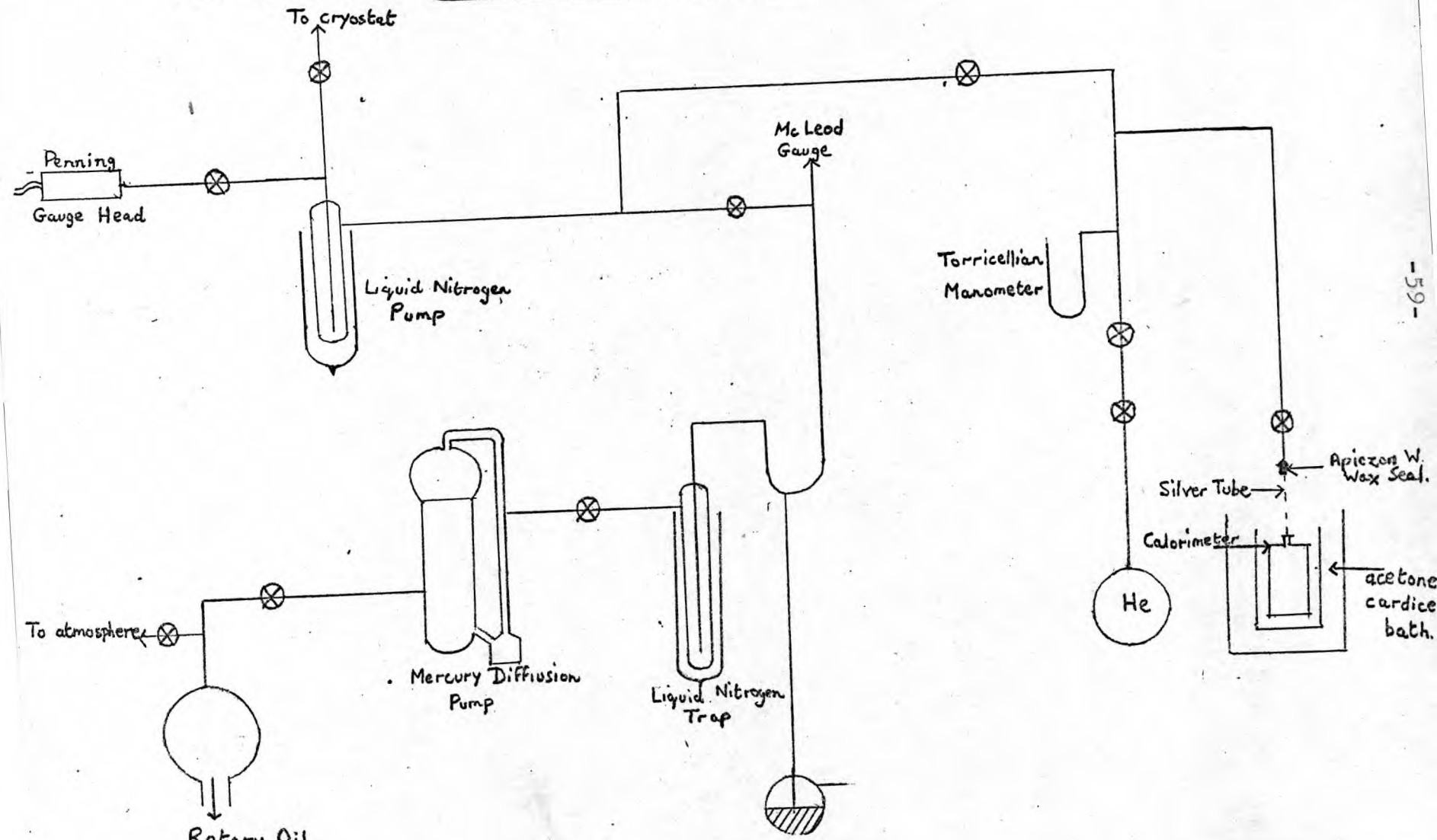
(i) Assembly of the calorimeter system

The sample was introduced into the calorimeter vessel through the German silver tube in the top plate (Figure 2.2). A hollow silver tube of external diameter 1mm was soldered into a hole of suitable size in a brass cap which was then soldered with the tube onto the brass rim of the German silver tube. A low melting point solder was used (40% Pb; 40% Sn; 20% Bi) and the low temperature necessary to solder on the cap together with the very low thermal conductivity of German silver ensured that heat-sensitive adducts did not decompose.

The top of the silver tube was then fixed with Apiezon W wax to make a vacuum tight seal with the glass-line (see Figure 3.1). When the sample was unstable to pumping at room temperature it was surrounded by an acetone-cardice bath. The calorimeter was evacuated to about 5×10^{-5}mm then the system was isolated from the pumps and a dose of helium (pressure about 1 cm of mercury) was introduced into the calorimeter. This was to improve heat exchange between the calorimeter heater and the sample.

The silver tube was then sealed just above the calorimeter by squeezing hard with a pair of pliers. The tube was then cut at the seal and a small amount of low melting point solder was applied to the cut surface. Finally

FIGURE 3.1. THE VACUUM LINE.



the thermometer with a coating of Apiezon T grease was put into position.

Weighings were made during the loading procedure to determine the wieghts of the sample, the empty calorimeter, the silver tube, the low melting point solder and the Apiezon T grease. These were determined so that the appropriate corrections could be made to the heat capacity of the empty calorimeter.

The vessel was then mounted in position within the shields. By making fine adjustments to the three nylon threads suspending the calorimeter it was situated in exactly the same position with respect to the calorimetry rig for each set of heat capacity measurements. The thermometer, calorimeter and thermocouple wires were then connected to the appropriate wires at the base of the side shield and the circuits were checked for the correct resistances and absence of short circuits. The copper submarine was soldered into position around the shield assembly using Sn/In Eutectic solder (Johnson Matthey Ltd.). Decompostion of the sample and charring of the electrical wiring during soldering is prevented by surrounding the submarine with and ice/water bath. The submarine was evacuated for about two days until a vacuum of 1×10^{-6} mm of mercury was achieved.

The hydrogen tungsten bronze sample decomposed in the presence of oxygen. To avoid any decomposition of the

sample the loading procedure was carried out in a polythene 'dry-bag' which had first been repeatedly flushed through with oxygen-free nitrogen gas and then placed under a slightly greater than atmospheric pressure of the nitrogen for about an hour. When the brass cap and silver tube had been soldered into position the calorimeter was removed from the dry-bag, attached to the glass line and pumped out.

(ii) The heat capacity measurements

The heat capaicty of the sample and calorimeter is defined by

$$C = \lim_{\Delta T \to 0} \left(Q/\Delta T \right) = \frac{dQ}{dT}$$

where ΔT is the temperature rise of the sample and calorimeter due to a heat input Q. However finite temperature increments ($\Delta T \neq 0$) must be employed in real systems and so when C is not a linear function of T a curvature correction should be employed. However except in regions of abnormally high curvature the correction will be less than 0.1% if the ΔT's are less than 10% of the temperature and thus may be neglected.

A correction must be made for heat exchange between the calorimeter and surrounds and for internal heating by the thermometer current. This was effected as follows: instead of taking just one temperature reading before heating t e calorimeter and one after the calorimeter had equilibrated,

two series of readings were taken over a period of about ten minutes in each case. From these readings the fore and after 'drifts' of the temperature with time were determined and the exact temperature of the calorimeter when the calorimeter heater was switched on and switched off were calculated.

The heat supplied to the calorimeter was determined by taking several measurements of Vi and Vv (see Figure 2.3). The average values of these quantities were then inserted in the equation

$$E = (R_u + s)\left(\frac{V_v}{R_v}\right)\left(\frac{V_i}{R_i} - \frac{V_v}{R_v}\right)$$

where E is the heat supplied, s is the resistance of the leads from the base of the side shield to the measuring circuits and the other quantities are as shown in Figure 2.3.

A programme has been written for the London University Atlas Computer evaluating the heat capacity of the sample plus calorimeter in absolute Joules K^{-1} from the temperature drift and heating data and the thermometer calibration. The heat capacity of the sample was then obtained by subtracting the corrected heat capacity of the calorimeter from the bulk heat capacity. The empty calorimeter heat capacity was determined by Cope (Cope 1967).

CHAPTER 4

THE PREPARATION AND ANALYSIS OF THE CHANNEL COMPOUNDS STUDIED

(i) Urea Adducts

(A) Preparation

The literature contains many different methods for the preparation of urea adducts (Bengen, 1940), (Zimmerschied, 1950), (Schlenk, 1951), (Hermann, 1962), (McAdie, 1962). Two slightly different methods were used in this thesis for the preparation of urea adducts, the method chosen depending on the physical nature of the guest.

The adducts of 1-dodecene and 1-tetradecene were prepared by adding the hydrocarbon slowly to a satuarated methanolic solution of urea until the hydrocarbon was in excess with respect to the urea. The mixture was then warmed until the precipitate initially formed dissolved.

For the 1-octadecene adduct and the long chain n-alkane molecules (prepared for D.T.A. measurements) the method of McAdie (1962) was used. Here the hydrocarbon (liquid or solid) was added to a saturated methanolic solution. The mixture was then warmed to 60°C and isopropanol added drop by drop until a homogeneous solution was obtained.

In both methods of preparation the adduct crystals were allowed to form slowly overnight then filtered and washed with a little n-pentane. The adducts were then left to dry in air for several hours.

The reagents used in adduct preparation were:

Compound	Source	Grade
urea	Hopkins and Williams Ltd.	Analar
methanol	Hopkins and Williams Ltd.	Analar
isopropanol	Hopkins and Williams Ltd.	Analar
n-pentane	B.D.H.	G.P.R.
1-dodecene	B.P. Research Sample	S 240
1-tetradecene	B.D.H.	Laboratory Reagent
1-octadecene	B.D.H.	Laboratory Reagent
n-octadecane	Koch-Light Labs Ltd.	Pure (better than 95%)
n-eicosane	B.P. Research Sample	
n-docosane	Koch-Light Labs Ltd.	Pure
n-tetracosane	B.P. Research Sample	S 313
n-octacosane	Koch-Light Labs Ltd.	Pure
n-dotriacontane	B.P. Research Sample	1202A

The purity of the three 1-alkenes used in calorimetric measurements was checked by gas chromatography. No detectable impurity was found. The infra-red absorption spectra of the 1- alkenes were also measured. In addition to all the characteristic absorptions of the 1-alkene molecules (Showell, Russell and Swern, 1962) small peaks were also noted for all the 1-alkenes at about 970 cm^{-1} and for 1-dodecene and 1-tetradecene at 1700 cm^{-1}.

The 1700 cm^{-1} peaks coincide with the very strong C=O stretching frequency absorption and therefore are probably

indicative of very small amounts of aldehydes or ketones being present.

The 970 cm^{-1} peaks coincide with the 968 cm^{-1} peak characteristic of a trans internal isomer.

( ) Analysis

The urea: guest molecule ratio was calculated by determining theweight of urea in a known weight of adduct. This was effected by hydrolysing the urea to ammonium carbonate against standard hydrocloric acid. Cope (1967) tested the method with pure urea and achieved agreement of analytically determined weight to actual weight to within 0.3%.

The procedure used in this thesis was as follows: About 0.6g of urea adduct were dissolved in water and the solution was made up to 250mls. Four 25 ml aliquots of this solution (1 control and 3 samples) were treated in the following way:

Control	Samples
2 ml of 0.5% $HgCl_2$ solution added and mixture agitated.	-
10 mls of enzyme suspension added and mixtures left stoppered overnight.	(suspension is 5 B.D.H. urease tablets in 50 mls water)
1 ml of 10% NH_4Cl soln added	2 mls of 0.5% $HgCl_2$ soln added

Few drops of screened methyl orange indicator added.

0.1M HCl added until end point reached.	0.1M HCl added until end point then nitrogen gas bubbled through solution for 5 mins and acid

The titre used to calculate the weight of urea in the adduct was the mean of the three samples minus the control titre. The effect of the mercuric chloride solution was to 'kill off' the enzyme solution and the nitrogen gas was used to displace any carbon dioxide in solution.

The three 1-alkene adducts studied calorimetricly were analysed before and after the calorimeter measurements; these results are listed in Table 4.1. together with Redlich's (1950) analyses in adduct solutions.

TABLE 4.1 ANALYSES OF THE UREA-1-ALKENE ADDUCTS

Adduct	% of urea		urea/guest weight ratio	molar ratio	
	before	after		present work	Redlich
1-dodecene	76.9	77.3	3.36	9.43	9.3
1-tetradecene	75.3	74.9	3.00	9.31	-
1-octadecene	75.2	75.2	3.03	12.74	-

The density of these adducts was required in order to determine a buoyancy correction to their weighings. This was determined from the analysis results above and the X-ray data of Smith (1952) for unit cell composition and dimensions.

(c) X-ray analysis

Because of the proposal by Lenné (1963) that for many urea adducts including urea-n-tetracosane the urea alttice exhibits 'two-dimensional disorder' it was thought advisable to study single crystals of urea-n-alkanes and urea-1-alkenes by X-ray techniques.

Single-crystal rotation photographs about the adduct c-axis were made by Miss P.S. Osbourne of the Chemistry Department, Imperial College using a Unicam S.C. Goniometer. The urea adducts studied were those of n-eicosane, n-tetracosane and n-dotriacontane, 1-decene, 1-dodecene, 1-tetradecene, 1-hexadene, 1-octadecene and 1-eicosene.

All the adducts studied gave rotation photographs consistent with a hexagonal unit cell and and the c-axis repeat distance was 11.15 $\pm$ 0.15 Å in good agreement with Smith (1952). A typical photograph, the n-hexadecene adduct isshown in Figure 4.1 (a). The n-tetracosane and n-dotriacontane adducts exhibited rather blurred urea lattice points. However these are best explained by a distorted urea lattice from poorly formed crystals rather than by two-dimensional disorder in the urea lattice. The rotation photograph for the urea-n-tetracosane adduct is shown in Figure 4.1 (b).

All photographs showed, to a greater or less extent, diffuse bands attheir centre due to the ordering of the guest molecules. Discrete lattice points are not exhibited by the guest-molecules because their lattice repeat distance is not rationally related to the urea lattice repeat distance.

FIGURE 4.1(a) ROTATION PHOTOGRAPH OF UREA - n-TETRACOSANE ADDUCT

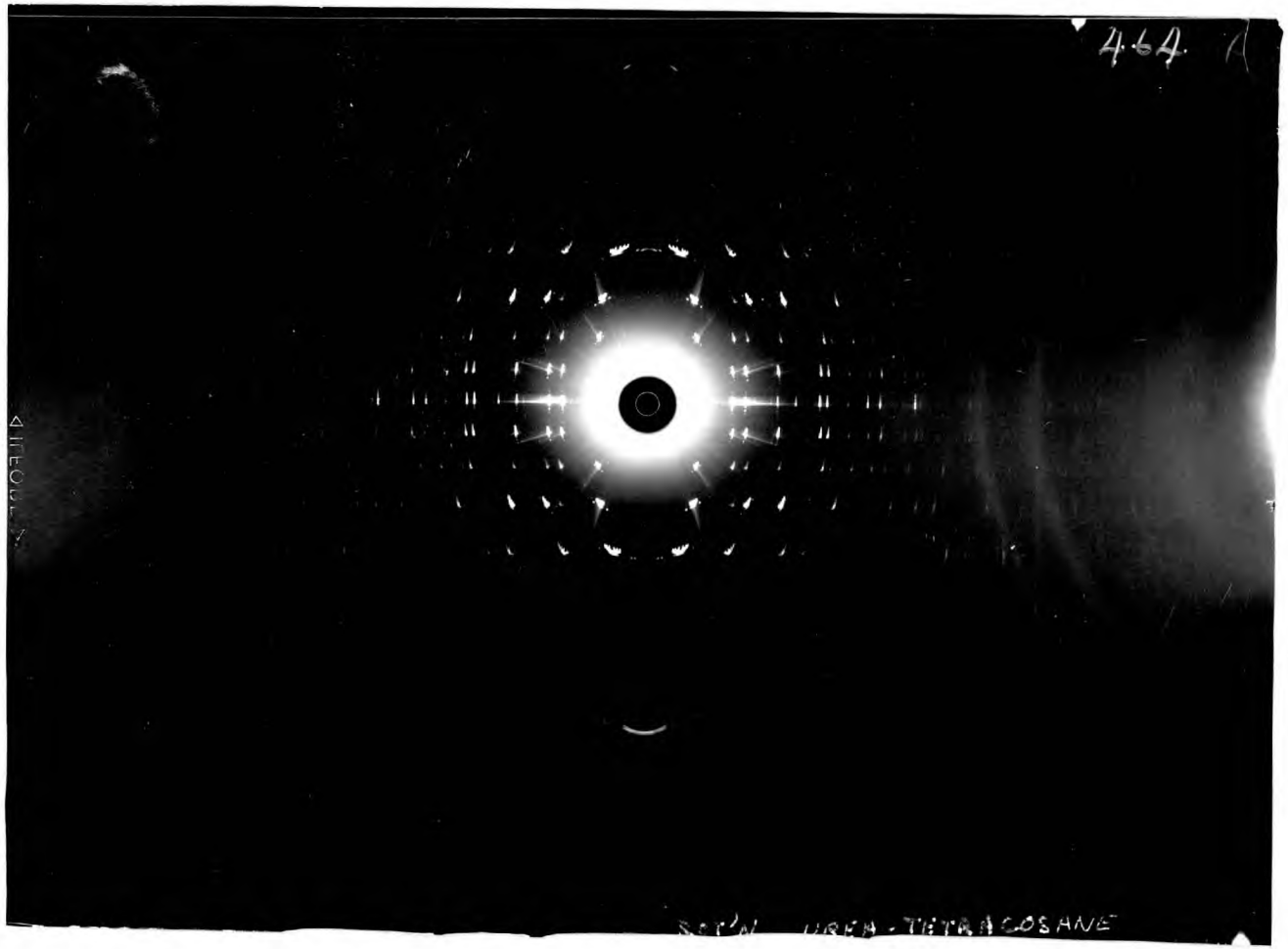
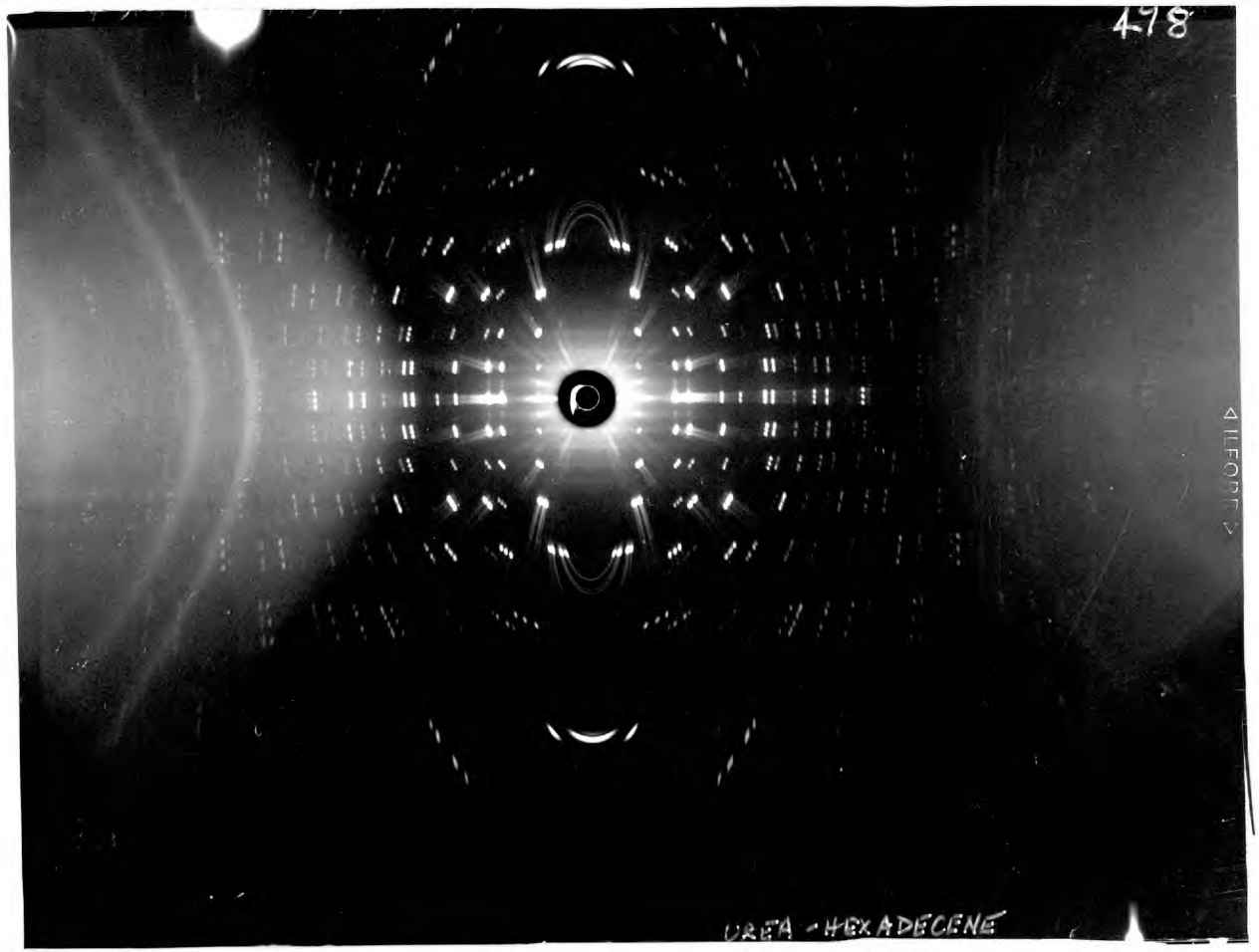


FIGURE 4.1.(b) ROTATION PHOTOGRAPH OF UREA - 1 - HEXADECENE



(ii) Thiourea Adducts

(A) Preparation

The thiourea adducts of cycloheptane and cyclooctane were prepared by the same procedure as the urea 1-dodecene and 1-tetradecene adducts. Various workers (Redlich, 1950) (Lenne, 1954), (Cope, 1967) have noted the instability of thiourea adducts in air at room temperature. However it was found from analysis results (see section B (ii)) and from physical appearance (a white powder is deposited on the surface of thiourea adduct crystals on decomposition) that the adducts of cycloheptane and cyclooctane are quite stable. The thiourea-cycloheptane adduct showed no signs of decomposition at 12°C for at least 24 hours whereas the cyclooctane adduct first showed signs of decomposition after about 5 hours.

Therefore the two thiourea adducts after filtration from their mother liquor were washed with a little of their respective constituent cycloalkanes and dried in air at about 12°C for two hours.

The reagents used were:

thiourea	Hopkins and Williams Ltd.	Analar
methanol	Hopkins and Williams Ltd.	Analar
cyclohexane	Hopkins and Williams Ltd.	G.P.R.
cycloheptane	Koch Light Labs Ltd	Puriss
cyclooctane	Koch Light Labs Ltd	Pure

The purity of the cycloheptane and cyclooctane used was checked by gas chrometography. No impurity was detected in

(i) Analysis

The weight of thiourea in a known weight of thiourea adduct may be determined by oxidising the thiourea to urea. This oxidation is quantitative if iodine in alkaline solution is employed as the oxidising agent (Cuthill and Atkins, 1937). The following procedure was adopted here:

Standard sodium thiosulphate solution (0.1N B.D.H. Ampoule) was titrated against 25ml of approximately 0.1N iodine solution in 10 ml of 4N sulphuric acid. The end point was indicated by the disappearance of the blue starch-iodine complex.

An aqueous solution of a known concentration of thiourea adduct (to give about 0.2g thiourea per 250 mls of solution) was prepared. 25mls of this solution was treated with 10ml of 2N sodium hydroxide, the solution was well shaken and then 50 mls of the iodine solution were added. This mixture was stored in the dark for 10-20 minutes to ensure complete oxidation of the thiourea to urea.

The excess iodine was then back titrated with sodium thiosulphate solution (20 mls of 4N H_2SO_4 were first added to the stored solution).

The oxidation proceeds according to the equations:

$$2NaOH + I_2 \rightarrow NaIO + NaI + H_2O$$

$$H_2O + 4NaOI + CS(NH_2)_2 \rightarrow CO(NH_2)_2 + 4NaI + H_2SO_4$$

$\therefore$ 4 moles $I_2 \equiv$ 1 mole $CS(NH_2)_2$

Cope (1967) showed by comparing the weight of pure thiourea found from this analysis with its actual weight that the procedure was accurate to about $\pm$ 1 %.

Both thiourea-cycloheptane and thiourea-cyclooctane adducts were analysed twice before heat capacity measurements were made. These analyses were made during the drying of the adducts at one hour intervals to determine the rate of adduct decomposition. The adducts were again analysied after the heat capacity runs. These analyses are listed in Table 4.2.

TABLE 4.2. ANALYSES OF THIOUREA-CYCLOALKANE ADDUCTS

Adduct	% thiourea			thiourea/guest molecule	
	1	2	After	wt ratio	molar ratio
cycloheptane	69.4	69.6	70.0	2.32	2.99
cyclooctane	67.0	66.6	67.4	2.02	2.98

(c) X-ray analysis

Lenne (1954) from single crystal rotation photographs of thiourea-cyclohexane found that the cyclohexane molecules formed discrete lattice points due to the molecules being situated near the sulphur atom plane in the thiourea channels and forming an ordered three dimensional array.

Single crystal rotation photographs of thiourea cycloheptane and thiourea cyclooctane were taken by Miss R. S. Osbourne of the Chemistry Department, Imperial College. The photographs of both adducts were consistent with a

rhombohedral unit cell and the c-axis lattice repeat distance 12.5 ± 0.1 Å agreed well with that found for the cyclo-hexane adduct. (see Figures 4.2 (a) and (b))

However neither the cycloheptane nor the cyclooctane adduct exhibited any lattice structure due to the guest molecule. This effect is discussed in Chapter 7(iii).

(iii) Tungsten Bronzes

The three bronzes studied in this thesis were prepared and analysed both quantititavely and structurally by Mr. D. Murphy and Dr. P. G. Dickens of the Inorganic Chemistry Department, Oxford.

(a) Preparation

Ammonium tungsten bronze was prepared by heating ammonium paratungstate to 400-450°C in an atmosphere of hydrogen.

$$5(NH_4)_2O.12WO_3.xH_2O \xrightarrow[pump]{} 5(NH_4)_2O\ 12.WO_3.1H_2O$$

$$\downarrow H_2,\ 400\text{-}450^{\circ}C$$

$$(NH_4)_{0.26}WO_3$$

The potassium tungsten bronze was prepared by heating together potassium tunstate, tungsten metal, and tungsten trioxide mixed in the correct proportions to give the bronze $K_{0.26}WO_3$.

The hydrogen tungsten bronze, $H_{0.40}WO_3$ was prepared by treating polycrystalline tungsten trioxide with zinc and hydrochloric acid in the absence of air.

FIGURE 4.2(a) ROTATION PHOTOGRAPH OF THIOUREA-CYCLOHEPTANE.



FIGURE 4.2(b) ROTATION PHOTOGRAPH OF THIOUREA - CYCLOOCTANE



(B) Analysis

All three bronzes were analysed thermogravimetrically. The hydrogen and ammonium tungsten bronzes were both oxidised to tungsten trioxide. The potassium tungsten bronze was converted with oxygen to potassium tungstate and tungsten trioxide. The K^+ ion was also estimated quantitatively by atomic absorption spectroscopy and the K:W ratio was determined by X-ray fluorescence spectroscopy.

Both the hydrogen and ammonium mole fractions were also determined by oxidation; hydrogen by titration with warm potassium dichromate solution and ammonium by reaction with silver thiocyanate. The ammonium content was also determined by the Kjeldahl method.

(C) Structural analysis

The structure of the potassium tungsten bronze was first determined by Magneli (1953) using X-ray methods. He found that the unit cell was hexagonal (space group D^3_{6h} - C_6/mcm) with six WO_3 units per unit cell. Unit cell dimensions for $K_{0.27}WO_3$ were a = 7.40 ± 0.01 Å, c = 7.56 ± 0.01 Å. Murphy (1968) found that $(NH_4)_{0.26}WO_3$ possessed the same crystal structure with a = 7.39 ± 0.015 Å c = 7.56 ± 0.015 Å.

The structure of the cubic hydrogen tungsten bronze has been studied by Dickens and Wiseman (1970) using neutron diffraction. The space group is cubic I_{3m} . The WO_6

octahedra are distorted in the sodium, lithium and hydrogen bronzes, the degree of distortion increasing in the order H > Li > Na.

CHAPTER 5

Optical Birefringence Measurements

(i) Introduction

Crystals may be classified by their optical properties into three different types: these are isotropic, uniaxial and biaxial crystals. For an isotropic crystal the velocity of light in the crystal is the same in all directions whereas for an anisotropic crystal (uniaxial or biaxial) the velocity varies with the direction of propagation.

A ray of light entering an anisotropic crystal will in general be divided into two rays travelling with different velocities and plane polarised at right angles to one another. Crystals of the hexagonal, tetragonal and trigonal systems have only one direction, the optic axis in which double refraction does not occur and thus are known as uniaxial crystals. Orthorhombic, monoclinic and triclinic crystals possess two directions in which double refraction does not occur and are known as biaxial crystals.

The optic axis of the hexagonal crystal system is the c - axis (see Figure1.1). Thus if we consider the hexagonal urea host lattice, neglecting the occluded guest molecules, light passing along the c axis should not be doubly refracted. If the guest molecules are rotating (they have no preferred orientation) then they will have

isotropic optical properties like a liquid or gas.

At low enough temperatures the guest molecules may cease to rotate and adopt an ordered low-energy arrangement. Two possible types of ordered arrangements may be imagined (Figures 5.1 a and b).

In the anisotropic arrangement the guest molecules are aligned in parallel. In Figure 5.1 a) the molecules are all pointing in the same direction (as in a ferromagnet) but the arrangement in which all the molecules point in the opposite direction to their nearest neighbours (as in an antiferromagnet) would be another possible anisotropic arrangement. For the anisotropic arrangements light passing along the c - axis will be doubly refracted.

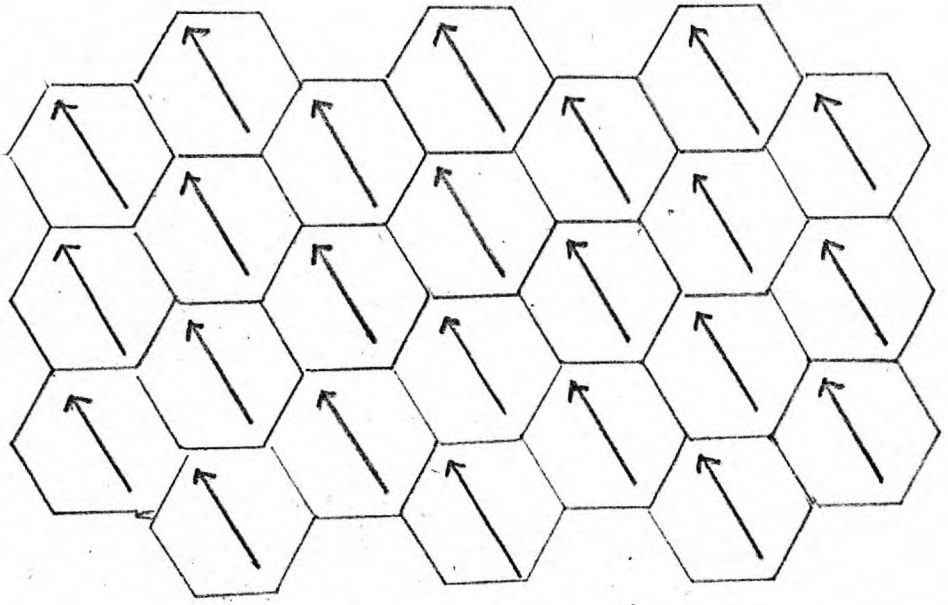
In Figure 5.1 b) the guest molecules are arranged in cyclic closed systems and this type of arrangement yields an isotropic section and so light passing along the crystal c - axis will not be doubly refracted.

Similar guest molecule arrangements may be envisaged for the thiourea - cycloalkane adducts.

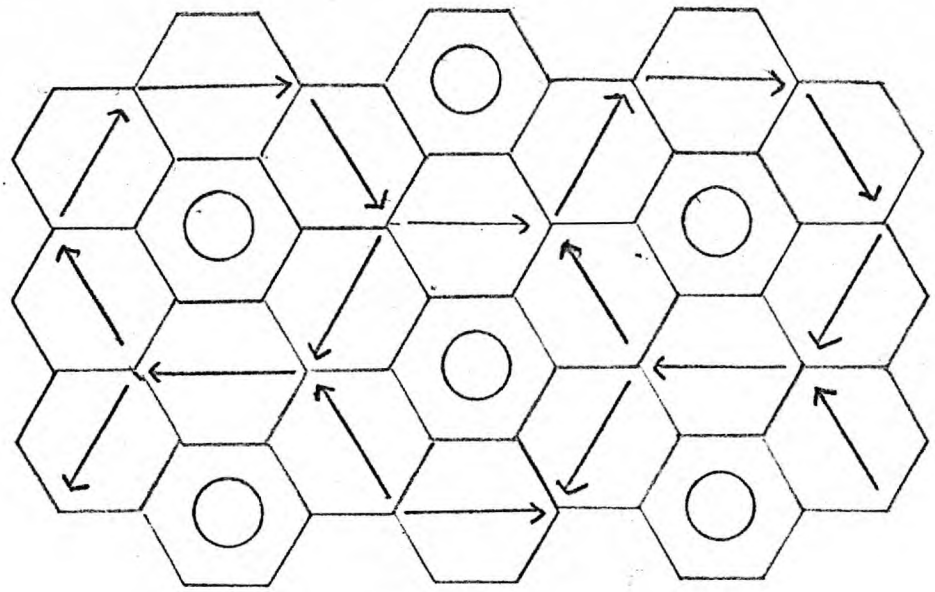
If the guest molecules of the urea or thiourea adducts undergo a transition on cooling from a rotating (isotropic) phase to an anisotropic phase then light passing along the crystal c - axis will change from being singly refracted to doubly refracted and optical birefringence will be observed below the transition temperature.

FIGURE 5.1.

ORDERED ARRANGEMENTS OF THE GUEST MOLECULES IN THE UREA HOST LATTICE. (PROJECTIONS ALONG THE 'C' AXIS)



a) Anisotropic Arrangement.



b) Isotropic Arrangement.

◯ = guest molecule with no preferred orientation.

However if the guest molecules go from the rotating phase to an isotropic ordered arrangement (as in Figure 5.1 b)) no optical birefringence will be observed.

The optical observation of polymorphous phase transitions was first achieved by Koptsik, Strukov and Nevedomskaya (1960). They measured the variation of optical birefringence with temperature for crystal sections of ammonium sulphate and ammonium fluoberyllate of unspecified thickness cut perpendicular to their ferroclectric axes. For these measurements they used a polarising microscope fitted with a thermostatic stage cooled with liquid nitrogen and a Berek Compensator. They found for both compounds that the optical birefringence changed sharply at the ferroclectric-paraelectric phase transition temperature.

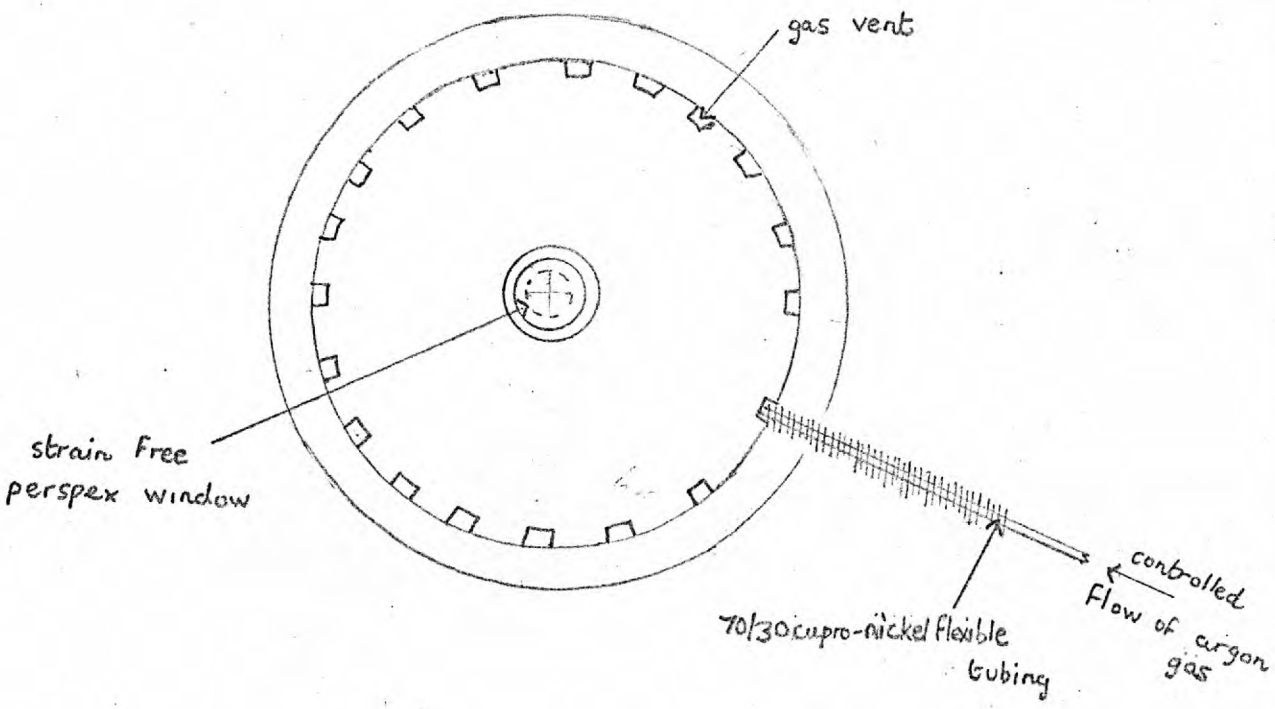
In the present work the variation of optical birefringence with temperature was studied using a polarising microscope with a miniaturised Joule-Thompson rapid-cooling cryostat as the cold stage.

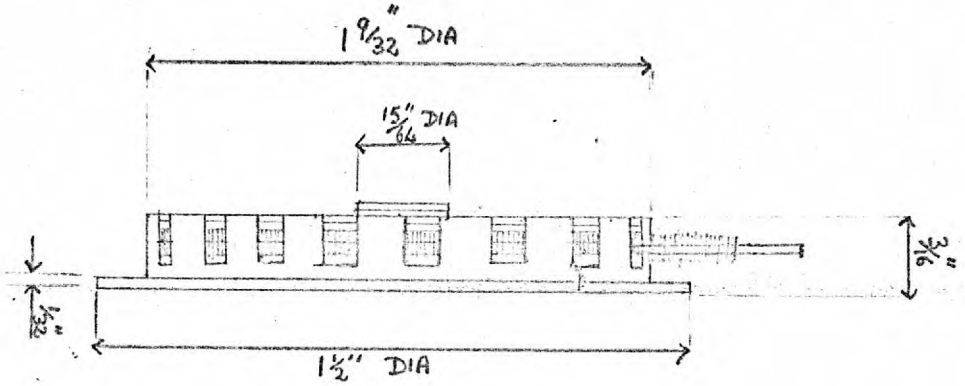
(ii) The apparatus

(a) The Joule-Thompson Cryostat.

The cryostat used was an 'Emicooler' rapid cooling cryostat (see Figure 5.2) ~~was~~ made by E.M.I. Electonics Limited. The gas passed through the cryostat was argon. With this gas liquid argon (bp -185·9°C) was produced by the

FIGURE 5.2. THE 'EMICOOLER' CRYOSTAT.





The system for regulating the pressure supplied to the Emicooler and purifying the argon gas is shown in Figure 5.3. The tubing leading from the argon cylinder and the tubing leading to the Emicooler was 3/8"o.d./3/16"i.d. cupro-nickel, used here because of its high flexibility. All other tubing in the system was 5/16"o.d./1/8"i.d. stainless steel (Tubesales Ltd.). All couplings and adoptors from the tubing were stainless steel 'Ermeto' couplings (British Ermeto Corporation Limited). Steel adaptors from the Ermeto couplings to the molecular sieve container and the pressure gauges were made by Industrial Hydraulics Limited.

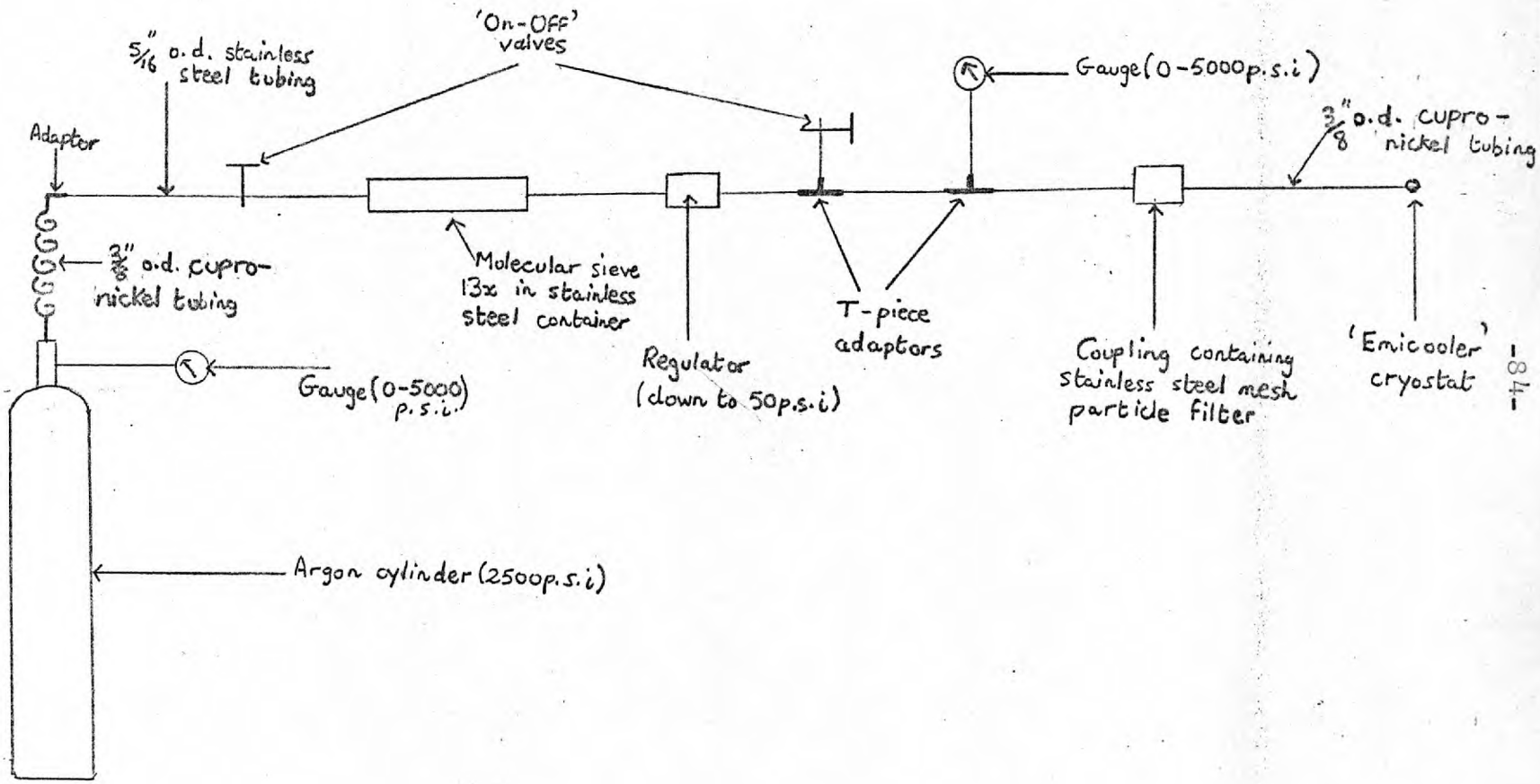
The regulator (Hymatic Limited) enabled variation of the pressure on the low pressure side from 50 p.s.i. to full gas cylinder pressure (about 2500 p.s.i.). Pressure gauges (Budenberg United) read from 0 to 5000 p.s.i. The stainless steel molecular sieve container was machined in the Chemistry Department Workshop, Imperial College.

All components in the system were designed to have a minimum burst pressure at least six times the maximum working pressure (2500 p.s.i.).

(b) The optical system.

A Zeiss polarising microscope (type 110A) with a mechanical stage and incorporating a Bertand lens was used to study the crystal sections. To determine the optical birefringence quantitatively a Berek compensator was

FIGURE 5.3. THE JOULE-THOMPSON CRYOSTAT SYSTEM



available.

The Emicooler fitted on to the mechanical stage and its perspex window showed no strain through crossed polars. However when the Emicooler was working water vapour condensed and froze on the window. To avoid this a box of perspex was constructed with a hole for the microscope lens. The microscope lens was surrounded by polyurethane foam to make a reasonably airtight fit with the perspex box when in position. With this arrangement the argon gas from the Emicooler purged the box and prevented any water vapour condensing.

To determine the temperature variation of the optical properties of a crystal section it was necessary to know the temperature of the clear perspex window at the centre of the Emicooler. However any temperature measuring device on this window would block the light passing though the microscope and make microscopic investigation of crystal sections impossible.

This difficulty was overcome by securing a copper-constantan thermocouple near the window (but not over it) with a little plasticine. Liquids of known freezing point were then viewed between crossed polars. The liquids being isotropic do not exhibit double refraction and so no light is transmitted. On freezing small anisotropic crystals are formed which give birefringence. The e.m.f. of the thermocouple at this point was measured. The e.m.f.

at which birefringence ceased on warming the crystals was also noted and the average value of the two e.m.f.s was taken to be the literature melting point of the substance. Each time the thermocouple was removed and resecured to the Emicooler recalibration was necessary. One such calibration is shown in Figure 5.4.

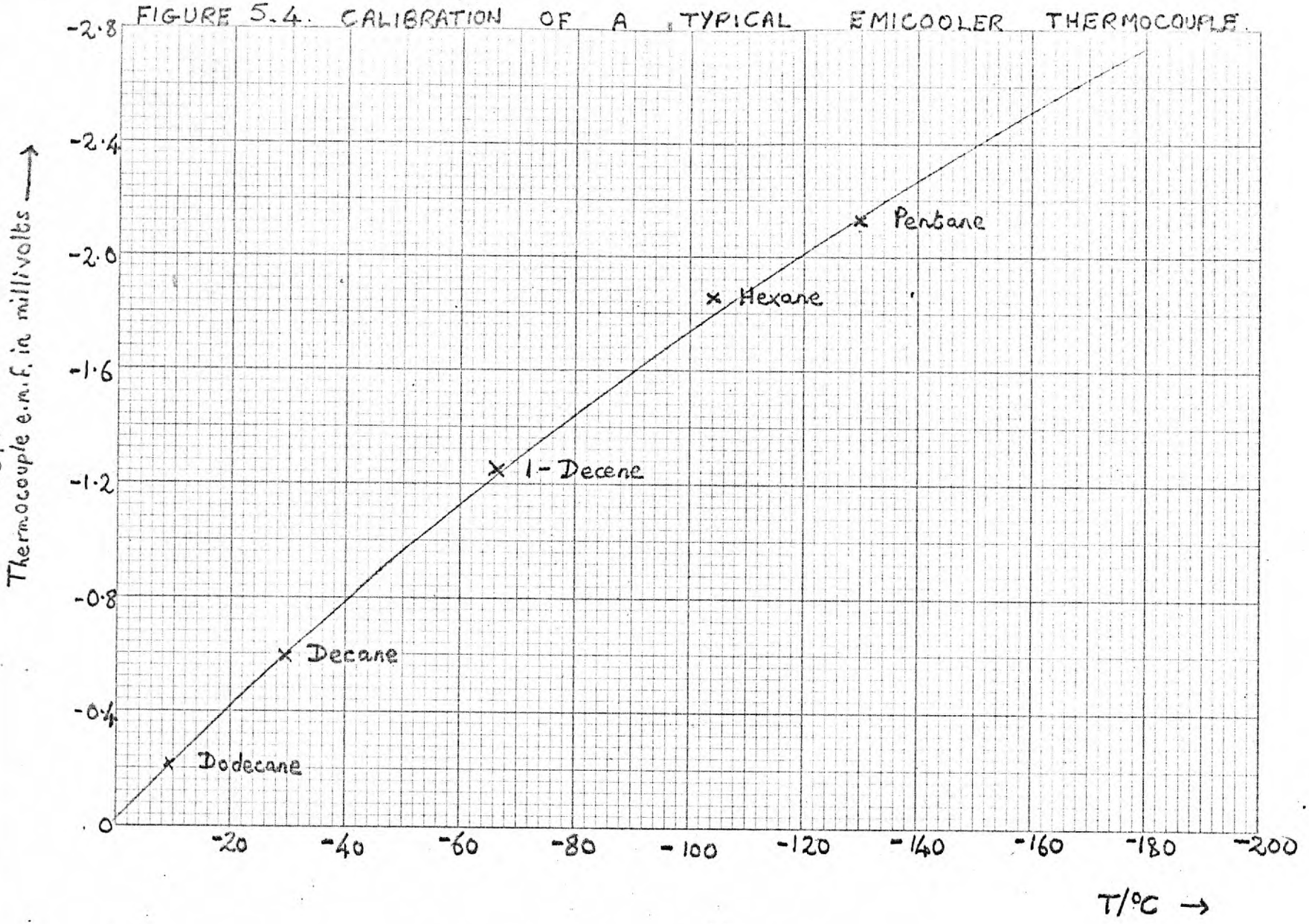
(iii) Birefringence measurements of ammonium sulphate crystal sections

In order to test the optical arrangement and determine the accuracy of the thermocouple calibrations the variation of optical birefringence of ammonium sulphate crystals was measured and the results compared with those of Koptsik et al (1960).

Single crystals of ammonium sulphate measuring 30mm x 10mm x 4mm were grown from a saturated solution by evaporation at constant temperature over several days. Sections of about 100 microns thickness were then cut perpendicular to the 'c' axis using a razor blade. These sections were then viewed at various temperatures.

Although the section thicknesses were not accurately determined so that quantitative birefringence comparison with Koptsik was not possible, qualitatively the crystal sections showed identical behaviour to Koptsik's sections. The optical path difference decreased slowly down to about $-48^{o}C$ where it suddenly increased sharply corresponding to a paraelectric-ferroelectric first order transition.

FIGURE 5.4. CALIBRATION OF A TYPICAL EMICOOLER THERMOCOUPLE.



(iv) Preparation of adduct crystal sections

In the introduction to this chapter it was demonstrated that any guest molecule 'order-disorder' transition would be exhibited most clearly in birefringence studies by viewing polarised light passing along the c-axis of the host lattice. This is because in this direction the host lattice will make no birefringence contribution. Thus crystal sections cut perpendicular to the c-axis should be viewed and to obtain first order interference colours these sections should be less than 100 microns thick. However as Smith (1952) notes the urea adduct crystals will cleave readily along the a c plane but will fracture if cleavage is attempted in any other direction. It is apparent from Figure 1.1 that only the a c plane passes through no urea molecules and that cleavage along this plane involves only the breaking of four hydrogen bonds per unit cell.

To cut crystal sections perpendicular to the c-axis it was obvious that the crystal must be supported in an inert matrix to try and avoid crystal fracture. This was effected by placing a crystal in a small gelatin capsule and immersing it in butyl methacrylate (containing a little α-α'-azo-bis-isobutyronitrile initiator). The capsule was then irradiated with ultraviolet light for about a day. The methacrylate polymerised to give a fairly hard non-brittle perspex which could be pared down with a

razor blade to the region containing the crystal. This sample was then cut into parallel faced sections perpendicular to the crystal c-axis of about 60 microns thickness using a microtome with a razor blade cutting edge.

Although urea is insoluble in butyl methacrylate the guest molecules are significantly soluble in it and while it is likely that the guest molecules would be only very slowly removed from the urea channels it was thought possible that the urea adducts would be destroyed during the polymerisation. For this reason crystal sections were also cut from polymer-crystal samples where the adduct crystals had not been added until the methacrylate had polymerised to form a very viscous liquid.

Very thin adduct crystal sections (less than 50 microns) were also cut along the a c cleavage plane using a razor blade.

v) Birefringence studies on urea adduct crystal sections.

The crystal sections supported in perspex were viewed between crossed polars at room temperature. Many of the crystal cuts transmitted light in some regions and not in others suggesting that the crystal was very strained or had fractured. Some sections transmitted no light however and in these cases the temperature of the emicooler was lowered slowly to liquid argon temperature whilst the crystal sections were studied for any changes in birefringent properties. No changes were observed for any of the crystal sections studied.

The crystal sections cleaved along the a c plane were also observed between crossed polars. These sections were highly birefringent at room temperature (due to the urea lattice contribution). No changes in birefringence properties were found on lowering the temperature.

It was thought that reflection from the top crystal section surface might be obscuring any changes in crystal optical properties and to reduce this reflection a suitable immersion fluid was sought. Such a fluid must be immiscible with both urea and the guest component and have a very low freezing point. The compound whose properties most closely matched those required was 'fluorolube', a fluorocarbon (I.C.I. Ltd.). In this fluid urea is completely insoluble and long chain hydrocarbons are miscible only to a very limited extent. Fluorolube freezes at about -30°C. So fluorolube was tested as an immersion fluid. However

no change in birefringent properties was observed for either the crystal sections supported in perspex or the a c plane sections.

It must be concluded that these measurements give no definite information about the ordering of the guest molecules in the urea channels. No real improvement in this system will be achieved unless a more satisfactory method of sectioning the urea adducts perpendicular to to their optic axis is found. 'Ion beam machining',used in electron microscopy to obtain very thin crystal sections, might be employed to get strain-free urea adduct sections if the section temperature could be kept low enough.

CHAPTER 6

Thermodynamic Properties of some Urea-hydrocarbon Adducts

(i) Differential Thermal Analysis Measurements on some Urea-n-Alkane Adducts

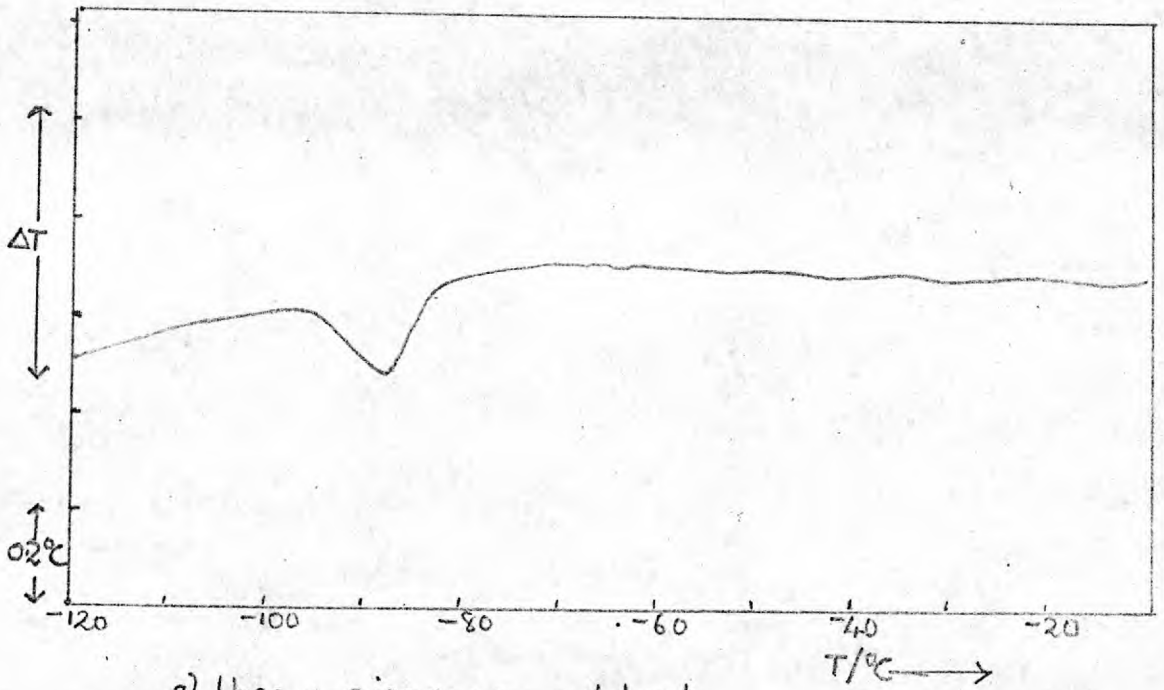
Differential thermal analysis (D.T.A.) is a very convenient method of determining the temperatures at which major anomalies in the heat capacity of a compound occur. The technique consists of comparing the rate of temperature rise of a sample of the compound with that of a standard substance on subjecting both to a very similar rate of heat input. It is important to note that D.T.A. involves taking non-equilibrium measurements and thus may confuse kinetic and thermodynamic effects. However it was decided that D.T.A. would afford a simple method of determining the transition temperatures of various even urea-n-alkane adducts. These could then be compared with the transition temperatures of the four even n-alkane adducts studied by calorimetric methods (Pemberton and Parsonage, 1965).

The instrument used for this study was a Dupont 900 Differential Thermal Analyser kindly made available by Dr. J. A. Barrie. The adduct sample crystals were crushed so that they could be introduced into the capillary tubes which fit into the heating block of the analyser. Silica was used as the standard substance and a heating rate was $2^{o}C$/minute in all cases. The accuracy of the method was

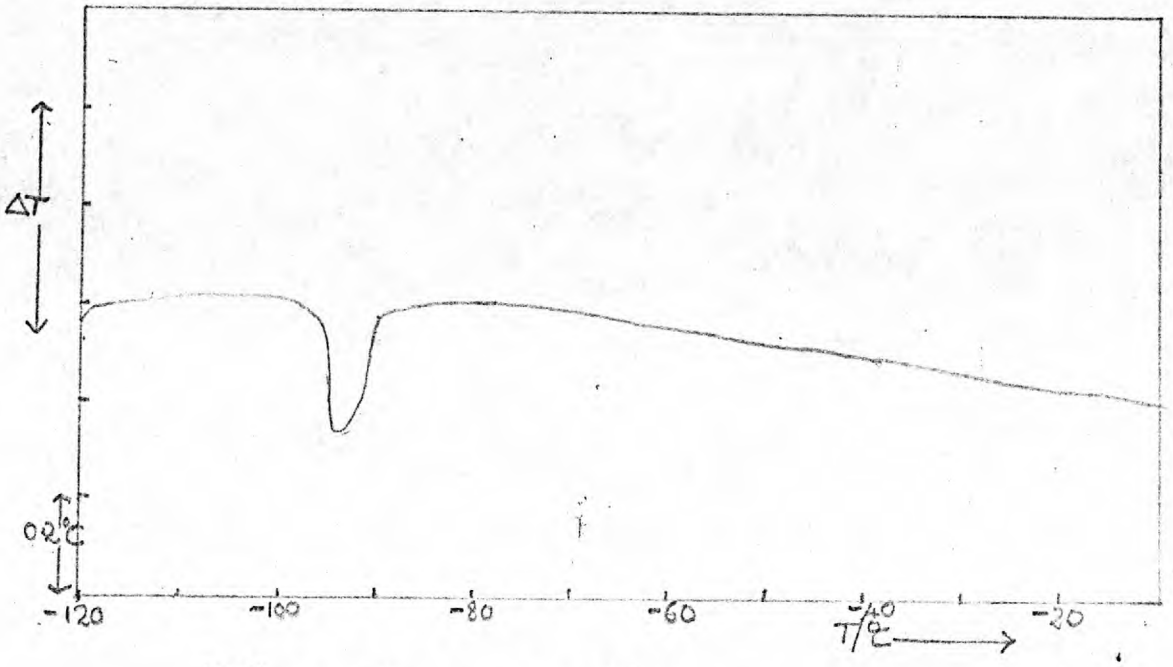
tested by employing urea-n-eicosane (whose transition temperature was known accurately from calorimetric measurements) as a sample. The D.T.A. plot for this adduct is shown in Figure 6.1 a. The temperature of the anomaly agrees with the calorimetric value to within a degree. The urea-eicosane D.T.A. anomaly occurs over a wider temperature range than any of the other paraffin adducts studied (again in agreement with calorimetric results). A more typical D.T.A. anomaly is shown for the urea-tetracosane adduct in Figure 6.1 b.

The transition temperatures determined by D.T.A. measurements together with those determined by calori etry are plotted against hydrocarbon chain length in Figure 6.2. Also plotted are the results of Ising-Weiss model calculations for four urea-n-alkane adducts (Parsonage and Pemberton, 1967). While most of the experimental points lie near a smooth curve, the urea-eicosane adduct has an unusually high transition temperature. The D.T.A. measurements show that the Ising-Weiss calculation points lie on a curve of shape similar to the experimentally determined curve.

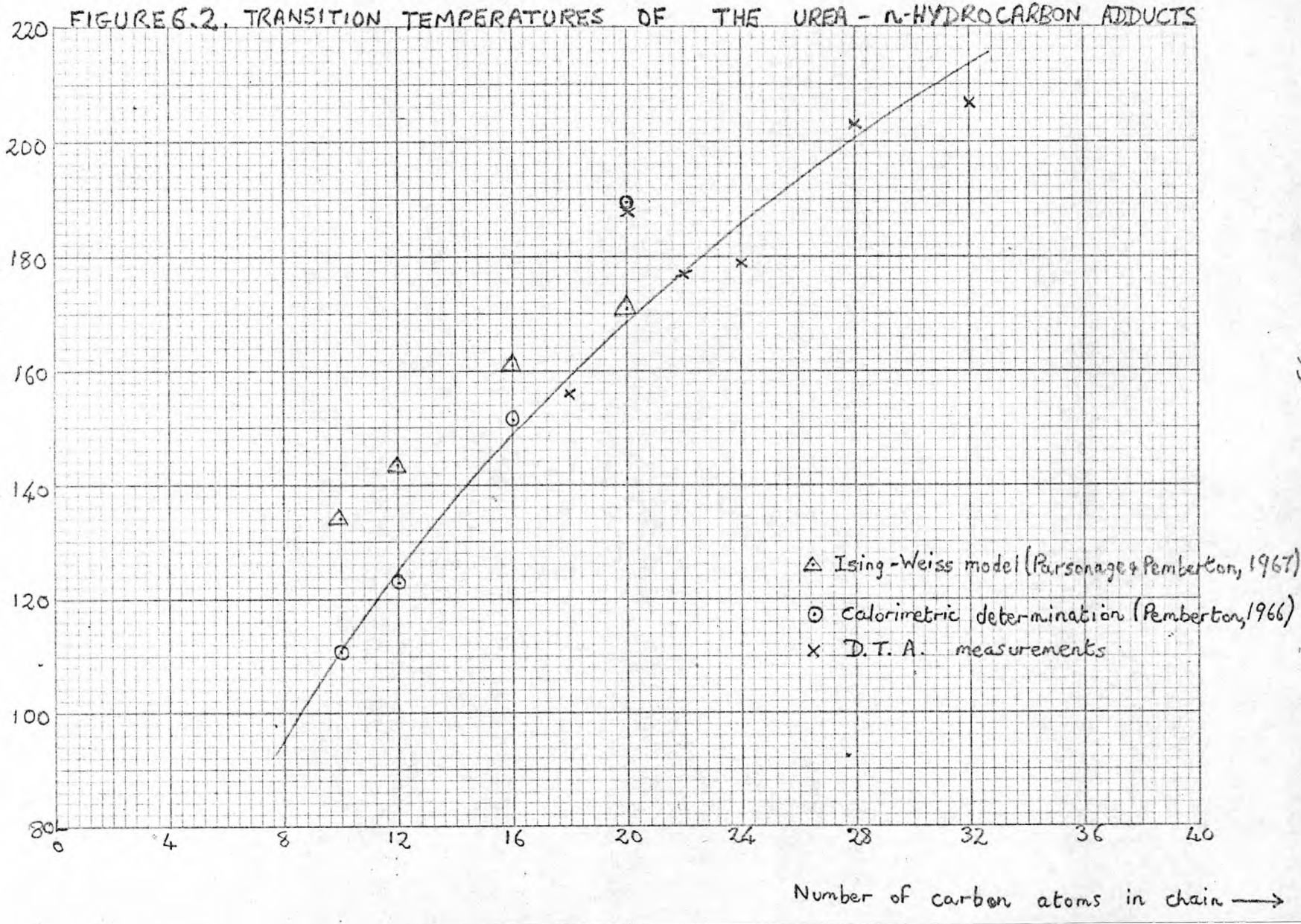
FIGURE 6.1 DIFFERENTIAL THERMAL ANALYSES OF UREA - n - ALKANES



a) Urea - eicosane adduct.



b) Urea - tetracosane adduct.


FIGURE 6.2. TRANSITION TEMPERATURES OF THE UREA - n-HYDROCARBON ADDUCTS
T/K →
220
200
180
160
140
120
100
80
0
4
8
12
16
20
24
28
32
36
40
Number of carbon atoms in chain →
△ Ising-Weiss model (Parsonage & Pemberton, 1967)
⊙ Calorimetric determination (Pemberton, 1966)
× D.T.A. measurements

(ii) Experimental Determination of the Heat Capacities of some Urea-1-Alkene Adducts

The heat capacity of the urea adducts were measured by the method described in Chapter 3. The experimental results for the heat capacity of urea-1-dodecene, urea-1-tetradecene and urea-1-octadecene are presented in Tables 6.2 to 6.4 respectively. ΔT values in these tables refer to the temperature ranges over which the heat capacity measurements were taken. Cp/mole values refer to heat capacity of the adduct in Absolute Joules per Degree-Kelvin per Mole of Urea (1 mole of urea = 60.058g). These heat capacity points were plotted against temperature using a large scale and a smooth curve of best fit drawn between the points. From these graphs smoothed heat capacity values were read at 5K intervals and these points are tabulated in Table 6.5. Small scale graphs of heat capacity versus temperature for the three adducts are shown in Figure 6.3. to 6.5.

A measure of the precision of the experimental results is given by the percentage root mean square deviation of the points from the smooth curve. The percentage root mean square deviations for the three adducts are tabulated below in Table 6.1.

Table 6.1	Temperature Range		
Adduct	12-25K	25-80K	80-300K
urea-1-dodecene	0.76	0.26	0.16
urea-1-tetradecene	0.80	0.34	0.17
urea-1-octadecene	0.69	0.22	0.11

In Table 6.6 the adduct entopies determined at 10K intervals by graphical integration under a large scale plot of Cp/T against T are listed. For this the adduct heat capacities below 12K had to be estimated. The heat capacities of urea adducts below 12K have been estimated in previous work (Pemberton and Parsonage, 1965 and Cope and Parsonage, 1969) using a modified Debye relations (Ahlbery, Blanchard and Lundberg, 1937). However it was found that the entropy difference for the Debye extrapolation and a curve drawn by eye between the lowest heat capacity measurements and zero heat capacity at zero degrees Kelvin was negligible. Hence for the compounds studied in this thesis the latter procedure was adopted.

TABLE 6.2

EXPERIMENTAL VALUES OF THE HEAT CAPACITY OF UREA-1-DODECENE

Wt. of sample in calorimeter = 12.0154g (9.2639g of urea + 2.7515g of 1-dodecene)
Heat capacity of sample, Cp, in Joules K^{-1}
Heat capacity per mole of urea, Cp/mole, in Joules K^{-1} $mole^{-1}$

Run No.	T/K	ΔT	Cp	Cp/mole
1	156.00	3.41	11.560	74.944
2	159.58	3.80	11.762	76.253
3	163.33	3.75	11.915	77.245
4	167.03	3.71	12.094	78.408
5	170.67	3.66	12.388	80.312
6	174.29	3.64	12.465	80.814
7	177.89	3.61	12.680	82.207
8	181.63	3.90	12.878	83.488
9	185.52	3.92	13.061	84.676
10	189.39	3.88	13.321	86.362
11	194.12	4.59	13.541	87.787
12	199.03	5.29	13.788	89.391
13	204.43	5.59	14.126	91.579
14	210.11	5.88	14.461	93.751
15	216.07	6.16	14.810	96.014
16	222.05	5.95	15.143	98.173
17	227.25	5.15	15.435	100.07
18	232.66	5.81	15.737	102.02
19	238.71	6.46	16.025	103.89
20	244.41	5.12	16.260	105.42
21	247.72	4.59	16.582	107.50
22	252.43	4.74	16.765	108.69
23	257.15	4.90	17.050	110.54
24	262.36	5.66	17.330	112.35
25	268.09	5.99	17.630	114.30
26	274.13	6.29	18.104	117.37
27	280.40	6.49	18.572	120.40
28	286.72	6.42	18.376	122.11
29	293.17	6.64	19.229	134.66
30	299.52	6.56	19.618	127.58
31	305.96	6.48	19.969	129.46
32	79.86	3.77	7.729	50.108
33	84.17	4.85	8.119	52.635
34	88.95	4.73	8.077	52.363
35	93.57	4.56	8.362	54.212
36	98.16	4.66	8.549	55.425
37	102.85	4.76	8.842	57.325

TABLE 62 (continued)

Run No.	Temp/K	ΔT	Cp	Cp/mole
38	107.53	4.64	9.020	58.476
39	112.09	4.52	9.269	60.091
40	116.61	4.56	9.544	61.873
41	121.32	4.85	9.712	62.965
42	126.18	4.94	9.941	64.450
43	131.14	5.03	10.258	66.505
44	135.70	5.12	10.566	68.500
45	140.74	5.01	10.741	69.634
46	145.79	5.13	10.998	71.300
47	150.96	5.25	11.290	73.195
48	156.14	5.16	11.571	75.015
49	161.23	5.08	11.798	76.488
50	166.24	5.00	12.080	78.316
51	171.16	4.93	12.306	79.781
52	176.02	4.86	12.561	81.433
P1	50.80	3.29	4.807	31.162
P2	54.19	3.53	5.189	33.639
P3	57.92	3.94	5.572	36.125
P4	62.02	4.29	5.992	38.848
P5	66.46	4.65	6.422	41.635
P6	70.96	4.36	6.787	43.999
P7	75.18	4.13	7.178	46.534
P8	79.35	4.27	7.763	50.329
P9	83.51	4.07	8.239	53.413
H1	11.12	1.03	0.308	2.000
H2	12.24	1.15	0.381	2.469
H3	13.67	2.00	0.509	3.301
H4	15.63	2.39	0.693	4.494
H5	18.87	4.49	0.945	6.125
H6	22.49	3.00	1.355	8.786
H7	25.46	2.97	1.647	10.678
H8	28.38	2.87	1.993	12.920
H9	31.21	2.82	2.316	15.016
H10	34.05	2.95	2.699	17.497
H11	37.01	3.00	3.110	20.163
H12	40.31	3.61	3.515	22.786
H13	44.70	5.21	4.062	26.334
H14	49.54	4.49	4.668	30.263
H15	53.79	4.03	5.152	33.409
T1	74.16	1.95	7.047	45.685
T2	76.08	1.90	7.265	47.099
T3	77.77	1.50	7.358	47.702
T4	79.24	1.46	7.642	49.543
T5	80.67	1.42	8.074	52.346
T6	81.98	1.21	8.505	55.137

TABLE 6.2 (continued)

Run No.	Temp/K	ΔT	Cp	Cp/mole
T7	83.11	1.04	8.262	53.564
T8	84.24	1.23	8.126	52.647
T9	85.55	1.38	8.151	52.840
T10	87.09	1.72	8.000	51.869
T11	89.13	2.37	8.153	52.856
T12	91.48	2.33	8.246	53.459
T13	93.78	2.30	8.359	54.191

TABLE 6.3

EXPERIMENTAL VALUES OF THE HEAT CAPACITY OF UREA-1-TETRADECENE

Wt. of sample in calorimeter = 18.2869 g (13.7079 g urea + 4.5790 g 1-tetradecene)
Heat capacity of sample, Cp, in Joules K^{-1}
Heat capacity per mole of urea, Cp/mole, in Joules K^{-1} $mole^{-1}$

Run No.	Temp/K	ΔT	Cp	Cp/mole
1	194.73	5.58	20.420	89.478
2	200.43	5.86	20.996	92.002
3	206.21	5.76	21.573	94.531
4	211.59	6.05	22.097	96.827
5	217.52	5.87	23.042	100.97
6	223.34	5.83	23.234	101.81
7	229.09	5.76	23.626	103.53
8	234.95	6.02	24.236	106.20
9	240.86	5.89	25.084	109.92
10	246.79	6.06	26.389	115.63
11	252.70	5.84	30.599	134.08
12	258.37	5.56	32.451	142.20
13	264.57	6.89	26.595	116.54
14	271.34	6.79	27.106	118.78
15	278.37	7.25	27.729	121.51
16	285.61	7.22	28.399	124.44
17	292.73	7.15	28.939	126.808
18	299.72	7.04	29.622	129.801
19	95.18	3.87	12.737	55.812
20	99.22	4.21	13.125	57.512
21	103.38	4.55	13.489	59.107
22	107.70	4.55	13.762	60.304
23	112.19	4.45	14.081	61.701
24	116.57	4.32	14.409	63.139
25	121.03	4.62	14.775	64.743
26	125.61	4.53	15.063	66.443
27	129.99	4.25	15.355	67.284
28	134.17	4.15	15.767	69.089
29	138.47	4.45	16.120	70.636
30	142.97	4.55	16.363	71.701
31	146.74	4.27	16.681	73.094
32	151.13	4.54	17.070	74.799
33	155.71	4.60	17.631	77.257
34	160.36	4.70	18.048	79.085
35	165.11	4.83	18.230	79.805
36	169.66	4.78	18.413	80.684
37	174.50	4.88	18.914	82.879

TABLE 6.3 (continued)

Run No.	Temp/K	ΔT	Cp	Cp/mole
38	179.51	5.00	19.162	83.966
39	184.67	5.33	19.596	85.868
40	189.94	5.26	20.014	87.699
P1	55.59	3.27	8.023	35.156
P2	58.76	3.07	8.441	36.988
P3	62.24	3.85	8.958	39.253
P4	66.18	4.04	9.516	41.698
P5	70.26	4.06	10.016	43.889
P6	74.64	4.68	10.591	46.409
P7	79.41	4.84	11.302	49.524
P8	84.15	4.60	11.950	52.364
P9	89.29	5.65	12.234	53.608
H1	14.36	1.50	0.738	3.234
H2	16.71	2.32	1.061	4.649
H3	19.11	2.52	1.403	6.148
H4	22.81	4.82	1.903	8.339
H5	26.76	3.34	2.710	11.875
H6	30.49	4.08	3.306	14.487
H7	34.51	3.91	4.059	17.786
H8	38.63	4.34	4.889	21.423
H9	43.67	5.75	5.775	25.305
H10	48.96	4.86	6.739	29.530
H11	53.34	3.90	7.573	33.184
T1	245.65	2.51	25.524	111.84
T2	248.03	2.37	26.534	116.27
T3	250.33	2.30	27.863	122.09
T4	252.56	2.20	29.473	129.15
T5	254.64	2.03	34.228	149.98
T6	256.51	1.77	41.942	183.79
T7	258.52	2.31	27.209	119.227
T8	260.80	2.37	26.303	115.26
T9	263.13	2.38	25.949	113.71

TABLE 6.4

EXPERIMENTAL VALUES OF THE HEAT CAPACITY OF UREA-1-OCTADECENE

Wt. of sample in calorimeter = 20.3782 g (15.3244 g of urea + 5.0538 g of 1-octadecene)
Heat capacity of sample, Cp, in Joules K^{-1}
Heat capacity per mole of urea, Cp/mole in Joules K^{-1} $mole^{-1}$

Run No.	Temp/K	ΔT	Cp	Cp/mole
1	121.15	3.90	16.360	64.115
2	125.18	4.15	16.746	65.628
3	129.28	4.06	17.118	67.085
4	133.46	4.30	17.577	68.884
5	137.85	4.50	18.012	70.589
6	142.29	4.40	18.567	72.764
7	146.72	4.45	19.094	74.829
8	151.09	4.30	19.877	77.898
9	155.10	3.73	26.051	102.09
10	158.83	4.21	20.644	80.904
11	163.06	4.23	20.158	78.999
12	167.27	4.19	20.471	80.226
13	171.58	4.42	20.783	81.449
14	175.96	4.36	21.133	82.820
15	180.44	4.62	21.492	84.227
16	185.01	4.56	21.854	85.646
17	189.56	4.56	22.326	87.496
18	194.21	4.75	22.906	89.769
19	198.03	4.63	22.948	89.933
20	202.80	4.72	23.531	92.218
21	207.59	4.77	23.851	93.472
22	212.31	4.70	24.338	95.381
23	216.94	4.64	24.882	97.513
24	221.56	4.59	25.175	98.661
25	226.19	4.50	25.647	100.51
26	230.84	4.65	26.115	102.34
27	235.61	4.92	26.626	104.35
28	232.61	5.26	26.270	102.95
29	237.80	5.16	26.977	105.72
30	242.92	5.10	27.338	107.14
31	245.13	5.07	27.526	107.87
32	250.47	5.64	27.998	109.72
33	256.05	5.58	28.401	111.30
34	261.55	5.49	28.965	113.51
35	267.14	5.73	29.470	115.49
36	272.94	5.94	29.931	117.30
37	278.92	6.09	30.585	119.86

TABLE 6.4 (continued)

Run No.	Temp/K	ΔT	Cp	Cp/mole
38	285.53	7.20	31.239	122.43
39	292.64	7.10	31.981	125.33
40	299.05	7.04	32.580	127.68
P1	59.42	2.82	9.541	37.391
P2	62.66	3.61	10.094	39.558
P3	66.19	3.42	10.564	41.400
P4	69.87	3.96	10.785	42.266
P5	73.98	4.28	11.279	44.202
P6	78.15	4.08	11.824	46.338
P7	82.21	4.03	12.376	48.502
P8	86.22	4.00	12.884	50.492
P9	90.23	4.00	13.332	52.248
P10	94.24	4.01	13.779	54.000
P11	98.33	4.17	14.144	55.430
P12	102.05	3.56	14.475	56.728
P13	105.57	3.48	14.868	58.268
P14	109.31	4.00	15.221	59.651
H1	14.10	2.15	0.803	3.147
H2	16.32	1.99	1.093	4.283
H3	19.05	2.30	1.469	5.757
H4	21.09	1.81	1.858	7.282
H5	23.10	2.22	2.183	8.555
H6	25.75	3.01	2.677	10.491
H7	28.98	3.36	3.300	12.933
H8	32.87	4.41	4.150	16.264
H9	37.08	4.01	5.052	19.799
H10	41.41	4.64	5.936	23.263
H11	45.74	4.01	6.805	26.668
H12	50.00	4.52	7.670	30.059
H13	54.30	4.07	8.502	33.319
H14	58.19	3.71	9.341	36.607
T1	149.02	2.00	19.384	75.966
T2	150.71	1.41	19.748	77.392
T3	152.05	1.26	19.964	78.239
T4	153.23	1.11	20.251	79.364
T5	154.20	0.82	20.728	81.233
T6	155.06	0.90	23.539	92.249
T7	155.84	0.67	37.785	148.08
T8	156.64	0.93	27.992	109.70
T9	157.67	1.10	20.570	80.614

TABLE 6.5

SMOOTHED VALUES OF THE HEAT

CAPACITIES OF UREA-1-ALKENE ADDUCTS

$0^{\circ}C = 273.15K$

HEAT CAPACITIES, C_p, PER MOLE OF UREA IN JOULES K^{-1} $MOLE^{-1}$

T/K	1-DODECENE	1-TETRADECENE	1-OCTADECENE
0	0.000	0.000	0.000
5	0.481	0.444	0.343
10	1.615	1.573	1.510
11	1.971	1.870	1.887
12	2.402	2.201	2.272
13	2.929	2.598	2.682
14	3.506	3.088	3.109
15	4.105	3.632	3.640
16	4.636	4.205	4.180
17	5.130	4.770	4.636
18	5.648	5.443	5.197
19	6.297	6.096	5.791
20	6.933	6.749	6.456
25	10.38	10.30	9.920
30	14.64	14.12	13.80
35	18.42	18.21	18.11
40	22.53	22.25	22.20
45	26.59	26.31	26.06
50	30.64	30.43	30.00
55	34.16	34.59	33.95
60	37.53	37.93	37.96
65	40.60	40.97	40.75
70	43.42	43.82	42.50
75	46.21	46.53	45.09
80	50.88	49.58	47.58
85	52.81	51.76	49.88
90	52.95	53.83	52.06
95	54.58	55.82	54.25
100	56.23	57.77	56.11
105	57.86	59.53	57.97
110	59.53	61.02	59.83
115	61.18	62.59	61.72
120	63.26	64.34	63.62
125	64.51	65.86	65.57
130	66.17	67.29	67.55
135	67.84	69.46	69.53

TABLE 6.5 (continued)

T/K	1-DODECENE	1-TETRADECENE	1-OCTADECENE
140	69.51	71.10	71.51
145	71.13	72.27	73.83
150	72.81	74.26	76.78
155	74.48	76.88	88.08
160	76.16	78.98	79.24
165	77.86	80.11	79.64
170	79.38	80.77	80.93
175	81.14	82.50	82.54
180	82.85	84.27	84.18
185	84.59	86.03	85.80
190	86.28	87.84	87.44
195	88.00	89.62	89.47
200	89.77	91.69	90.67
205	91.76	93.79	92.77
210	93.71	96.06	94.36
215	95.57	99.34	96.48
220	97.48	101.3	98.35
225	99.33	102.3	100.2
230	101.1	104.2	102.1
235	102.8	106.1	104.3
240	104.3	108.4	106.4
245	105.9	111.6	107.8
250	107.8	119.8	109.4
255	109.7	153.8	111.0
260	111.7	116.3	112.8
265	113.6	116.1	114.7
270	115.6	118.0	116.6
273.15	116.9	119.2	117.8
275	117.6	119.9	118.5
280	119.6	121.9	120.4
285	121.4	123.9	122.4
290	123.5	126.0	124.3
295	125.4	128.0	125.2
298.15	126.6	129.2	127.4
300	127.4	130.0	128.1

FIGURE 6.3 HEAT CAPACITY OF UREA-1-DODECENE

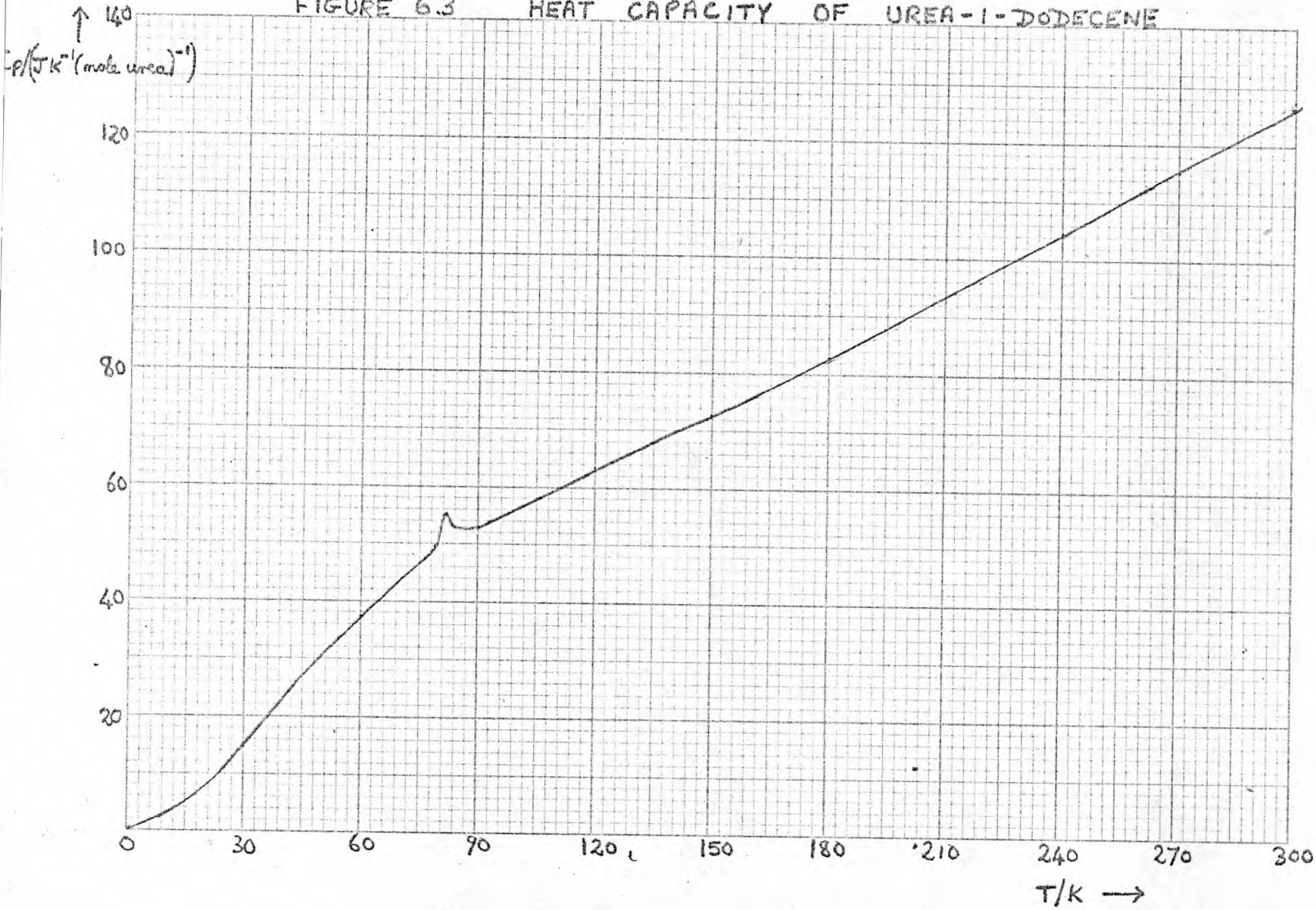


FIGURE 6.4 HEAT CAPACITY OF UREA – 1 – TETRADECENE

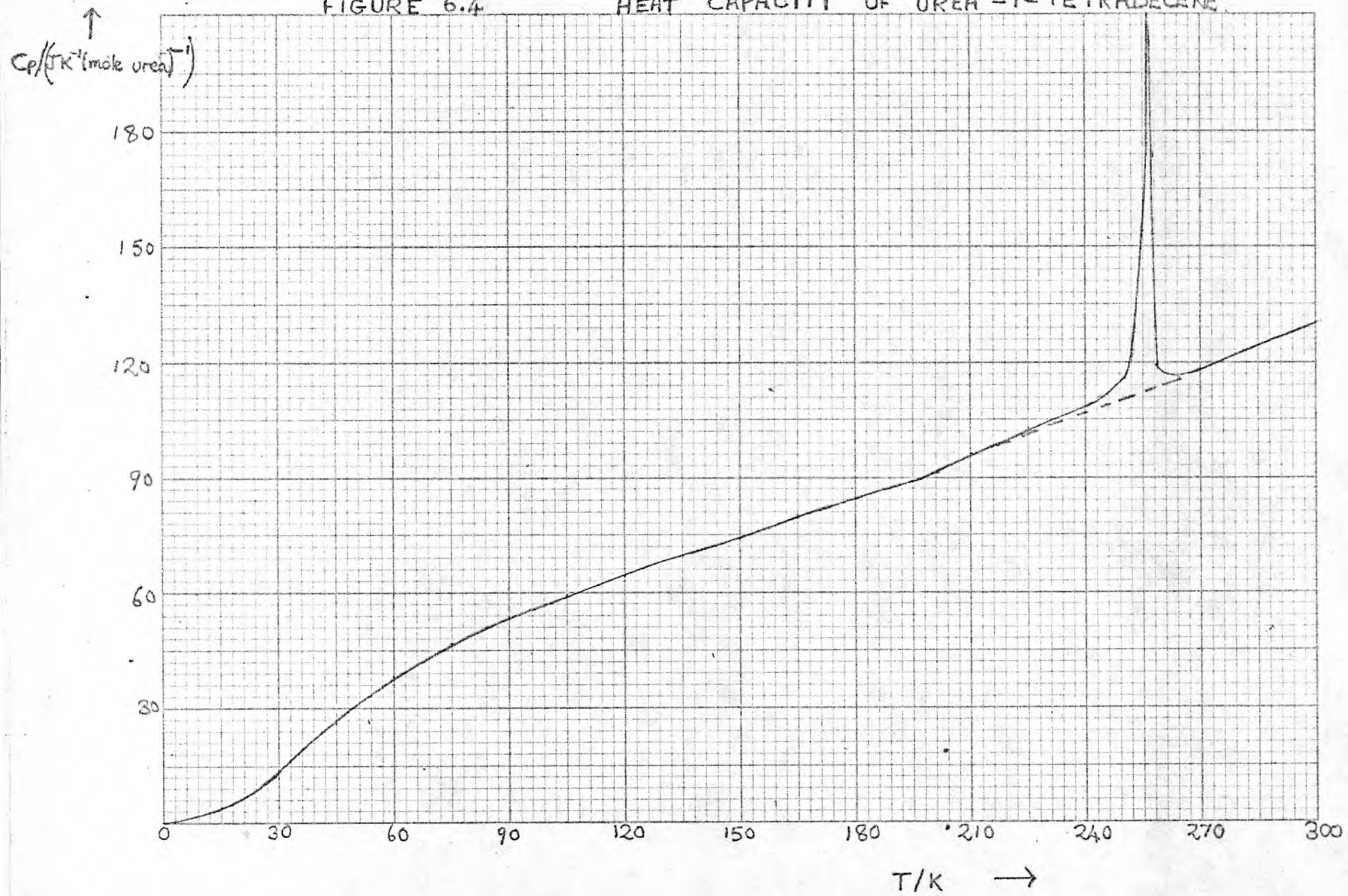


FIGURE 6.5 HEAT CAPACITY OF UREA-1-OCTADECENE.

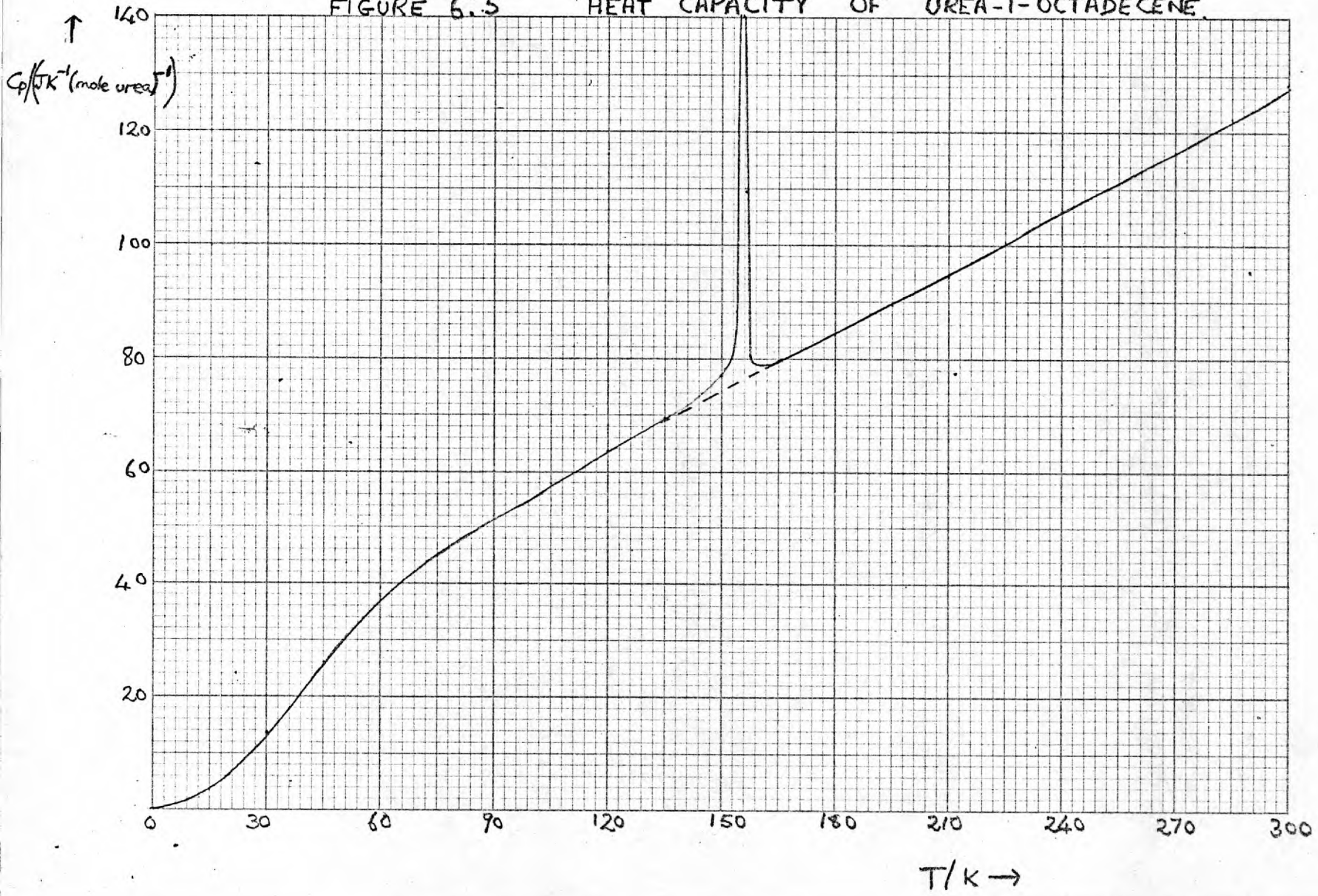


TABLE 6.6

THE ENTROPY $(S_T - S_o)$ OF UREA-1- ALKENE ADDUCTS IN JOULES K^{-1} (MOLE UREA)$^{-1}$

$0^oC = 273.15K$

T/K	1-DODECENE	1-TETRADECENE	1-OCTADECENE
0	0.00	0.00	0.00
10	0.83	0.74	0.75
20	3.45	3.19	3.14
30	7.63	7.28	7.09
40	12.89	12.46	12.22
50	18.80	18.32	18.01
60	25.00	24.59	24.19
70	31.25	30.89	30.44
80	37.45	37.11	36.46
90	43.73	43.20	42.33
100	49.48	49.07	48.03
110	54.99	54.74	53.55
120	60.33	60.19	58.91
130	65.50	65.45	64.15
140	70.53	70.59	69.31
150	75.44	75.58	74.41
160	80.24	80.52	80.14
170	84.95	85.38	84.97
180	89.59	90.10	89.91
190	94.17	94.75	94.34
200	98.68	99.35	98.91
210	103.2	103.9	103.4
220	107.6	108.5	107.9
230	112.0	113.1	112.4
240	116.4	117.6	116.8
250	120.7	122.2	121.2
260	125.0	128.5	125.6
270	129.3	132.9	129.9
273.15	130.7	134.3	131.3
280	133.6	137.2	134.2
290	137.8	141.6	138.5
298.15	141.3	145.1	142.0
300	142.1	145.9	142.8

The three adducts studied all showed a large region of anomalously high heat capacity. However the urea-1-dodecene major anomaly did not possess such a sharp peak as the other two adducts and appeared to occur over a much greater temperature range. The excess heats of the major anomalies in the urea-1-tetradecene and urea-1-octadecene adducts were determined by measuring graphically the area between the smooth heat capacity curve (see dotted lines in Figure 6.4 and 6.5) and the peaks. To determine the anomaly entropies the corresponding areas for the Cp/T versus T plot were measured. These quantities are listed together with the transition temperatures (the temperature at which the maximum value of heat capacity occurs) in Table 6.7.

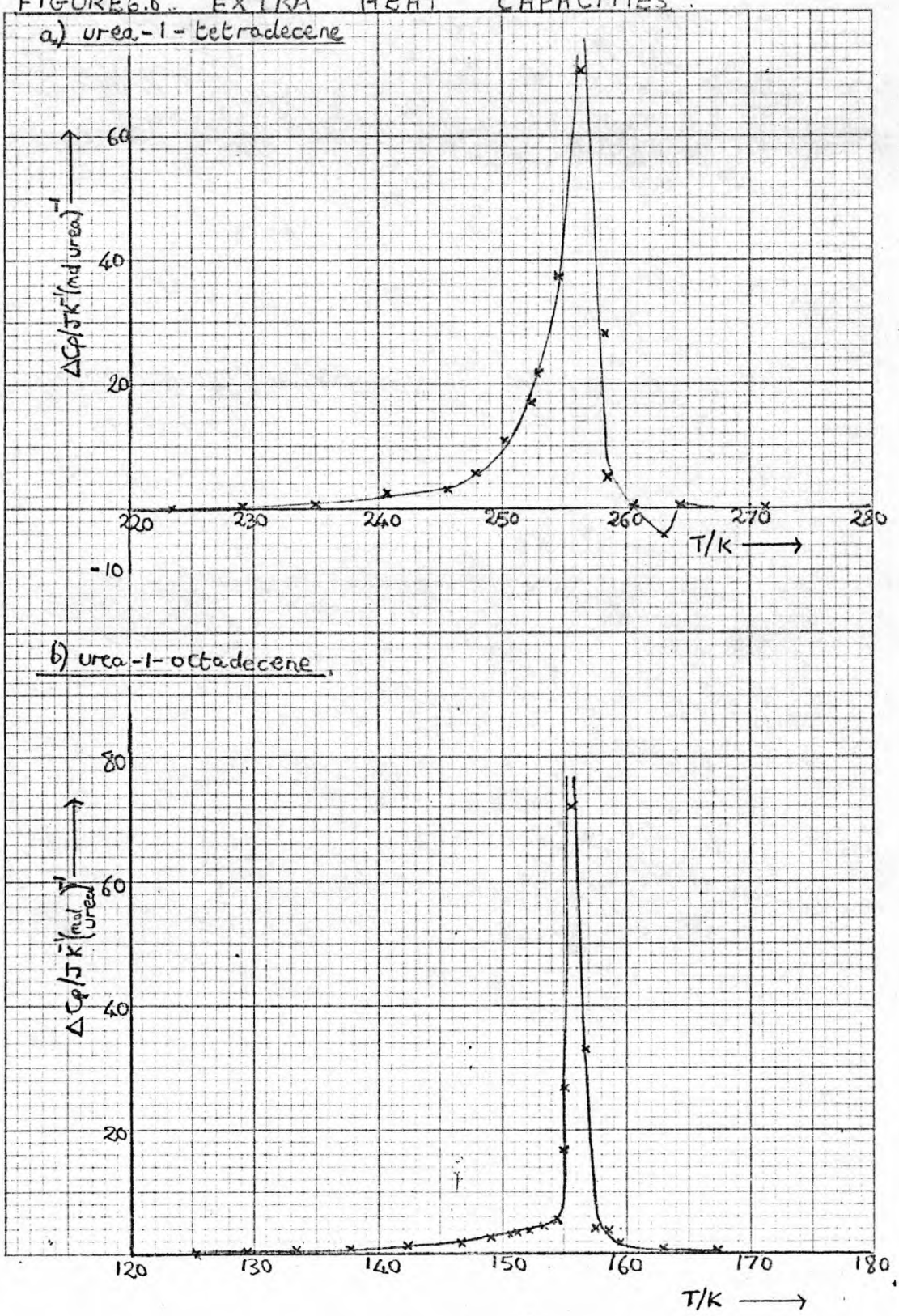
TABLE 6.7 Properties of the major anomalies in the heat capacities of urea-1-tetradecene and urea-1-octadecene

Adduct	1-tetradecene	1-octadecene
Transition Temp/K	256.6	155.9
Excess heat, Δ H/J (mole urea)$^{-1}$	370.4	151.2
Excess heat, ΔH/J (mole alkene)$^{-1}$	363.4	192.6
Excess entropy, ΔS/JK^{-1} (mole urea)$^{-1}$	1.22	1.00
Excess entropy, ΔS/JK^{-1} (mole alkene)$^{-1}$	12.0	12.7

In Figure 6.6 are plotted the 'extra' heat capacities (difference between actual heat capacity and the value expected in the absence of the transition) for urea-1-tetradecene and urea-1-octadecene.

The major anomaly in the heat capacity of 1-dodecene

FIGURE 6.6 'EXTRA' HEAT CAPACITIES.



adduct was spread over too great a temperature range to allow an accurate 'smooth heat capacity' baseline to be drawn. However Pemberton (1966) showed that the heat capacity of the urea-n alkane adducts excluding anomalous regions could be represented to about 1% by adding the component heat capacities in the correct ratio. Cope and Parsonage (1969) later used a similar method to determine the excess heat and entropy of the urea-1-decene adduct in which the anomalous region is exhibited as smooth humps over a very large temperature range.

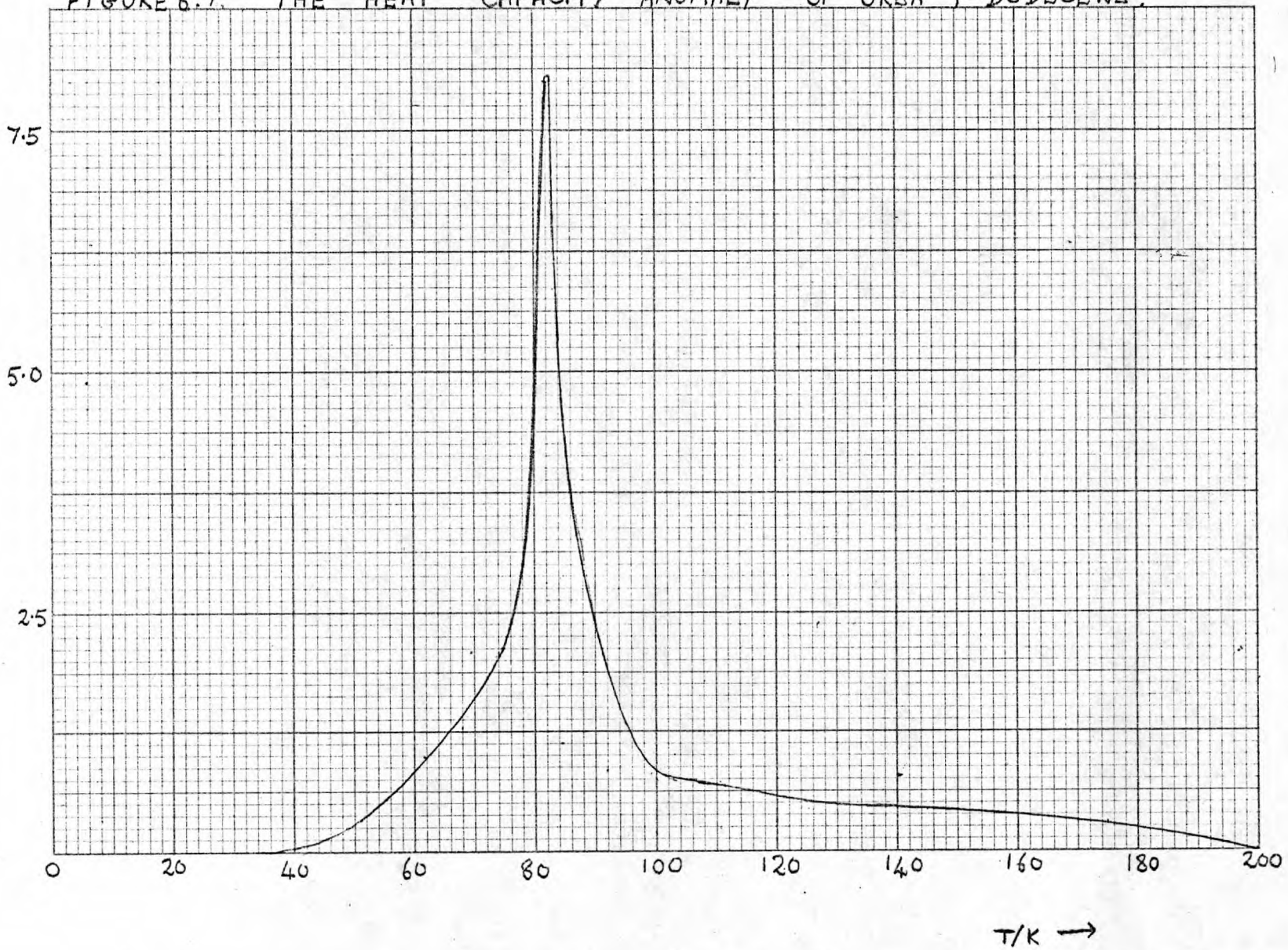
The same procedure was adopted to determine the excess heat and entropy of the 1-dodecene adduct anomaly. The relationship used to estimate the adduct heat capacity excluding irregular contributions was:

$$C_{pene\ adduct}^{estimated} = C_{pane\ adduct} + (X_{ene} - X_{ane})\ C_{pene}$$

Where ene = 1-dodecene, ane = dodecane, Cp is the heat capacity and X the mole fraction. The Cpane adduct and the Xane values were taken from Pemberton and Parsonage (1965) and the Cpene values were from Finke, Gross, Waddington and Huffmann (1954).

Below 40K and from 200K to 300K the experimentally measured and estimated urea-1-dodecene heat capacities differed by only about 1%. However between 40 and 200K the difference in measured and estimated heat capacities, ΔCp, has the form of a well defined peak with a very long high temperature tail (see Figure 6.6). By graphical integration under this curve the excess heat, ΔH of the

FIGURE 6.7. THE HEAT CAPACITY ANOMALY OF UREA 1-DODECENE.



adduct anomaly was determined. The excess entropy, ΔS, was determined by graphical integration under the $\Delta Cp/T$ versus T curve.

$$\Delta H = (128 \pm 20)\ J(\text{mol urea})^{-1}$$
$$= (1210 \pm 190\ J(\text{mol hydrocarbon})^{-1}$$
$$\Delta S = (1.1 \pm 0.1)\ JK^{-1}(\text{mol urea})^{-1}$$
$$= (10.8 \pm 0.9)\ JK^{-1}(\text{mol hydrocarbon})^{-1}$$

In estimating the error in ΔCp it is useful to rewrite ΔCp in terms of specific heat capacities, C^g, and molar masses, M.

$$\Delta Cp = (M\,\text{urea} + X_{ene}M_{ene})\,C^g_{ene\ adduct} - (M\,\text{urea} + X_{ane}M_{ane})\,C^g_{and\ adduct} - {}_{ene}C_{ene} + {}_{ane}C_{ene}$$

The error in ΔCp, $\delta\Delta Cp$ is given by

$$\delta\Delta Cp = \Big\{ (C^g_{ene\ adduct}M_{ene} - C_{ene})^2(\delta X_{ene})^2 + (C^g_{ane\ adduct}M_{ane} - C_{ane})^2(\delta X_{ane})^2 + (M\,\text{urea} + X_{ene}M_{ene})^2(\delta C^g_{ene\ adduct})^2 + (M\,\text{urea} + X_{ane}M_{ane})^2(\delta C^g_{ane\ adduct})^2 \Big\}^{\frac{1}{2}}$$

Errors in mole fractions lead to molar heat capacity errors and thus an estimate which assumes that these errors are independent gives far too large a value for $\delta\Delta Cp$.

For the 1-dodecene adduct anomaly temperature range $\delta C^g_{ene\ adduct}$ and $\delta C^g_{ane\ adduct}$ are approximately constant at 0.18 and 0.08 per cent of the parent quantities. δX_{ene} and δX_{ane} are both taken as 0.002. These figures lead to an error of 20 $J(\text{mol urea})^{-1}$ in ΔH and 0.1 $JK^{-1}(\text{mol urea})^{-1}$ in ΔS .

ΔCp should also contain a contribution from the difference in heat capacities of adducted n-dodecane and

1-dodecene. In estimating this contribution for the 1-decene adduct (Cope and Parsonage, 1969), ΔCp was estimated using the procedure discussed above for the urea-1-hexadecene adduct as the urea-n-hexadecane adduct and the urea-1-hexadecene adduct both have particularly clearly defined anomalies (ΔCp here excluded the excess heat of the major transition). This gave $S = (2.9 \pm 1.2)$ $JK^{-1}(\text{mol hydrocarbon})^{-1}$. As the urea lattice holds the alkenes and alkanes in an extended configuration the difference in their molar entropy contributions should be independent of chain length. Thus we may use the ΔS value for urea-1-hexadecene adduct to give a corrected entropy value ΔS^1 for the urea-1-dodenene of (7.9 ± 2.1) $JK^{-1}(\text{mol hydrocarbon})^{-1}$.

Although similar estimates of ΔCp for urea-1-tetradecene and urea-1-octadecene were thought desirable the lack of any heat capacity data for the corresponding n-alkane adducts or for pure 1-tetradecene and 1-octadecene rendered the calculation impossible.

The three 1-alkene adducts each exhibited two further small anomalies. These were of similar magnitude and occurred at similar temperatures to those previously observed by Pemberton (1966) and Cope (1967).

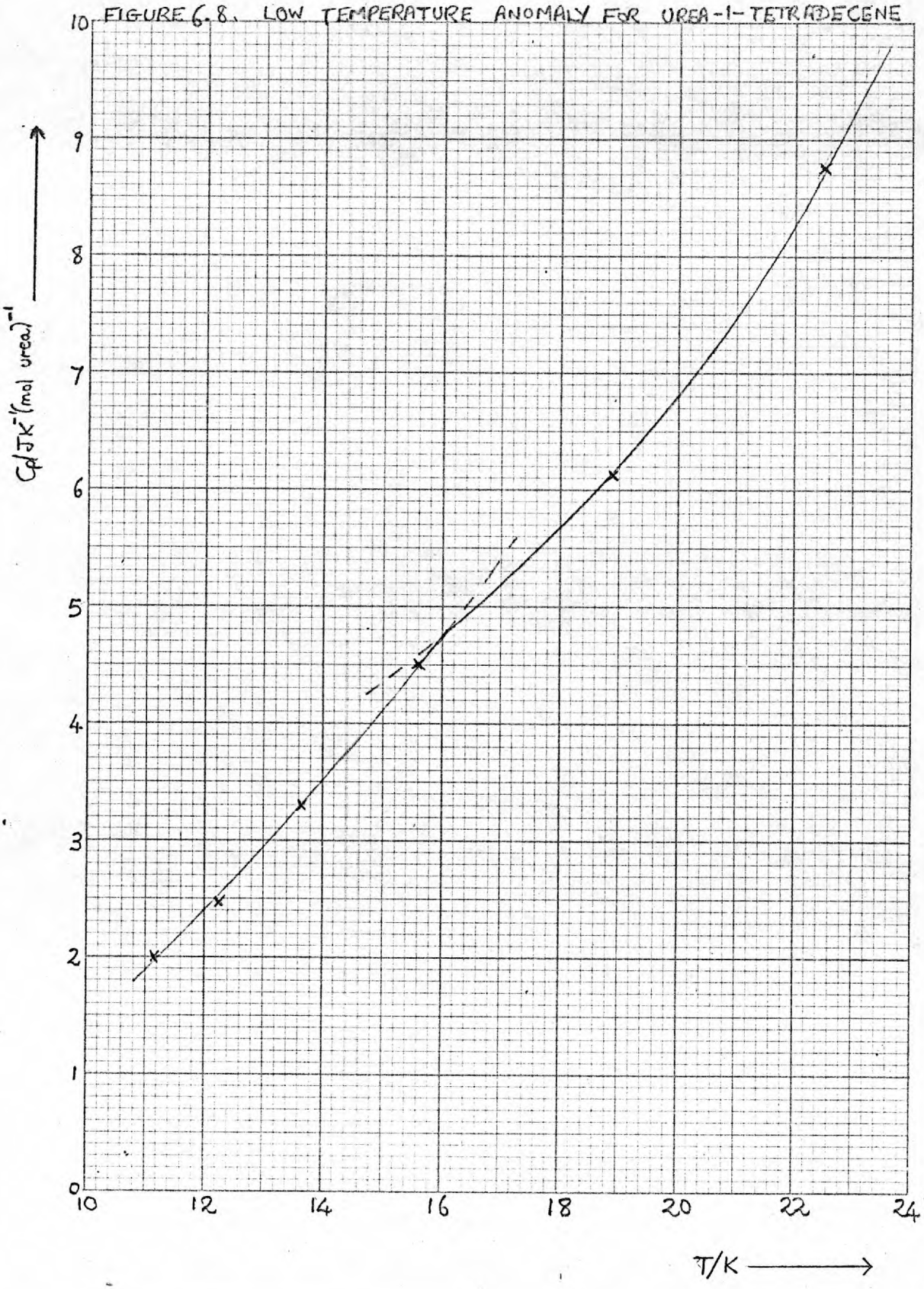
The first type, known as the low temperature anomaly, was a small excess heat (about 5J $(\text{mol urea})^{-1}$) at around 16K. The anomaly for urea-1-tetradecene is shown in Figure

6.8. A more complete study of these low temperature anomalies is hindered by the inaccuracy of measurements in this temperature range and by the small magnitude of the anomalies. However as in all measurements made with this calorimeter system other than those on urea adducts no 16K anomaly was observed the effect can be safely attributed to the urea adducts.

The second type, known as the high temperature anomaly, were small heat excesses observed in the temperature region 210-250K. Although the percentage root-mean-square deviation of points in this range in somewhat greater than the quoted values for the 80-300 K range these deviations are too small to throw any doubt on the existence of the anomaly. The excess heats and entropies for the high temperature anomalies are summarised below.

Adduct	1-Dodecene	1-Tetradecene	1-Octadecene
$\Delta H/(J\ (mol\ urea)^{-1})$	2.45 ± 1.8	14.6 ± 1.9	11.7 ± 1.2
$\Delta H/(J\ (mol\ alkene)^{-1})$	23.0 ± 17.0	143.2 ± 18.6	149.1 ± 15.3
$\Delta S/(JK^{-1}(mol\ urea)^{-1})$	0.010 ± 0.008	0.067 ± 0.008	0.049 ± 0.005
$\Delta S/(JK^{-1}(mol\ alkene)^{-1})$	0.094 ± 0.075	0.657 ± 0.078	0.624 ± 0.064

FIGURE 6.8. LOW TEMPERATURE ANOMALY FOR UREA-1-TETRADECENE



(iii) Discussion of the Heat Capacity Anomalies of the Urea-1-alkenes studied

(a) The low temperature (~ 16K) and high temperature (200-240K) anomalies

Pemberton (1966) suggested two possible explanations for the high temperature anomalies. The first was that put forward by Ruehrwein and Huffman (1946) to explain the small anomalously high heat capacity region in pure urea from 255-265K. They suggested that this was due to melting of a urea-water eutectic. However the anomalies in the urea adducts are found between 20 and 60K lower than the urea-water eutectic point, ~ 262K (Chadwell and Politi, 1938) and it seems unlikely that the properties of aqueous urea solution will be modified to this extent in the urea adducts.

The second explantion was first proposed by Gilson and McDowell (1961). To explain the sudden drop in the second moments of N.M.R. spectra of urea-d_4-alkane adducts at 224-230K they suggested that the urea lattice expanded lightly in this temperature range. This would allow the guest molecules greater motional freedom. However as it is thought that the guest molecules already have considerable rotational freedom a large entropy change would not be expected.

The heat capacity measurements made by Ruehrwein and Huffman (1946) on pure urea covered the temperature range 20-320K and so it is not known whether the heat capacity

of pure urea exhibits an anomaly near 16K similar to those found in the urea-n-alkane and 1-alkane adducts.

In view of the uncertainty in the origin of the low and high temperature adduct anomalies it was decided to study the possible vibrational and translational motion of the guest molecules along the urea channels and to see what contribution to the adduct heat capacity this motion of guest molecules might make.

(1) Monte-Carlo Study of Translation of Guest Molecules

The following computations were carried out on the Atlas Computer, University of London.

To simplify the computation the guest molecules (n-hexadecane was chosen for detailed study) are considered to occupy the sites of a simple cubic lattice. A cube of 512 molecules is chosen, 8 per cube side. Rotation of the guest molecules in the lattice is not considered and the lateral and longitudinal guest molecule interactions are determined by averaging those calculated by Parsonage and Pemberton (1967) over all guest molecule orientations (see Figures 6.9 and 6.10).

In a real adduct crystal the number of guest molecules near the crystal surfaces is negligible compared with the number in the interior of the crystal. However with a model of 512 molecules almost half of the molecules are on the surface. In these calculations the molecules on the surface are made to experience equivalent interactions to those in the centre of the cube by surrounding the cube by

FIGURE 6.9. VARIATION OF LONGITUDINAL ANE-ANE INTERACTION WITH CHANNEL SEPARATION (AVERAGED OVER ALL ORIENTATIONS)

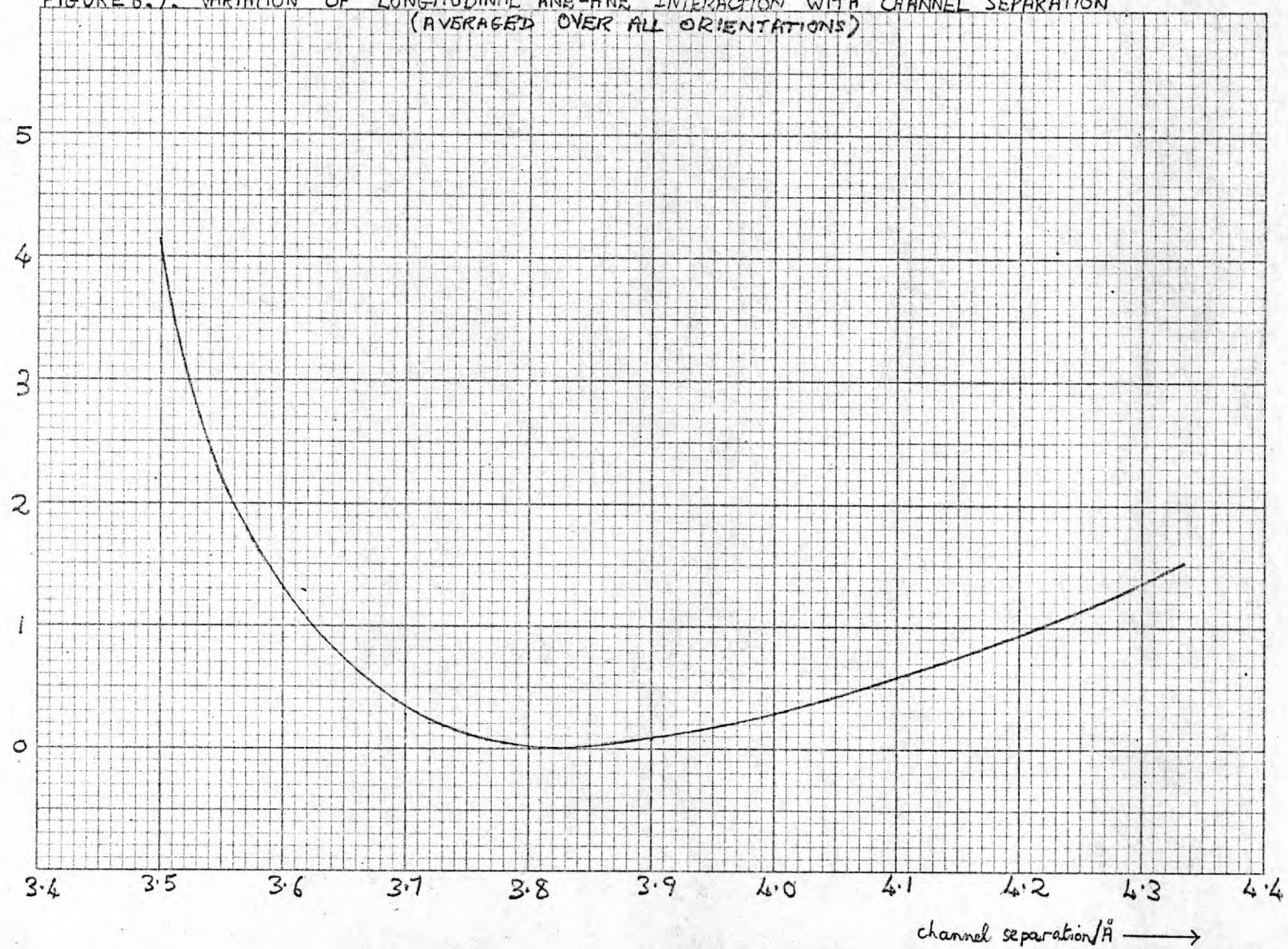
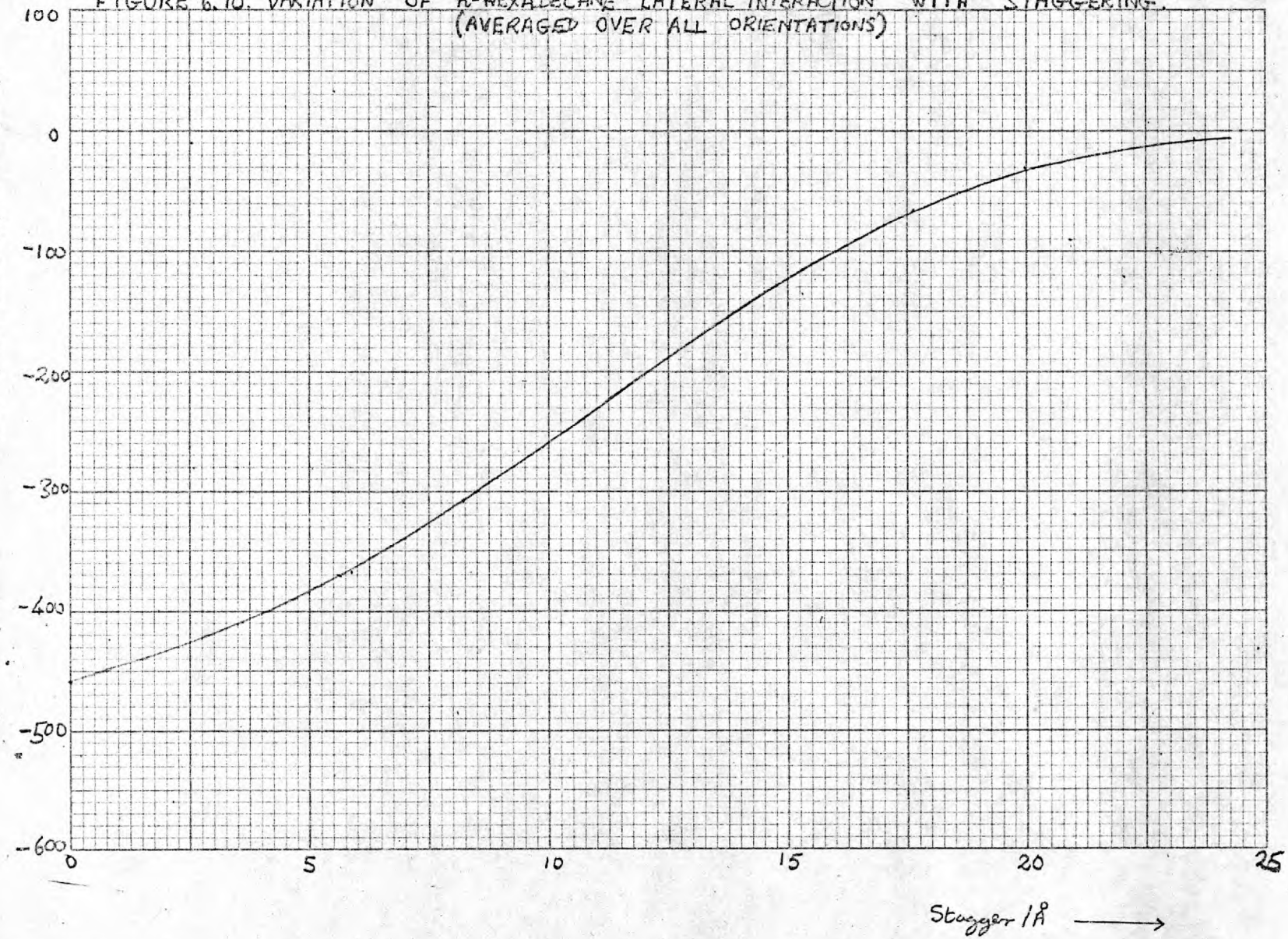


FIGURE 6.10. VARIATION OF n-HEXADECANE LATERAL INTERACTION WITH STAGGERING.
(AVERAGED OVER ALL ORIENTATIONS)



'ghost' systems i.e. the cube is surrounded by cubes of molecules whose configurations match the central cube at all times.

The energy (E) of a molecule (a) in the cube is determined by summing its two longitudinal interactions and its lateral interactions with molecules in the surrounding channels within 25Å of either end of (a). The total (E_T) energy of the cube is the sum of the E's for all 512 molecules. E_T is determined for a cube of molecules with all molecules initially in an ordered array. Then one molecule is allowed to move a random distance between 0 and 'x' in a positive or negative direction along the channel. The new E_T is calculated. If the energy of the new configuration of molecules is lower than the original one the new configuration is accepted. If the new energy is higher the Baltzmann factor of the energy increase $e^{-\frac{\Delta E}{kT}}$ is compared with a random number between 0 and 1; if the factor is larger, the move is accepted, if it is smaller the original configuration is retained. This process is repeated for all the molecules in the cube. After a certain number of cycles of the cube the average energy $\langle E \rangle$ and the average of the square of the energy $\langle E^2 \rangle$ are determined. The heat capacity of the model may then be determined from the formula

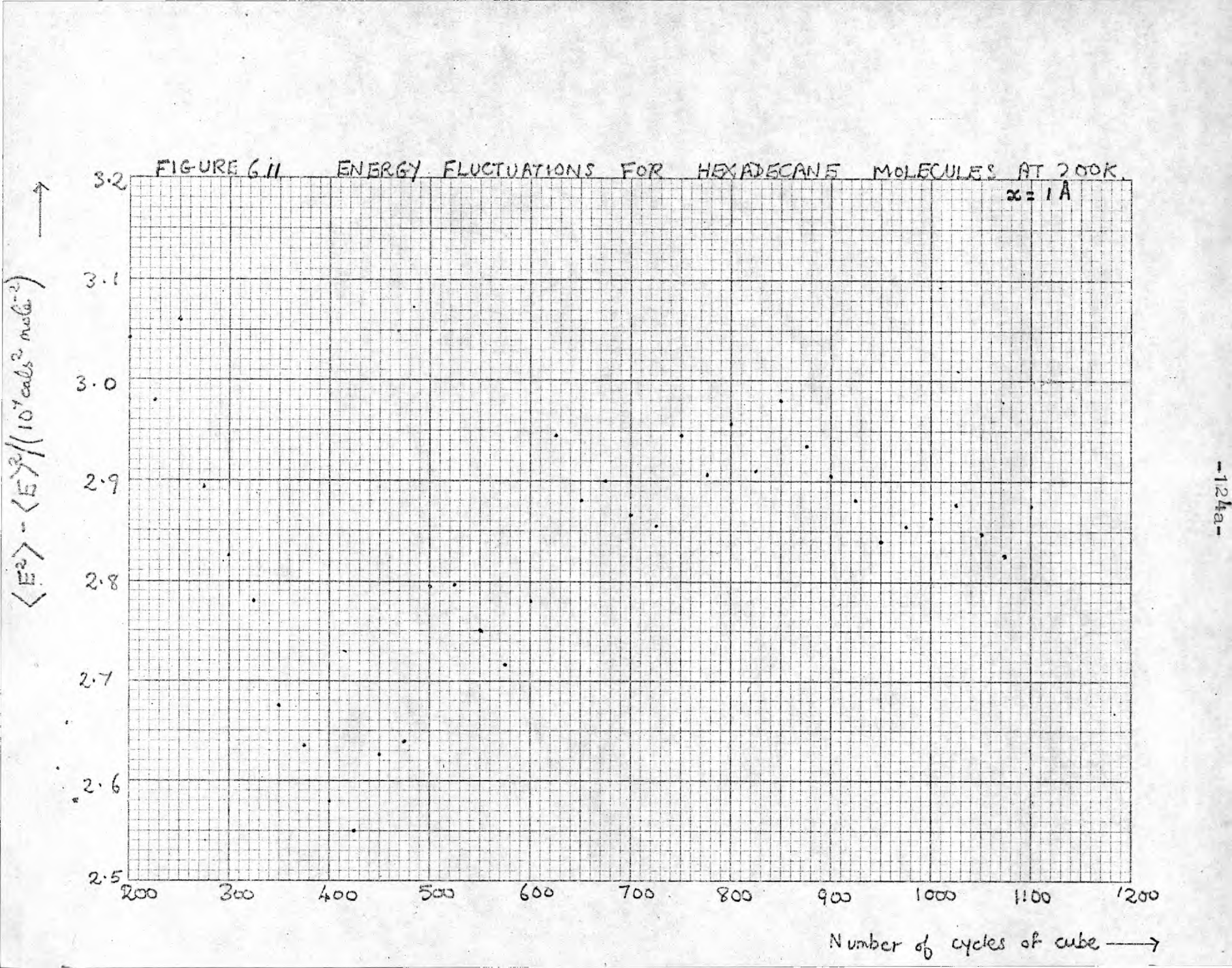
$$\frac{C}{R} = \frac{\langle E^2 \rangle - \langle E \rangle^2}{(kT)^2 N}$$

where R is the gas constant, C is the heat capacity, T

the temperature and N the number of molecules considered. A plot of $\langle E^2 \rangle - \langle E \rangle^2$ versus number of cycles of cube for hexadecane molecules at 200K is shown in Figure 6.11

It will be observed that the $\langle E^2 \rangle - \langle E \rangle^2$ term still has relatively large fluctuations even after 1000 cycles of the cube. Varying x (the maximum allowed move for a molecule) did not improve convergence and neither did starting with a cube with alternate rows translated by half a lattice repeat distance. The effect of moving random molecules in the cube (instead of the normal method of proceeding from one molecule to the next in a row and then from one row to the next etc.) was also tested. This also did not improve the convergence.

The position to which the molecules in the cube had moved after many cycles of the cube were noted. It was found that the molecules generally moved very little from their original positions - this was true even in the case where alternate rows were translated by half a lattice repeat distance although this arrangement has a higher energy than the unstaggered cube. This rules out the possibility that there is little molecular movement because the initial system is the configuration of lowest energy. Thus it was decided that the lack of convergence of $\langle E^2 \rangle - \langle E \rangle^2$ and the small movement of the molecules from their original positions was a kinetic effect and that if the cube was cycled enough times the true behaviour of the molecules might be established.


FIGURE 6.11 ENERGY FLUCTUATIONS FOR HEXADECANE MOLECULES AT 200K
α = 1 Å
$\langle E^2 \rangle - \langle E \rangle^2 / (10^4 \text{ cals}^2 \text{ mole}^{-2})$
3.2
3.1
3.0
2.9
2.8
2.7
2.6
2.5
200
300
400
500
600
700
800
900
1000
1100
1200
Number of cycles of cube

However computations employing a greater number of cycles of the cube could not be made due to the prohibitive amount of computer time required.

(2) Born-von Kármán and Einstein Oscillators

The possibility of guest molecules behaving as one dimensional Born-von Kármán oscillators and Einstein oscillators in the urea lattice has been considered by Dr. N. G. Parsonage.

Einstein (1907) first applied Planck's theory of quantised oscillators to the vibrations of a crystal. His model consisted of oscillators all vibrating with the same frequency, ν . The energy levels available to an oscillator are

$$E_n = h\nu\left(n + \tfrac{1}{2}\right) \qquad n = 0, 1, 2 \ldots\ldots \qquad (1)$$

and the partition function is given by

$$q = \sum_{n=0}^{\infty} e^{\frac{-nh\nu}{k_B T}} = \frac{1}{1 - e^{-\frac{h\nu}{k_B T}}} \qquad (2)$$

But entropy, S, is related to the partition function, q, by

$$S = k_B \left[\ln q + T \frac{d\ln q}{dT} \right] \qquad (3)$$

$$\therefore \quad S = k_B \left[- \ln\left(1 - e^{-h\nu/k_B T}\right) + \frac{h}{T} \cdot \frac{e^{-h\nu/k_B T}}{\left(1 - e^{-h\nu/k_B T}\right)} \right] \qquad (4)$$

However Einstein's model was found to agree only qualitatively with experimentally determined low temperature heat capacities. He concluded that the failure of his formula to agree with experiment at low temperatures was the result of the use of a single frequency and suggested that a whole band of

frequencies be employed in the theory.

Debye (1912) and Born and von Kármán (1912) followed this suggestion and achieved a substantial improvement in the theory. Whereas Debye treats solids as continua the theory of Born and von Kármán allows for the fact that real solids have a discrete lattice structure.

In one dimension the Born-von Kármán lattice consists of equidistant identical particles. Harmonic forces exist between the molecules which may be represented by weightless springs obeying Hooke's low which join the particles. If 'a' is the separation distance of the molecules, M is their mass and α' is Hooke's constant then it can be shown from considerations of the equations of motion of the molecules (de Launay, 1956) that

$$\nu^2 = \frac{\alpha'}{\pi^2 M} \sin^2 \pi a k^1 \qquad (5)$$

where k^1 is the wave number. The entropy of a one-dimensional array is given by

$$S = -k_B \sum_{\nu} \ln \left(1 - e^{-h\nu/k_B T}\right) + \frac{h}{T} \sum_{\nu} \nu \frac{e^{-h\nu/k_B T}}{1 - e^{-h\nu/k_B T}} \qquad (6)$$

If we consider an infinitely long array the frequency summation may be replaced by an integral over frequency distribution and (6) may be rearranged to give

$$\frac{S}{k_B} = -\int_0^{\pi/a} \ln\left(1 - e^{-\alpha \sin \frac{k^1 a}{2}}\right) dk^1 + \int_0^{\pi/a} \alpha \sin \frac{k^1 a}{2} \cdot \frac{e^{-\alpha \sin \frac{k^1 a}{2}}}{1 - e^{-\alpha \sin \frac{k^1 a}{2}}} dk^1 \qquad (7)$$

Therefore for an Avogadro Number of oscillators and putting

$$\theta = \frac{k^1 a}{2},$$

$$\frac{S_{Evk}}{R} = -\frac{2}{\pi}\int_0^{\pi/2} \ln\left(1 - e^{-\alpha \sin\theta}\right) d\theta + \frac{2}{\pi}\int_0^{\pi/2} \frac{\alpha \sin\theta}{e^{\alpha \sin\theta} - 1} \cdot d\theta \qquad (8)$$

The first integral in (8) may be integrated by parts.

$$\int_0^{\pi/2} \ln\left(1 - e^{-\alpha \sin\theta}\right) d\theta = \left[\theta \ln\left(1 - e^{-\alpha \sin\theta}\right)\right]_0^{\pi/2} - \int_0^{\pi/2} \frac{\theta \alpha \cos\theta \cdot d\theta}{e^{\alpha \sin\theta} - 1}$$

$$= \frac{\pi}{2} \ln\left(1 - e^{-\alpha}\right) - \int_0^{\frac{\pi}{2}} \frac{\theta \alpha \cos\theta}{e^{\alpha \sin\theta} - 1} \cdot d\theta \qquad (9)$$

The integrand in the second term of (9) tends to unity as (6) tends to zero. Thus the integrand is well-behaved throughout the range 0 to $\pi/2$ and may be enumerated by Simpson integration. The second integral in (8) may also be evaluated by Simpson integration since the intergrand again tends to unity at (6) tends to zero.

Hooke's constant, α, is given by

$$\alpha = \frac{h}{2\pi k_B T}\sqrt{\frac{4f}{M}} \qquad (10)$$

where f is the force constant for molecule-molecule interaction which for n-alkane molecules may be estimated from Figure 6.9.

For an Avogadro's Number of Einstein oscillators the entropy is given by

$$\frac{S_E}{R} = -\ln\left(1 - e^{-\frac{h\nu_E}{k_B T}}\right) + \frac{h\nu_E}{k_B T} \cdot \frac{1}{\left(e^{\frac{h\nu_E}{k_B T}} - 1\right)} \qquad (11)$$

The choice of value for ν_E is not obvious. As for each molecular displacement two molecular distances are altered the best assignment is probably

$$\nu_E = \frac{1}{2\pi}\sqrt{\frac{2f}{M}} \qquad (12)$$

The upper limit for ν_E is the maximum value of ν for the Born-von Kármán model with

$$\nu_E = \frac{1}{2\pi}\sqrt{\frac{4f}{M}} \qquad (13)$$

Dr. N. G. Parsonage has written a computer program finding S_{DvK} and S_E for the two values of ν_E, (12) and (13), for various values of α. The results are shown in Table 6 below.

TABLE 6 ENTROPIES FOR BORN-VON KARMAN AND EINSTEIN OSCILLATORS

α	S_{DvK}/R	$S_E(12)/R$	$S_E(13)/R$
1.000	1.714	1.367	1.041
0.700	2.060	1.713	1.377
1.500	1.333	9.867×10^{-1}	6.833×10^{-1}
3.000	7.556×10^{-1}	4.166×10^{-1}	2.083×10^{-1}
10.000	2.127×10^{-1}	6.863×10^{-3}	4.994×10^{-4}
30.000	6.992×10^{-1}	1.368×10^{-8}	6.333×10^{-11}
100.000	2.094×10^{-1}	1.386×10^{-29}	3.720×10^{-42}

From Figure 6.9 the value of f for n-alkane molecules will be $\sim 5 \times 10^3$ kcals cm^{-1}. Now we can see if the transition from Born-von Kármán to Einstein oscillators ($S_{DvK} - S_E$) for n-alkane molecules in urea channels might explain either the low or high temperature anomalies.

If T ~ 220-240K then $\alpha \sim 0.9$. This will give an entropy of transition of ~0.4 R if (12) is used for ν_E and ~0.7 R if (13) is used for ν_E. These values are at least an order of magnitude larger than the entropies of the high temperature anomalies in the urea adducts. Clearly then, this model will not predict the high

temperature anomalies.

If T $\sim$ 16K then $\alpha \sim 12$. This leads to an entropy of transition of $\sim$ 0.2 R whether (12) of (13) is used for ν_E. This value falls well within the range of entropies found for the low temperature anomaly (1-2 JK^{-1}(mole hydrocarbon)$^{-1}$). Due to the inaccuracy of the experimental heat capacity points around 16K, the broadness of the anomaly and the crude model employed, itis not possible to come to any definite conclusions about the origin of the low temperature anomaly. However these calculations suggest that a transition of the guest molecules from Born-von Karman oscillators to Einstein oscillators may well be responsible for this anomaly.

(b) The major anomalies

The heat capacities of the urea adducts of 1-dodecene, 1-tetradecene and 1-octadecene were studied in this thesis primarily to gain more information about the major anomalies of the urea-1-alkene series and to try to understand the head-tail ordering of the guest molecules in the urea channels. However the anomalies found for these three adducts do little to clarify the situation.

Both urea-1-tetradecene and urea-1-octadecene exhibit major co-operative-type anomalies and the transition temperature of the1-octadecene adduct is in the same temperature region as the anomalies found for urea-1-hexadecene and urea-1-eicosene (Cope and Parsonage, 1969). The

1-tetradecene adduct anomaly, however, occurs at 256K, about 100K higher than would be expected by comparison with the other 1-alkene adducts.

The 1-dodecene adduct exhibited a broad peak from 40-200K i.e. a non-co-operative-type anomaly rather similar to the anomalous regions found in 1-decene. Ising-Monte Carlo calculations for a head-tail disordered adduct lattice (Cope, 1967) failed to reproduce the non-co-operative anomaly found for urea-1-decene. The origin of this lack of co-operation in the 1-decene and 1-dodecene adducts remains obscure.

The high temperature of transition in the 1-tetradecene might be explained on the basis of head-head tail-tail ordering of the 1-tetradecene molecules. Cope (1967) showed that the ene-ene potential barrier to rotation is very high and so it is possible that two molecules might begin to rotate together like one long molecule. However in this case the entropy should only be half that found for other 1-alkene adducts - in fact the entropy for the 1-tetradecene adduct anomaly is somewhat larger than for other 1-alkene adducts.

(iv) Proposals for further work

It seems unlikely that a real understanding of the molecular rearrangement of the 1-alkene molecules in the urea channels that leads to the major anomalies in the

adduct heat capacities will be achieved until the head-tail ordering of the guest molecules is definitively determined.

The only technique certain to give this information is the neutron diffraction study of adduct single crystals containing fully deuterated 1-alkene molecules. This method could actually locate the position of the deuterium atoms and hence determine the ordering. Unfortunately none of the 1-alkenes are yet available fully deuterated, and even if they were the time and cost of a full neutron diffraction study of just one adduct would probably prove prohibitive.

In principle it would be possible to obtain information on the head-tail ordering by measuring the entropy of solution of the adducts in a suitable solvent near room temperature. Since one would expect the entropy of the solution to change regularly with chain-length of the olefin any anomalies could be attributed to the adduct. From the measured values of $S_{300} - S_0$ it would then be possible to say whether the anomalous entropy was retained at the lowest temperatures.

The entropy of solution must be determined from the heat and free energy of solution. The solvent chosen must be one in which urea is very soluble while the guest molecules have a very low sulubility - water or methanol would be two possibilities. The heat of solution of 1 mole of urea

to infinite dilution in water is -15.1 kilojoules at 24°C: for urea in ethanol at 24°C it is also -15.1 kilojoules (E. Anderson, 1929). However the contribution to the entropy from loss of head-tail ordering on dissolving the adduct would be Rln2. This would contribute to the heat of solution at room temperature something of the order of 1.5 kilojoules per mole of olefin or about 150 joules per mole of adduct. This term therefore would be only about 1% of the total heat of solution. This suggests that entropies of solution of the adducts would be effected so little by any ordering term that the precision of the experimental measurements would be of too low an order to detect any ordering.

Casey and Runnels (1969) have devised a model, which predicts a thermodynamic singularity in a one-dimensional model arising from the rotation of non-spherical molecules. This differs from previous models (including the Ising model) which give no singularity in one dimension. The one-dimensional Ising model is not ordered above zero degrees Kelvin because the presence of one incorrectly oriented spin will remove all long range order in the lattice. Parsonage and Pemberton (1967) thus considered that the weak lateral alkane-alkane interactions were important in producing a co-operative order-disorder transition. However if the model of Casey and Runnels could be successfully applied to the guest molecules in urea adducts

it would be very interesting to see if the heat capacity anomalies might be predicted by a one dimensional model.

CHAPTER 7

THERMODYNAMIC PROPERTIES OF THIOUREA-CYCLOHEPTANE AND THIOUREA-CYCLOÖCTANE ADDUCTS

(i) Experimental Determination of the Heat Capacities

The heat capacities of the thiourea adducts of cycloheptane and cycloöctane were determined by the method described in Chapter 3. The values found for their heat capacities are listed on Tables 7.1. and 7.2. Cp/mole values refer to the heat capacity of the adduct per Mole of Thiourea (1 mole of Thiourea = 76.133g). These heat capacity points were plotted against temperature using a large scale and a smooth curve of best fit drawn between the points. From these graphs smoothed heat capacity values were read at 5K intervals and these points are tabulated in Table 7.3. Small scale graphs of heat capacity versus temperature for the cycloheptane and cycloöctane adducts together with the thiourea-cyclohexane adduct (Cope 1967) are given in Figure 7.1.

A measure of the precision of the experimental results is given by the percentage root mean square deviation of the points from the smooth curve. These values for the thiourea adducts of cycloheptane and cydo-öctane are given below in Table 7.1.

TABLE 7.1. ROOT MEAN SQUARE DEVIATIONS OF THE EXPERIMENTAL POINTS FROM A SMOOTH CURVE

Adduct	Temperature Range		
	12-25K	25-80K	80-300K
cycloheptane	0.79	0.23	0.12
cyclooctane	0.26	0.35	0.13

In Table 7.5 the adduct entropies determined at 10K intervals by graphical integration under a large scale plot of Cp/T against T are listed. For this the heat capacities below 12K must be estimated. For the cyclooctane adduct this was effected using the same procedure as in Chapter 6 section (ii). However for the cycloheptane adduct the experimental points did not extrapolate to zero heat capacity at zero degrees Kelvin. These points are shown in Figure 7.2. The entropy values were determined using Cp values of curve 'a' in the figure.

TABLE 7.2

EXPERIMENTAL VALUES OF THE HEAT CAPACITY OF THIOUREA-CYCLOHEPTANE

Wt. of sample in calorimeter = 10.8695 g (7.5543 g of thiourea + 3.3152 g of cycloheptane)
Heat capacity of sample, Cp, in Joules K^{-1}
Heat capacity per mole of thiourea, Cp/mole, in Joules K^{-1} $mole^{-1}$

Run No.	Temp/K	ΔT	Cp	Cp/mole
1	96.20	2.12	6.610	66.635
2	98.89	3.29	6.785	68.400
3	102.41	3.77	7.103	71.605
4	106.81	5.00	7.275	73.339
5	111.74	4.86	7.492	75.527
6	116.35	4.35	7.677	77.392
7	120.86	4.68	7.779	78.420
8	125.49	4.57	8.007	80.719
9	130.16	4.78	8.218	82.846
10	134.87	4.66	8.521	85.900
11	139.58	4.73	8.765	88.360
12	144.45	5.01	8.996	90.689
13	149.34	4.83	9.229	93.038
14	151.35	2.96	9.389	94.651
15	153.99	2.33	9.581	96.586
16	155.98	1.63	9.606	96.838
17	157.61	1.61	9.682	97.604
18	159.34	1.84	9.829	99.086
19	161.17	1.82	9.931	100.11
20	163.07	1.98	10.985	110.74
21	165.15	2.02	10.317	104.01
22	167.17	2.03	10.097	101.79
23	169.20	2.01	10.195	102.78
24	171.21	2.00	10.268	103.51
25	173.82	1.97	10.405	104.89
26	175.77	1.93	10.489	105.74
27	177.71	1.93	10.560	106.46
28	179.65	1.93	10.598	106.84
29	181.68	2.12	10.846	109.34
30	183.80	2.10	10.983	110.72
31	186.14	2.57	11.104	111.94
32	189.06	3.26	11.203	112.94
33	191.17	4.50	11.345	114.37
34	195.78	4.72	11.461	115.54
35	200.63	5.01	11.610	117.04
36	205.62	4.94	11.844	119.40
37	210.54	4.90	12.053	121.51

TABLE 7.2 (continued)

Run No.	Temp/K	ΔT	Cp	Cp/mole
38	215.42	4.86	12.263	123.62
39	220.27	4.81	12.498	125.99
40	225.08	4.80	12.593	126.96
41	229.84	4.77	12.758	128.61
42	231.83	3.20	13.072	131.78
43	234.61	3.02	13.181	132.88
44	237.14	2.60	13.110	132.16
45	239.63	2.54	13.691	138.02
46	242.14	2.48	13.881	139.93
47	244.67	2.40	12.986	130.91
48	247.18	2.50	12.940	130.45
49	249.71	2.46	13.006	131.11
50	252.20	2.58	13.099	132.05
51	252.35	2.70	12.946	130.51
52	255.03	2.62	13.041	131.47
53	257.67	2.58	13.127	132.33
54	259.86	2.20	13.352	134.60
55	262.03	2.16	13.921	140.34
56	264.23	2.24	13.415	135.24
57	266.52	2.36	13.184	132.91
58	268.91	2.50	13.456	135.65
59	271.12	2.40	13.625	137.35
60	277.29	5.64	13.785	138.97
61	283.05	5.92	14.024	141.38
62	289.13	6.28	14.247	143.62
63	295.13	5.81	14.553	146.71
64	300.52	4.99	14.790	149.10
P1	50.82	4.80	3.951	39.830
P2	55.24	4.50	4.153	41.866
P3	60.64	3.64	4.567	46.042
P4	64.26	4.24	4.920	49.599
P5	67.99	4.16	5.151	51.927
P6	72.29	4.45	5.293	53.359
P7	76.50	4.17	5.559	56.040
P8	80.81	4.44	5.888	59.357
P9	85.37	4.68	6.205	62.553
P10	90.16	4.91	6.525	65.778
P11	95.00	4.76	6.719	67.734
H1	12.17	1.62	0.605	6.099
H2	14.38	2.40	0.647	6.522
H3	16.67	2.30	0.743	7.492
H4	19.05	2.44	0.912	9.194
H5	22.06	3.58	1.277	12.873
H6	25.60	3.70	1.632	16.452
H7	30.52	6.00	2.135	21.523

TABLE 7.2 (continued)

Run No.	Temp/K	ΔT	Cp	Cp/mole
H8	35.75	4.46	2.628	26.493
H9	40.88	5.78	3.165	31.906
H10	46.18	4.82	3.629	36.584
H11	51.07	4.96	3.969	40.011
H12	55.68	4.10	4.192	52.260
T1	161.79	0.67	9.942	100.22
T2	162.43	0.50	12.363	124.63
T3	162.81	0.56	10.970	110.59
T4	163.73	0.64	10.567	106.53

TABLE 7.3

EXPERIMENTAL VALUES OF THE HEAT CAPACITY OF THIOUREA-CYCLOOCTANE

Wt. of sample in calorimeter = 20.9881 g (14.0620 g thiourea + 6.9261 g cyclooctane)
Heat capacity of sample, Cp, in Joules K^{-1}
Heat capacity per mole of thiourea, Cp/mole, in Joules K^{-1} $mole^{-1}$

Run No.	Temp/K	ΔT	Cp	Cp/mole
1	87.32	3.58	11.176	60.496
2	91.28	4.33	11.504	62.271
3	98.06	4.56	12.110	65.551
4	102.56	4.42	12.500	67.663
5	107.00	4.46	12.920	69.936
6	111.48	4.46	13.245	71.695
7	116.00	4.49	13.694	74.126
8	120.58	4.60	14.036	75.997
9	125.27	4.77	14.484	78.402
10	130.10	4.84	14.861	80.443
11	134.32	4.80	15.316	82.906
12	139.09	4.72	15.499	83.896
13	143.79	4.78	16.085	87.068
14	148.60	4.85	16.628	90.007
15	153.48	4.93	17.272	93.493
16	158.44	5.02	17.929	97.050
17	162.98	4.07	18.491	100.09
18	167.03	4.03	18.759	101.54
19	171.00	3.97	19.150	103.66
20	175.43	4.84	19.638	106.30
21	180.18	5.14	19.881	107.62
22	184.77	4.02	21.404	115.86
23	188.47	3.34	29.690	160.71
24	192.12	3.96	21.697	117.45
25	196.69	5.19	22.354	121.00
26	202.21	4.88	23.389	126.60
27	208.00	5.70	24.538	132.82
28	213.60	5.50	26.117	141.37
29	219.39	6.03	27.930	151.19
30	225.31	5.66	29.733	160.94
31	231.23	6.06	32.000	173.22
32	237.49	6.45	34.477	186.62
33	244.09	6.70	34.417	186.30
34	251.07	7.27	32.462	175.72
35	258.40	7.37	31.385	169.89
36	265.76	7.27	31.937	172.88
37	273.33	7.97	29.465	159.49

TABLE 73 (continued)

Run No.	Temp/K	ΔT	Cp	Cp/mole
38	281.29	7.93	29.660	160.55
39	289.19	7.87	29.834	161.49
40	296.97	7.78	30.315	164.09
P1	56.02	3.85	7.838	42.427
P2	60.31	4.20	8.279	44.814
P3	64.45	4.63	8.933	48.354
P4	69.28	3.99	9.345	50.584
P5	74.19	4.84	9.877	53.464
P6	78.92	4.60	10.311	55.813
P7	83.42	4.38	10.903	59.018
P8	87.71	4.20	11.423	61.833
H1	12.52	1.40	0.572	3.096
H2	14.42	1.71	0.656	3.551
H3	16.65	2.43	0.963	5.213
H4	20.02	4.23	1.579	8.547
H5	23.71	3.16	2.287	12.380
H6	27.70	4.65	3.044	16.477
H7	31.92	3.62	3.844	20.808
H8	35.89	4.37	4.604	24.921
H9	40.87	5.61	5.484	29.685
H10	46.29	5.23	6.372	34.492
H11	51.18	4.60	7.109	38.481
H12	55.56	4.16	7.778	42.102
T1	152.72	2.77	17.235	93.293
T2	155.48	2.74	17.533	94.909
T3	158.04	2.38	17.845	96.595
T4	160.40	2.35	18.135	98.165
T5	165.07	2.32	18.543	100.37
T6	167.36	2.28	19.072	103.24
T7	169.48	1.94	19.167	103.75
T8	171.28	1.63	18.836	101.96
T9	172.90	1.62	19.110	103.44
T10	174.97	2.57	19.533	105.73
T11	178.07	3.68	20.223	109.47
T12	181.41	2.97	20.646	111.76
T13	183.89	1.97	20.984	113.59
T14	185.82	1.91	21.199	114.75
T15	187.20	0.89	50.383	272.72
T16	188.37	1.46	22.792	123.37
T17	190.01	1.80	21.595	116.89
T18	192.19	2.56	21.848	118.26
T19	227.97	5.15	30.785	166.64
T20	232.41	3.74	32.531	176.09
T21	235.63	2.72	33.782	182.86
T22	238.04	2.10	34.112	184.65

TABLE 7.3. (continued)

Run No.	Temp/K	ΔT	Cp	Cp/mole
T23	239.98	1.78	34.724	187.96
T24	241.75	1.76	35.121	190.11
T25	243.69	2.07	34.630	187.84
T26	245.80	2.17	33.981	183.94
T27	261.79	2.17	31.729	171.75
T28	263.97	2.16	32.011	173.28
T29	266.09	2.08	33.863	183.30
T30	268.40	2.56	31.238	169.09

TABLE 7.4

SMOOTHED VALUES OF THE HEAT CAPACITIES OF THIOUREA-CYCLOHEPTANE AND THIOUREA-CYCLOOCTANE ADDUCTS

$0^{\circ}C = 273.15K$ HEAT CAPACITY IN JOULES K^{-1} (MOLE THIOUREA)$^{-1}$

T/K	CYCLOHEPTANE	CYCLOOCTANE
0	0.000	0.000
5	2.905	0.920
10	5.495	2.205
15	6.735	4.125
20	10.18	8.520
25	15.78	13.78
30	21.01	18.89
35	26.07	23.94
40	30.99	28.93
45	35.57	33.51
50	39.29	37.52
55	41.99	41.50
60	45.38	45.29
65	50.11	48.47
70	52.49	50.83
75	54.97	53.23
80	58.76	56.57
85	62.36	60.07
90	65.63	61.67
95	67.85	64.08
100	69.38	66.44
105	72.74	68.82
110	74.78	71.20
115	76.85	73.54
120	78.22	75.89
125	80.47	78.23
130	83.26	80.61
135	85.97	82.97
140	88.53	85.36
145	91.01	87.80
150	93.43	91.13
155	96.84	94.68
160	99.37	97.87
165	104.2	100.4
170	103.0	103.4
175	105.4	105.8
180	107.1	110.9
185	111.3	114.3
190	113.9	116.8

TABLE 7.4(continued)

T/K	CYCLOPHEPTANE	CYCLOOCTANE
195	115.2	119.7
200	116.8	123.9
205	119.1	129.3
210	121.2	135.6
215	123.4	143.8
220	125.4	152.1
225	126.9	160.3
230	128.8	170.2
235	132.8	181.3
240	139.6	188.4
245	130.7	185.3
250	131.3	176.9
255	131.6	171.3
260	134.8	170.4
265	134.3	176.2
270	136.6	164.9
273.15	137.8	161.2
275	138.5	159.4
280	139.9	160.2
285	141.7	161.0
290	144.1	162.1
295	146.5	163.3
298.15	148.3	164.3
300	148.8	164.6

FIGURE 7.1 HEAT CAPACITIES OF THE THIOUREA-CYCLOALKANE ADDUCTS

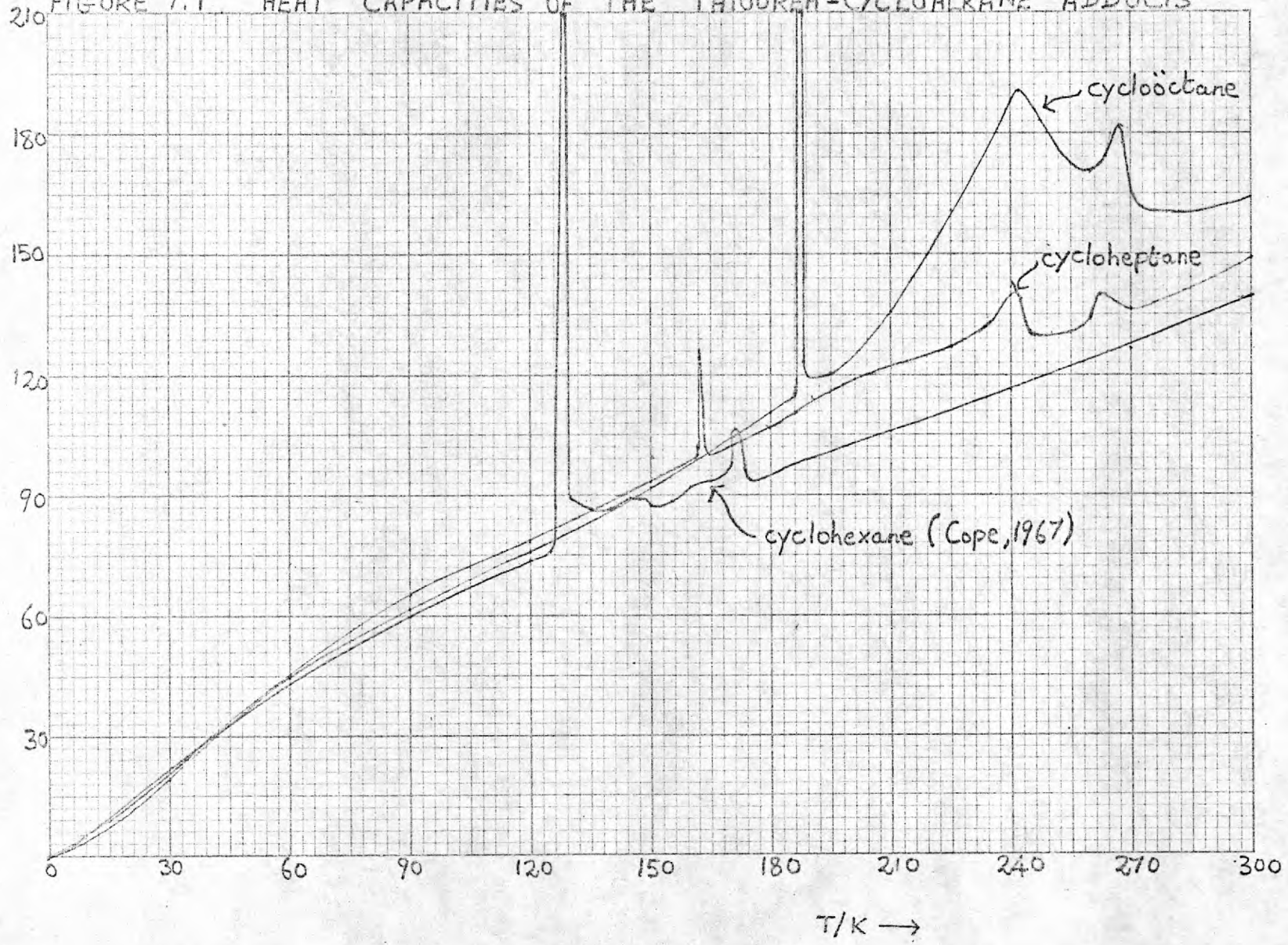


FIGURE 7.2. LOW TEMPERATURE HEAT CAPACITY OF THIOUREA-CYCLOHEPTANE

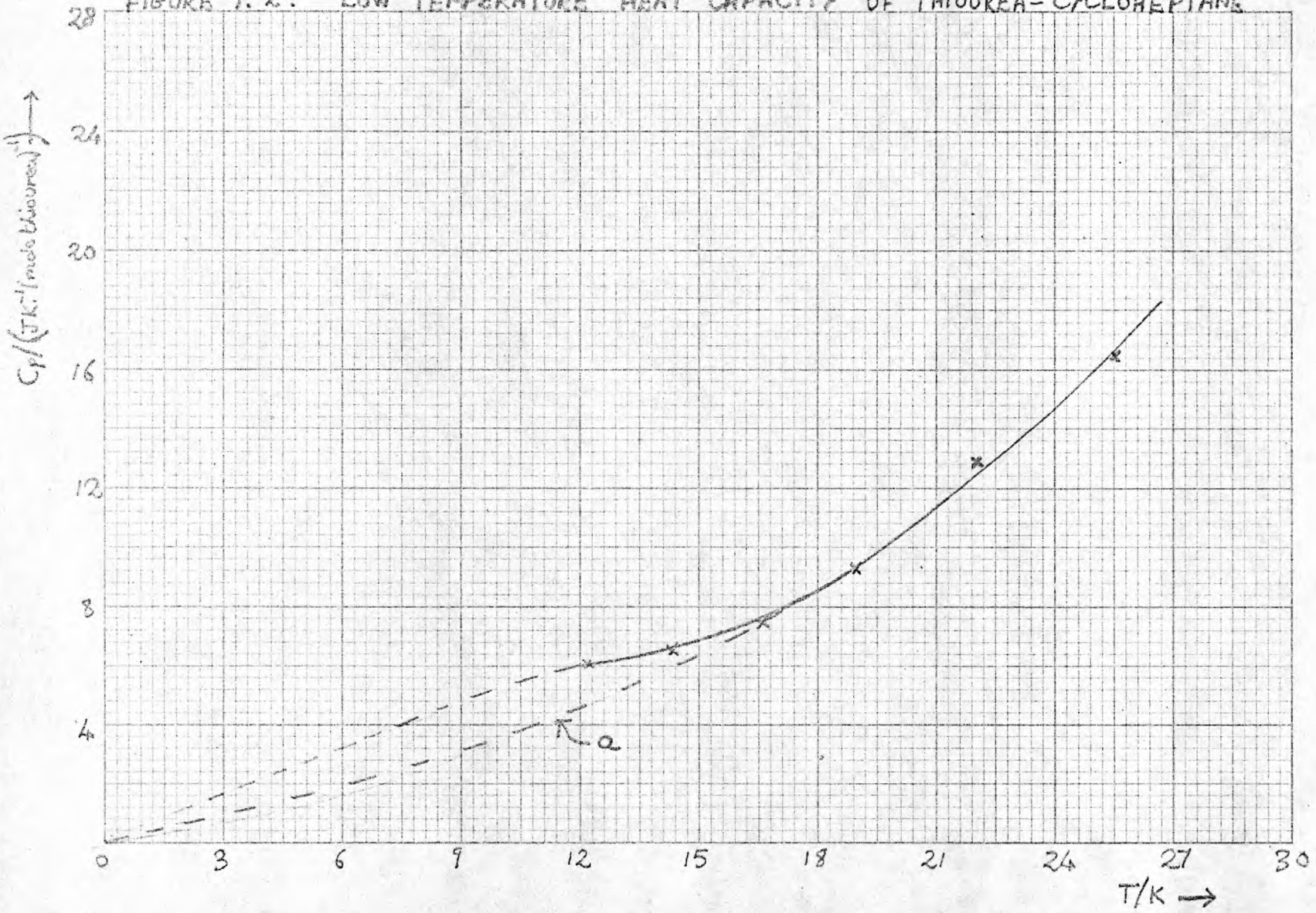


TABLE 7.5 THE ENTROPY ($S_T - S_o$) OF THIOUREA-CYCLOHEPTANE AND CYCLOÖCTANE ADDUCTS IN JOULES K^{-1} (MOLE THIOUREA)$^{-1}$

$0^oC = 273.15K$

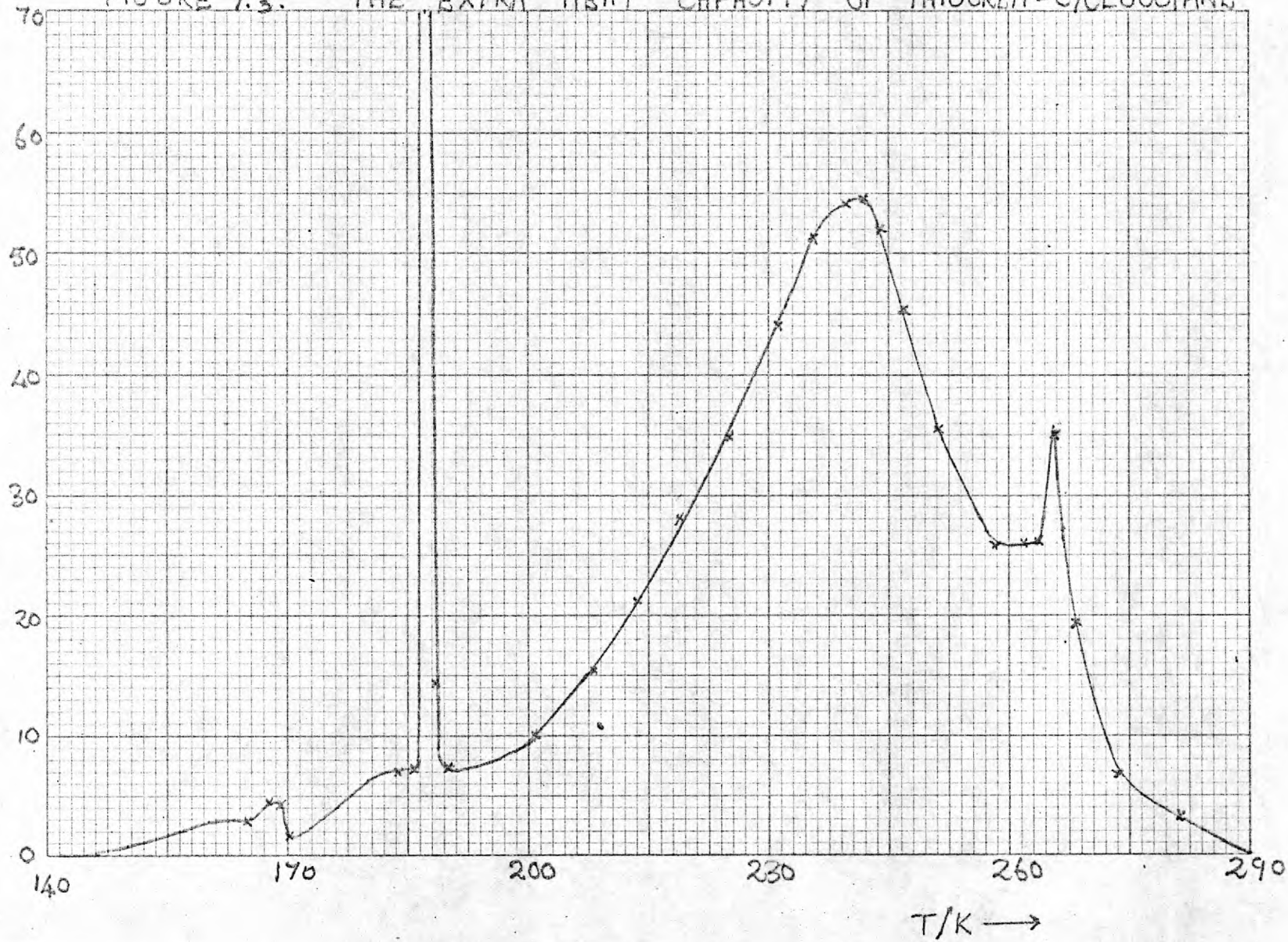
T/K	Cycloheptane	Cycloöctane
0	0.00	0.00
10	0.84	0.64
20	4.42	3.38
30	10.66	8.81
40	18.10	15.64
50	25.96	23.06
60	33.62	30.61
70	41.26	38.10
80	48.62	45.22
90	55.95	52.24
100	63.09	59.08
110	69.99	65.93
120	76.68	72.32
130	83.12	78.57
140	89.49	84.70
150	95.76	90.77
160	102.0	96.86
170	108.4	103.0
180	114.4	109.0
190	120.4	116.3
200	126.3	122.5
210	132.1	128.8
220	137.8	135.5
230	143.5	142.6
240	149.1	150.2
250	154.6	157.8
260	159.8	164.5
270	164.9	171.1
273.15	166.5	173.0
280	169.9	176.9
290	174.9	182.6
298.15	179.0	187.1
300	179.9	188.2

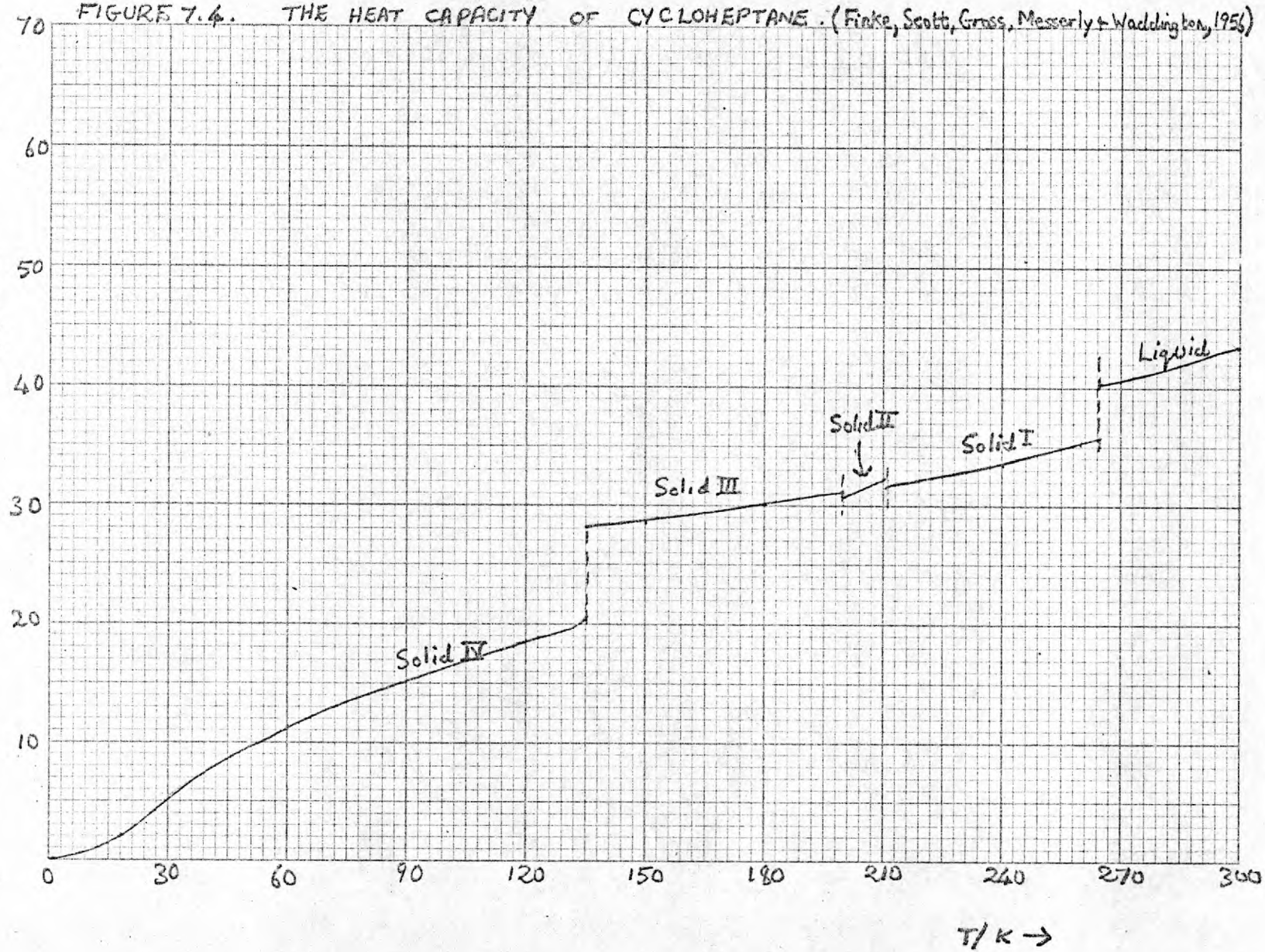
Both of the thiourea adducts studied showed a complex series of anomalously high heat capacity regions. For the cyclooctane adduct the excess heat of the anomalies was determined by measuring graphically the area between the actual heat capacity and the value expected in the absence of the anomalies. The excess entropy was determined by measuring the corresponding area in the Cp/T versus T plot. These quantities are listed in Table 7.6, and in Figure 7.3 the 'extra' heat capacity for the cyclooctane adduct is shown.

The heat capacity anomalies of the thiourea cycloheptane adduct although including several peaks are spread out over a very broad temperature range. For this reason the heat capacity baseline is very difficult to determine accurately by eye and a procedure similar to that used for the excess heats and entropies of urea-1-decene (Cope and Parsonage, 1969) and urea-1-dodecene (this thesis Chapter 6 (ii)) was sought.

However the heat capacity of pure cycloheptane at low temperatures (Finke, Scott, Gross, Messerly and Waddington, 1956) exhibits phase transitions between four solid phases. The cycloheptane heat capacity curve is shown in Figure 7.4. It is impossible to decide which heat capacity line should be used and in any case this would have to extrapolated all through the temperature range.

FIGURE 7.3. THE 'EXTRA' HEAT CAPACITY OF THIOUREA-CYCLOOCTANE




FIGURE 7.4. THE HEAT CAPACITY OF CYCLOHEPTANE. (Finke, Scott, Gross, Messerly & Waddington, 1956)
C_p/(cals K^{-1} mole^{-1}) →
70
60
50
40
30
20
10
0
30
60
90
120
150
180
210
240
270
300
T/K →
Solid IV
Solid III
Solid II
Solid I
Liquid

So an estimate of the heat capacity baseline of the thiourea-cycloheptane adduct was made by eye - the excess heat and entropy are given in Table 7.6 and the 'extra' heat capacity is shown in Figure 7.5. It must be stressed however that the uncertainties in these quantities cannot be determined unambiguously but are very high (see Table 7.6).

It was mentioned earlier in this section that the lowest measured experimental heat capacity points for the thiourea cycloheptane adduct did not extrapolate to zero heat capacity at zero degrees Kelvin. The root mean square deviation of points from a smooth curve in this region is only 5-10% of the deviation necessary for the curve to extrapolate to the origin. It therefore seems possible that this behaviour is caused by a small heat capacity anomaly partly occurring below 12K, the lowest temperature measured. In Figure 7.2 the possible size of this anomaly is sketched in. This anomaly would lead to an increase of about 2% in $S_{298.15}-S_0$. However as only the two lowest temperature heat capacity points suggest this anomaly is present, its existence is far from certain.

FIGURE 7.5. THE 'EXTRA' HEAT CAPACITY OF THIOUREA - CYCLOHEPTANE.

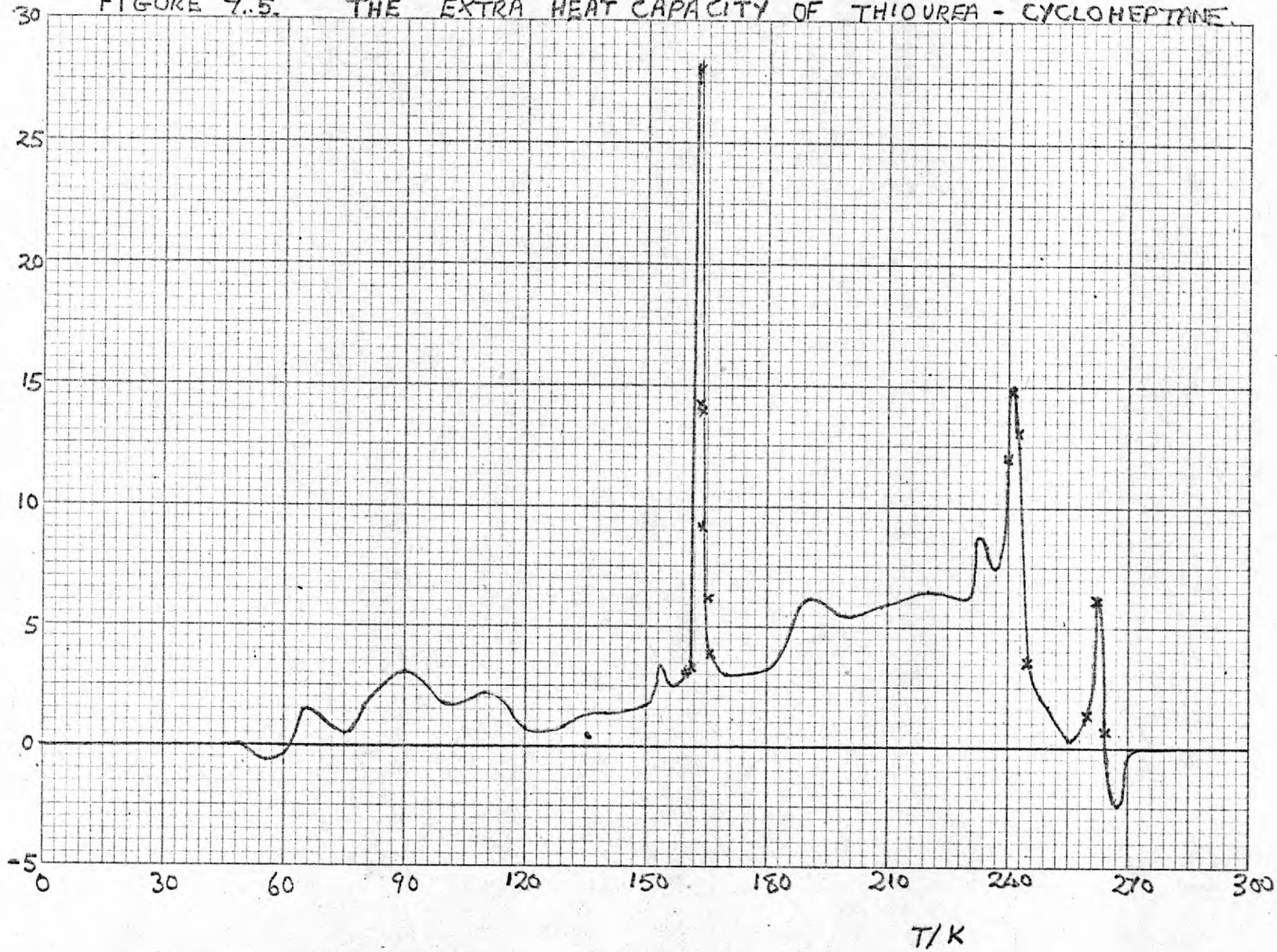


TABLE 7.6. ANOMALIES IN THE THIOUREA ADDUCTS

Adduct	cycloheptane	cyclooctane
$\Delta H/(J\ (\text{mole thiourea})^{-1})$	650 ± 100	2730 ± 40
$\Delta H/(J\ (\text{mole cycloalkane})^{-1})$	1950 ± 300	8130 ± 120
$\Delta S/(JK^{-1}(\text{mole thiourea})^{-1})$	4.4 ± 0.7	12.2 ± 0.3
$\Delta S/(JK^{-1}(\text{mole cycloalkane})^{-1})$	13.2 ± 2.1	36.4 ± 0.9

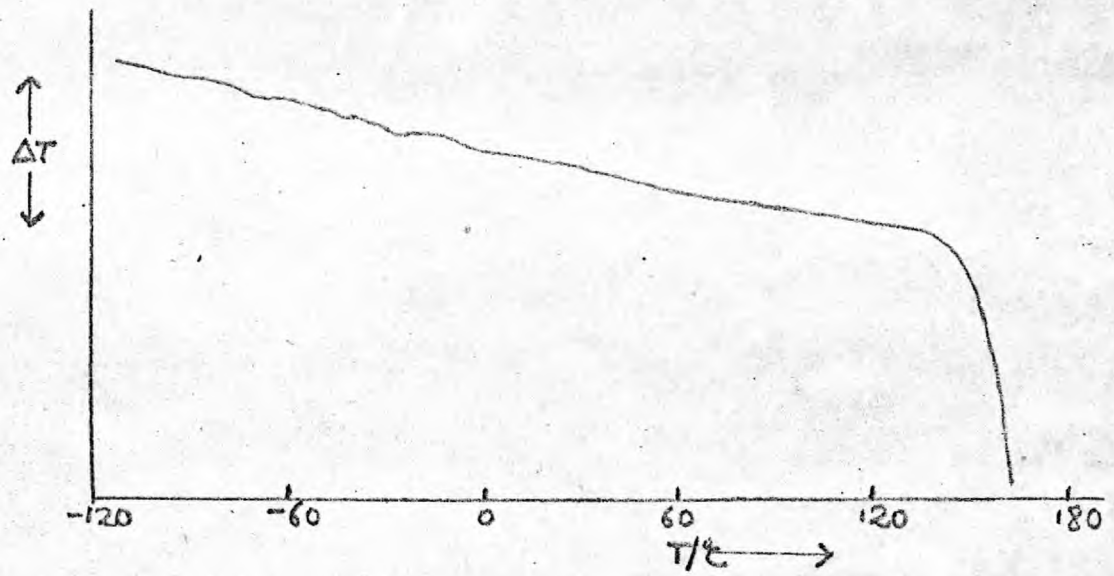
Differential thermal analysis measurements were carried out on samples of the two thiourea adducts from -100°C up to 160°C (see Chapter 6 section (i) for description of method). D.T.A. curves for the two adducts are shown in Figure 7.6. Below 300K the D.T.A. measurements were in accord with the heat capacity measurements, the thiourea-cyclooctane peaks showing up clearly in the D.T.A. scan. Above 300K neither adduct exhibited any observable anomaly up to about 160°C when the thiourea lattice melted.

(ii) Ferroelectric measurements

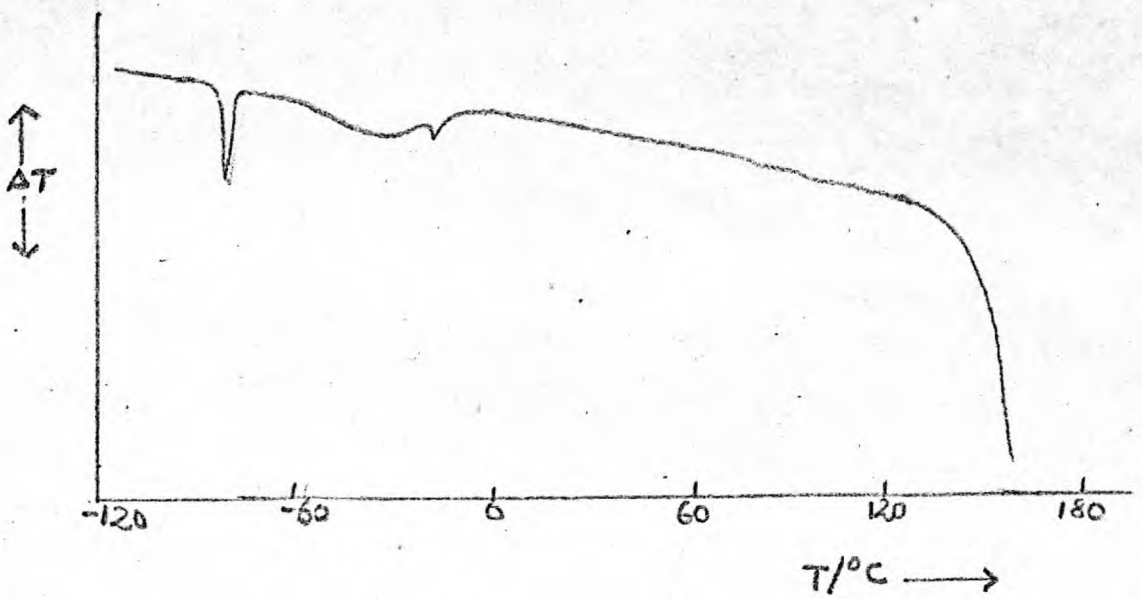
The ferroelectric behaviour of the stable, orthorhombic thiourea was noted in Chapter 1 of this thesis. In the adducts studied by Cope (1967) and in the cycloheptane adduct certain anomalous regions were observed in the heat capacity curve at about 170K similar to the ferroelectric-antiferroelectric transition observed by Chang and Westrum (1960). It was therefore decided to make some electrical measurements on the thiourea adducts to see if at low temperatures the crystals

FIGURE 7.6 D.T.A. MEASUREMENTS

a) thiourea - cycloheptane



b) thiourea - cyclooctane

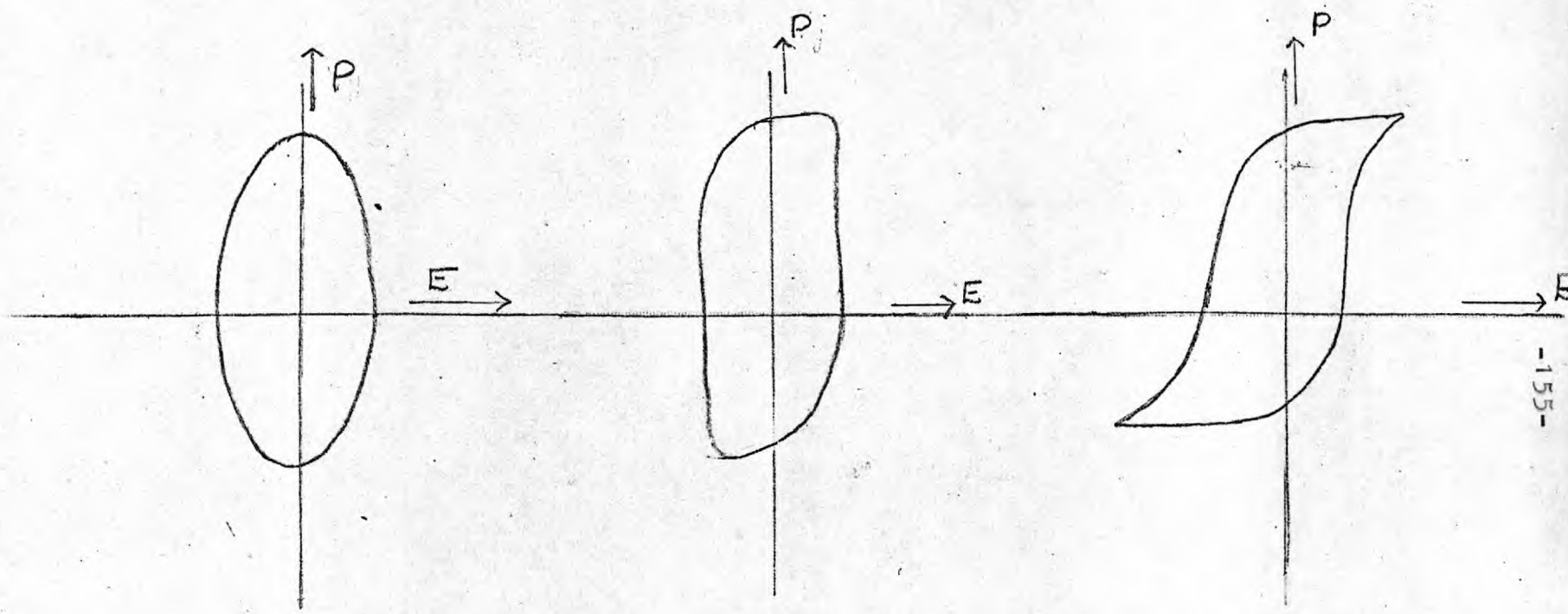


exhibited ferroelectric properties.

For this purpose crystal sections cut perpendicular to the ferroelectric axis (the crystal c axis) were required. However similar difficulties to those described in Chapter 5 for urea crystals sectioning were experienced in preparing ferroelectric-axis sections of the thiourea adducts. For this reason pellets (1-2 mm thick) of finely crushed crystals of the cyclohexane, cycloheptane and cyclooctane adducts of thiourea were prepared. Similar preparations are often used for ferroelectric investigations when single crystals cannot be prepared or sectioned (Furfoot, 1967) as in a powder many of the small crystals will be orientated in the desired direction.

The electrical measurements on the pellet were carried out in the Materials Section of the Electrical Engineering Department, Imperial College and very helpful instruction and advice on the preparation of samples and electrical measurements was given by Mr. E. J. Weidmann of that department. The apparatus employed to observe ferroelectric hysteriesis loops was a Sawyer-Tower loop tracer circuit (Sawyer and Tower, 1930). Fine silver wire electrodes were fixed to the pellet faces with 'silvadag', a colloidal silver paint. Two typical traces displayed on the cathode ray oscilloscope for the thiourea adduct pellets together with a fully saturated hysteresis loop are shown in Figures 7.7 (a), (b) and (c). At room temperature all three adducts exhibited loops very similar to type (a)

FIGURE 7.7. LOOPS DISPLAYED ON OSCILLOSCOPE FOR THIOUREA ADDUCT PELLETS



(a) Unsaturated Loop

(b) Partially Saturated Loop

(c) Fully saturated loop.

P= Polarisation , E = Electric Field.

which is characteristic of a condensor with imperfect electrical connections. However on cooling to liquid nitrogen temperatures the pellets of thiourea cyclohexane and thiourea cycloheptane showed loops more similar to type (b). No thiourea-cyclooctane pellets exhibited this change at low temperatures. The low temperature loops for the cyclohexane and cycloheptane adducts may indicate ferroelectric behaviour for these crystals but far more detailed and varied ferroelectric studies would be necessary to prove its existence.

Measurements were also made on adduct crystal sections cut parallel to their (possible) ferroelectric axes. No saturation was observed in the loops displayed for these specimens.

(iii) Discussion of the Heat Capacity Anomalies of the Thiourea Cycloalkane Adducts

Cope (1967) noted the very complex nature of the heat capacity anomalies in the thiourea-cyclohexane and 2.2-dimethylbutane adducts. The heat capacities of the thiourea adducts of cycloheptane and cyclooctane studied in this thesis exhibit a similar complexity. The two components which may contribute to anomalies in adduct heat capacities, the thiourea lattice and the guest molecules will be considered separately.

(a) The thiourea lattice

The heat capacity of pure thiourea is shown in Figure

1.5. Westrum and McCullough discussed the heat capacity and observed three anomalies:

T/K	$\Delta S/(JK^{-1}mole^{-1})$
169.33	0.17
171.20	0.04
150-200	0.70

Cope found a sharp anomaly in the heat capacity of the cyclohexane adduct at 170.3K with a ΔS of ~ 0.23 $JK^{-1}(\text{mole thiourea})^{-1}$ and humps in the range 130-160K with $\Delta S \sim 0.84JK^{-1}(\text{mole thiourea})^{-1}$. The cycloheptane adduct exhibited a sharp anomaly at 163.4K with $\Delta S \sim 0.25JK^{-1}$ $(\text{mole thiourea})^{-1}$. The entropy of smooth humps found in the heat capacity of thiourea cycloheptane in the 150-200K temperature range is difficult to estimate but is probably similar in magnitude to those found in the cyclohexane adduct. The heat capacity of thiourea-cyclooctane exhibited no sharp peak in the 160-170K temperature range. The sharp peak at 187.2K had an excess heat and an excess entropy several orders of magnitude larger than the ferroelectric anomalies in pure thiourea and thus is unlikely to be due to a ferroelectric transition.

Heat capacity measurements suggest therefore that while the thiourea adducts of cyclohexane and cycloheptane may exhibit ferroelectric behaviour similar to pure thiourea, thiourea-cyclooctane probably possess no ferroelectric properties. These tentative conclusions are in agreement with the ferroelectric measurements made on the

thiourea cycloalkane adducts. However it must be emphasised again that the ferroelectricity measurements are by no means unambiguous.

Goldsmith and White (1959) deduced from detailed X-ray structure analyses of pure thiourea at room temperature and at 120K that the transition from the high-temperature antiferroelectric structure to the ferroelectric structure is produced by small rotations of the thiourea molecules. This results in two molecules per unit cell (there are four thiourea molecules per unit cell) having different orientation to the ferroelectric axis from the other two molecules. The resultant molecular dipole moment is no longer zero. Similar X-ray structure analysis of the thiourea adducts at low temperatures might reveal small rotations of the thiourea molecules in the host lattice.

It is not unlikely that similar thiourea adducts will exhibit different ferroelectric properties as the host lattice will have varying interactions with different guest molecules. It is also possible that the thiourea molecules may be slightly displaced in some adducts in order to experience the most favourable interactions with the guest molecules. Lenne (1954) has reported that the positions of the thiourea nitrogen atoms vary from adduct to adduct.

(b) <u>The guest molecules</u>

Apart from the anomalous heat capacity behaviour observed for thiourea-cycloheptane in the 160-170K region

(discussed above) the following anomalous heat capacity regions were observed.

Thiourea-cycloheptane adduct: No sharp transitions but smooth anomalies in heat capacity from 50-270K. Two small heat capacity peaks - one at 240K and one at 260K. Total entropy of two peaks is $\sim 0.2 JK^{-1}$ (mole thiourea)$^{-1}$ and excess enthalpy is $\sim 60J$ (mole thiourea)$^{-1}$.

Thiourea-cyclooctane adduct: Major co-operative anomaly at 137.2K and very large broad anomaly from 160-230K. The excess enthalpy and entropy of the 137.2K anomaly cannot be determined accurately because the low temperature tail of the 160-230K anomaly partially masked the 137.2K transition. The excess enthalpy is of the order of 150J(mole thiourea)$^{-1}$ and excess entropy is about $0.8 JK^{-1}$(mole thiourea)$^{-1}$. 160-230K anomaly has excess heat of $\sim$ 2600J(mole thiourea)$^{-1}$ and excess entropy of $\sim 11.5 JK^{-1}$(mole thiourea)$^{-1}$.

To try and explain the origin of the thiourea cycloheptane and cyclooctane adduct heat capacity anomalies all the possible notional processes available to the cycloalkane molecules must be considered. As with the urea-hydrocarbon complexes the cycloalkane molecules in the thiourea channels may possess rotational and translational freedom. It also has been suggested that straight-chain hydrocarbons might flex (i.e. behave as springs rather than rigid rods) in the urea channels. However more than small angles of internal rotation will cause unfavourable

interactions with the urea lattice. For cycloalkane molecules in the larger thiourea channels flexing will also be possible and may lead to conversion from one cycloalkane conformation to another. The effect on the adduct heat capacity of possible conformational interconversions will be discussed in the next section.

(1) Conformational interconversions

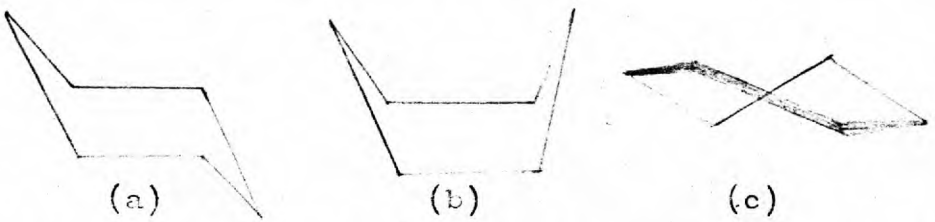
Cope (1967) in his discussion of the heat capacity of thiourea-cyclohexane did not consider the possibility of conformational 'flipping'. However consideration of the strain energy of the possible conformations of cyclohexane shows that only the chair form will exist at ordinary temperatures. In order to understand the possibility of interconversion of conformation of cycloalkanes it is first necessary to consider the factors comprising the strain energy.

Hendrickson (1961, 1964, 1967 (a), (b) and (c)) has computed the energies of the cyclohexane, cycloheptane and cyclooctane rings. The strain energy of a ring is made up of three main factors: bond angle strain, torsional strain due to rotation around a single bond (i.e. the extent of eclipsing of substituent hydrogens), and non-bonded interactions. Hendrickson found that changes in bond length were not a significant factor in the energy calculations.

The chair form of cyclohexane (Figure 7.8 (a)) is unique amongst the cycloalkanes conformations in that all

of the energy componenets listed above are minimised. The boat form (Figure 7.8 (b)) of cyclohexane has an energy 6.9 kcals/mole higher than the chair form. However, the boat form, unlike the chair, is flexible as it can exist in an entire spectrum of conformations all possessing unstrained tetrahedral angles and in fact one of these conformations, the twist boat (Figure 7.8 (c)) has an energy 1.6kcals/mole lower than the form (b).

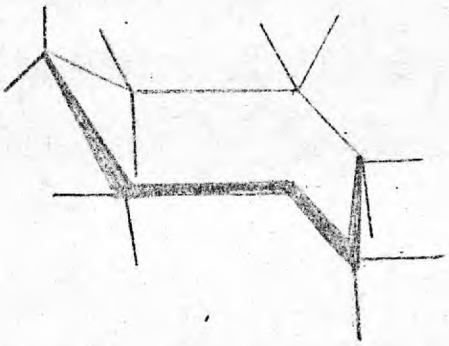
FIGURE 7. 8 CONFORMATIONS OF CYCLOHEXANE



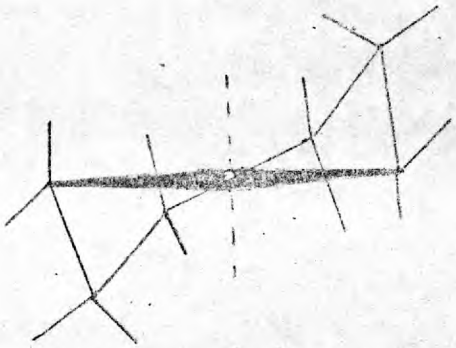
Therefore the chair form of cyclohexane is 5.3 kcals/mole more stable energetically than any other conformation and at ordinary temperatures will be the only conformation observed.

Cycloheptane also has a boat and chair form which can only be interconverted by deformation of bond angles. However in this case both forms are flexible and the two energetically favoured conformations are the twist chair and twist boat. The four forms and their energy diagram are shown in Figure 7.9. The twist chair form is 2.4 kcals $mole^{-1}$ more stable energetically than the twist boat. As the entropy gain for molecules 'flipping' from the chair to the boat form would be fairly small cycloheptane would be expected to exist entirely in the chair form to well above

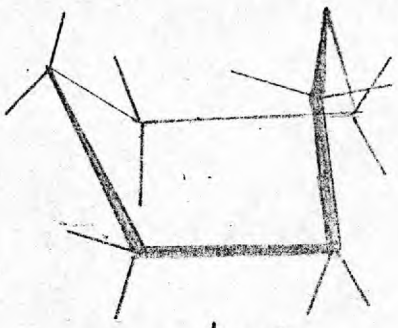
FIGURE 7.9. CONFORMATIONS OF CYCLOHEPTANE.



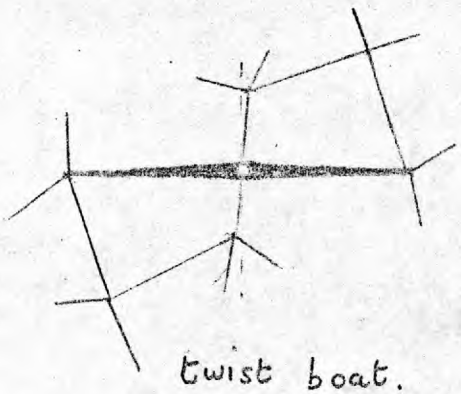
chair



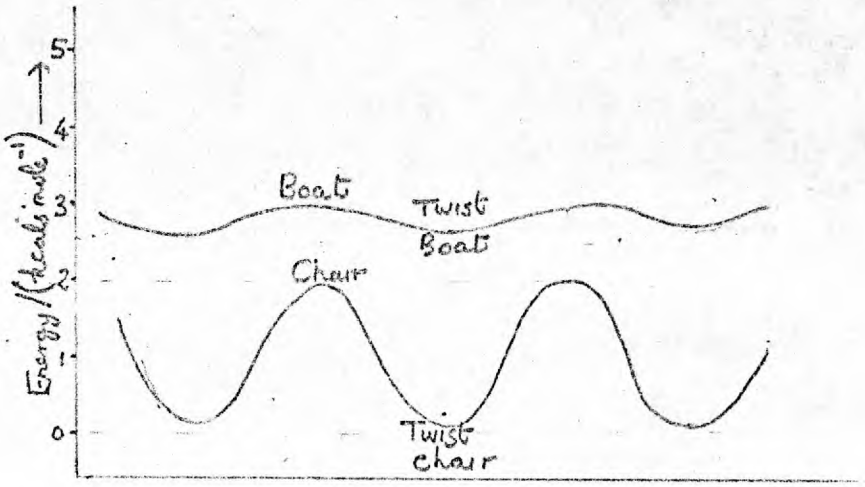
twist chair



boat



twist boat.



Calculated energies of cycloheptane (Hendrickson, 1961)

300K.

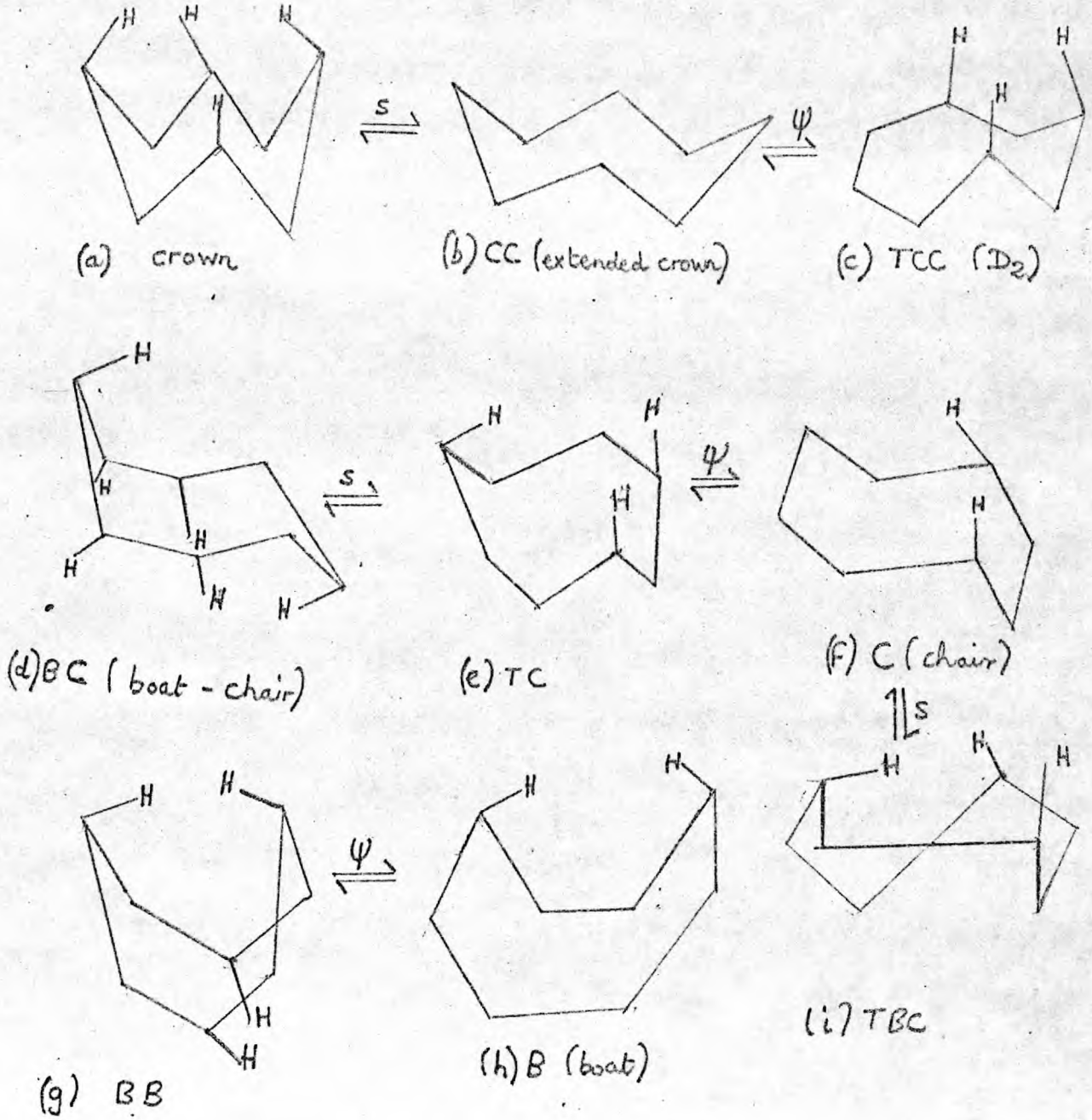
The nine forms of cyclooctane with definable symmetry are shown in Figure 7.10. Unlike cyclohexane and cycloheptane the conformation of cyclooctane having the lowest energy is not immediately obvious. Machine calculations of Hendrickson (1967 (a)) and Eixon and Lifson (1967) suggest that the boat-chair form (Figure 7.10(d)) is energetically favoured over the other forms by 1-2 kcal/mole. Wiberg (1965) suggested that (d) is a four hundred calories per mole less stable than the extended crown form (b). However Wiberg's boat-chair model contains an unnecessary restraint and relaxation of this restraint will lower its energy somewhat. The energy differences (ΔE) determined for the nine cyclooctane forms by Hendrickson with the boat-chair form as an energy zero are listed in Table 7.7.

TABLE 7.7 ENERGIES OF CYCLOOCTANE CONFORMATIONS

Form	$\Delta E/(kcals\ mole^{-1})$
BC	0
CC	1.9
[illegible]	1.4
TC	3.7
C	3.3
[illegible]	10.3
Crown	2.8
TCC(D_2)	1.7
TTC	2.0

These energy values led Hendrickson to suggest that at room temperature cyclooctane will exist as a mixture of several conformations. This suggestion is supported by the electron diffraction studies of Almenningen, Bastiensen Haaland, and Seip (1965) on cyclooctane. They found that

FIGURE 7.10 CONFORMATIONS OF CYCLOOCTANE.



S = symmetrical mode interconversion e.g. cyclohexane chair → boat (deformation of CCC angle)

ψ = pseudorotation interconversion e.g. cyclohexane chair → twist chair (no deformation of CCC angle)

the structure observed for cyclooctane at 40°C could only be explained by the existence of a mixture of cyclooctane conformers.

The 160-230K anomaly in the heat capacity of thiourea-cyclooctane has an excess heat of ~2600J(mole thiourea)$^{-1}$ and an excess entropy of ~11.2JK^{-1}(mole thiourea)$^{-1}$. This is an excess heat of ~7800 J (mole of cyclooctane)$^{-1}$ ≡ 1.86 kcals (mole cyclooctane)$^{-1}$. The entropy of the anomaly per mole of cyclooctane is equivalent to R ln 80 and so the anomaly would obviously be very difficult to explain on the basis of reorientation between potential minima. However the excess heat of the anomaly is very similar to that expected for conversion of boat-chair cyclooctane to higher energy forms. The large number of higher energy forms and their greater flexibility may explain the large entropy of the anomaly.

The absence of any similar anomaly in the heat capacity of the thiourea-cycloheptane adduct might be expected from the energetic stability of the twist chair molecule. The two small heat capacity peaks at 240 and 260K have an entropy which might be consistent with conversion of the cycloheptane chair form to the boat form, but the enthalpy of the peaks (~ 130J(mole cycloheptane)$^{-1}$ is only a tiny fraction of the necessary conversion energy, 2.4 k cals.

(2) Rotation and translation

The thiourea-cyclooctane adduct exhibits a major co-operative-type anomaly in its heat capacity at 187.2K.

Thiourea-cyclohexane has a similar peak at 128.8K (Cope, 1967). Cope suggested that this cyclohexane adduct transition might be due to reorientation of the cyclohexane molecules between potential minima in the thiourea channels. The 137.2K transition may likewise be due to reorientation of the cyclooctane molecules between potential minima in the thiourea channels.

There is not a similar co-operative-type anomaly in the heat capacity of thiourea-cycloheptane. In place of such an anomaly there is a broad region of anomalous heat capacity behaviour from 50-270K. However why the nature of the rotational transition in cycloheptane should differ so entirely in its degree of co-operation is not understood.

Translation of the cycloalkane molecules along the thiourea channels is a possible form of molecular motion. However Gilson and McDowell (1961) conclude from N.M.R. studies that the translational motion of cyclohexane molecules along thiourea channels is hindered and therefore it seems unlikely that the larger cycloheptane and cyclooctane molecules will have any significant translational freedom. Also the uniform thiourea:guest molecule ratio for the three cycloalkanes of 3.0 suggests that the guest molecules lie near the sulphur atoms plane and that translational motion is unimportant.

(c) X-ray studies

It was noted in Chapter 4 that the single crystal

rotation photographs of thiourea cycloheptane and cyclooctane adducts showed no discrete lattice points arising from the ordering of the cycloalkane molecules in the thiourea channels. Verné (1954) found discrete points in the single crystal rotation photograph of thiourea-cyclohexane which he put down to cyclohexane molecules being situated at each sulphur atom plane in the thiourean channels and hence giving an an ordered lattice of cyclohexane molecules. The absence of cycloalkane lattice points in the cycloheptane and cyclooctane adduct photographs may be due to:

(i) positional disorder of the cycloalkane molecules in the thiourea channels However it would be expected since all three cycloalkanes have very similar thiourea:guest molecule ratios that they would have similar channel ordering.

(ii) Motion of the cycloalkane molecules attenuating the intensity of the cycloalkane lattice points to below the observable level. Conformation interconversion might explain why the cyclohexane adduct photograph exhibits the guest molecule lattice points whereas cycloheptane and cyclooctane do not.

If the absence of lattice points were due to the interconversions of conformers, low temperatures X-ray photographs might exhibit guest molecule lattice points as the lowest energy conformation might be the only form existing at these temperatures.

(iv) Proposals for further work

It has already been suggested in this chapter that low temperature X-ray studies on the thiourea cycloalkane adducts may give very useful evidence about the ferroelctric properties of the thiourea lattice and the positioning and motion of the guest molecules.

How much other useful work can be carried out depends to a large extent whether the thiourea adduct lattice can be cleared successfully into thin sections perpendicular to the adduct lattice c-axis. If this can be achieved more refined ferroelectricity measurements should disclose if the adduct lattices are ferroelectric and if so in what temperature regions. Also the study of optical birefringence of such sections at low temperatures might give more information about the ordering of the guest molecules.

Further useful heat capacity measurements could be made on the thiourea adducts of completely deuterated cycloalkanes. The ferrodectric properties of the thiourea lattice should be unaltered and any conformational interconversion of the cycloalkane molecules would be substantially unchanged although the vibration of the ring segments would be altered by the substitution of deuterium for hydrogen. However any rotational transitions would be changed significantly by substitution of deuterium because of the alteration of the various guest molecule-guest molecule and guest molecule-host lattice interactions.

CHAPTER 8

Thermodynamic Properties of some Tungsten Bronzes

(i) Experimental Determination of the Heat Capacities of $(NH_4)_{0.26}WO_3$, $K_{0.26}WO_3$ and $H_{0.40}WO_3$

The heat capacities of ammonium, potassium and hydrogen tungsten bronzes (formulae shown above) were determined by the method described in Chapter 3. These values between 12 and 300K are listed in Tables 8.2, 8.3 and 8.4. Cp/mole values refer to the heat capacity of the bronze per Gram Formula Weight of Bronze. The heat capacity points were plotted against temperature using a large scale and a smooth curve of best fit was drawn between the points. From these graphs smoothed heat capacity values were read at 5K intervals and these points are tabulated in Table 8.4. Small scale graphs of heat capacity versus temperature for the bronzes are shown in Figures 8.1 and 8.2.

A measure of the precision of the experimental results is given by the percentage root mean square deviation of the points from the smooth curve. These deviations for the three bronzes are listed below in Table 8.1.

TABLE 3.1 ROOT MEAN SQUARE DEVIATIONS OF THE EXPERIMENTAL POINTS FROM A SMOOTH CURVE

Bronze	Temperature Range		
	12-25K	25-80K	80-300K
$(NH_4)_{0.26}WO_3$	12	4.5	1.2
$K_{0.26}WO_3$	3.5	2.8	0.9
$H_{0.40}WO_3$	7	2.9	1.0

It will be noticed immediately that the precision of the tungsten bronze heat capacity points is of a far lower order than that of the urea and thiourea adducts. In the case of the urea and thiourea adducts the sample heat capacity varied between 30% and 70% depending on the temperature and weight of sample. However for the bronzes the greatest mass of sample that could be prepared in one batch was about fifteen grams. This weight of sample contributed between 3% and 20% to the total heat capacity. The sample percentage heat capacity was particularly low below 40K. The loss of precision in heat capacity measurements on the tungsten bronzes stems directly from this small sample heat capacity percentage.

TABLE 8.2

EXPERIMENTAL VALUES OF THE HEAT CAPACITY OF AMMONIUM TUNGSTEN BRONZE

Wt. of sample in calorimeter = 16.2884 g_{-1}
Heat capacity of sample, Cp, in Joules K^{-1}
Heat capacity per mole of ammonium tungsten bronze, Cp/mole in Joules K^{-1} $mole^{-1}$

Run No.	Temp/K	ΔT	Cp	Cp/mole
1	88.49	5.41	2.122	30.784
2	93.97	5.17	2.329	33.787
3	98.88	4.99	2.442	35.426
4	103.81	4.83	2.540	36.848
5	108.58	4.71	2.637	38.255
6	113.37	4.88	2.785	40.402
7	118.44	5.27	2.917	42.317
8	123.66	5.16	3.071	44.551
9	128.76	5.02	3.215	46.640
10	133.83	5.10	3.276	47.525
11	138.87	5.00	3.415	49.541
12	143.83	4.94	3.542	51.384
13	148.52	4.89	3.633	52.704
14	153.46	4.97	3.721	53.981
15	158.51	5.15	3.860	55.997
16	163.58	4.92	3.923	56.911
17	168.59	5.09	4.066	58.985
18	173.88	5.52	4.153	60.248
19	179.36	5.42	4.278	62.061
20	184.83	5.54	4.341	62.975
21	190.24	5.23	4.491	65.151
22	195.53	5.28	4.604	66.790
23	200.77	5.23	4.710	68.328
24	204.68	5.21	4.672	67.777
25	210.31	6.06	4.793	69.532
26	216.35	6.06	4.859	70.489
27	222.32	5.99	5.037	73.072
28	232.91	9.55	5.073	73.594
29	242.35	9.45	5.182	75.175
30	251.68	9.36	5.215	75.654
31	260.85	9.18	5.501	79.803
32	273.22	9.57	5.516	80.021
33	282.33	8.67	5.504	79.847
34	291.25	9.48	5.510	79.934
35	300.08	8.53	5.622	81.558

TABLE 8.2 (continued)

Run No.	Temp/K	ΔT	Cp	Cp/mole
P1	57.66	6.07	1.193	17.307
P2	63.06	4.70	1.262	18.307
P3	67.53	4.31	1.481	21.485
P4	72.06	4.73	1.535	22.268
P5	76.63	4.44	1.704	24.720
P6	81.26	4.83	1.784	25.880
P7	85.95	4.55	1.993	28.912
P8	90.43	4.40	2.199	31.901
H1	12.81	3.18	0.001	0.014
H2	15.19	1.87	0.002	0.029
H3	17.27	2.02	0.115	1.668
H4	19.77	2.31	0.114	1.654
H5	22.35	2.63	0.065	0.943
H6	25.32	3.26	0.222	3.221
H7	29.27	4.28	0.273	3.960
H8	33.60	4.31	0.414	6.006
H9	38.18	4.79	0.530	7.689
H10	43.48	5.81	0.675	9.792
H11	49.41	6.08	0.875	12.694
H12	55.07	5.24	1.106	16.045
H13	60.02	4.68	1.219	17.684

TABLE 8.3

EXPERIMENTAL VALUES OF THE HEAT CAPACITY OF POTASSIUM TUNGSTEN BRONZE

Wt. of sample in calorimeter = 14.7124 g
Heat capacity of sample, Cp, in Joules K^{-1}
Heat capacity per mole of potassium tungsten bronze in Joules K^{-1} $mole^{-1}$

Run No.	Temp/K	ΔT	Cp	Cp/mole
1	96.13	5.47	1.899	31.185
2	101.48	5.20	1.987	32.631
3	106.66	5.13	2.079	34.141
4	112.95	7.45	2.234	36.687
5	120.31	7.23	2.355	38.674
6	127.71	7.57	2.493	40.940
7	135.32	7.66	2.720	44.667
8	143.54	8.84	2.824	46.376
9	153.20	8.76	2.965	48.691
10	160.57	8.70	3.135	51.480
11	168.17	8.65	3.259	53.519
12	177.31	9.66	3.420	56.163
13	186.89	9.47	3.552	58.331
14	196.24	9.31	3.687	60.548
15	204.89	9.08	3.786	62.174
16	214.41	10.00	3.919	64.358
17	222.33	9.90	4.067	66.788
18	234.10	9.75	4.181	68.660
19	244.33	10.80	4.223	69.350
20	255.41	11.64	4.286	70.385
21	267.16	11.96	4.351	71.452
22	278.97	11.88	4.393	72.142
23	290.59	11.79	4.426	74.840
24	301.05	9.50	4.561	74.900
P1	57.86	6.48	0.980	16.094
P2	63.95	5.71	1.142	18.754
P3	69.43	5.19	1.253	20.577
P4	74.53	4.86	1.363	22.383
P5	79.78	5.62	1.403	23.040
P6	85.23	5.28	1.605	26.357
P7	90.88	6.03	1.762	28.936
P8	96.78	5.70	1.909	31.350
H1	13.19	3.14	0.003	0.049
H2	16.15	2.00	0.002	0.033
H3	18.53	1.65	0.004	0.066
H4	21.70	3.48	0.074	1.215
H5	25.40	3.71	0.150	2.463

TABLE 8.3

Run No.	Temp/K	ΔT	Cp	Cp/mole
H6	29.83	4.98	0.215	3.531
H7	34.21	3.75	0.328	5.386
H8	38.21	4.21	0.442	7.259
H9	42.89	5.13	0.537	8.819
H10	48.85	6.79	0.745	12.234
H11	55.12	5.74	0.926	15.207

TABLE 3.4 EXPERIMENTAL VALUES OF THE HEAT CAPACITY OF $H_{0.40}WO_3$

Wt of sample in calorimeter = 14.7124g

Heat capacity of sample, Cp, in Joules K^{-1}

Heat capacity per mole of $H_{0.40}WO_3$ in Joules $K^{-1}mole^{-1}$

Run No.	Temp/K	ΔT	Cp	Cp/mole
1	83.60	4.60	1.509	22.115
2	88.10	4.38	1.693	24.816
3	92.64	4.73	1.885	27.638
4	97.48	4.91	1.935	28.340
5	103.26	6.66	2.095	30.683
6	109.55	5.94	2.260	33.120
7	115.51	5.98	2.464	36.088
8	121.29	5.53	2.566	37.582
9	126.98	5.80	2.747	40.233
10	131.70	5.05	2.794	40.921
11	136.79	5.14	2.922	42.796
12	142.13	5.57	3.033	44.421
13	147.81	5.92	3.234	47.365
14	153.68	5.81	3.400	49.796
15	159.53	5.83	3.293	48.229
16	164.31	5.66	3.534	51.759
17	169.91	5.57	3.645	53.385
18	175.41	5.45	3.802	55.684
19	180.82	5.41	3.902	57.149
20	186.41	5.77	4.079	59.741
21	192.60	5.66	4.098	60.019
22	199.20	6.51	4.174	61.132
23	205.95	6.96	4.352	63.739
24	212.83	6.88	4.491	65.775
25	219.62	6.81	4.607	67.474
26	226.45	7.01	4.675	68.470
27	231.43	6.89	4.935	73.010
28	238.19	6.81	5.188	75.983
29	244.87	6.69	5.323	78.034
30	251.43	6.63	5.358	78.473
31	258.34	7.31	5.402	79.118
32	265.53	7.27	5.395	79.015
33	273.05	8.10	5.479	80.245
34	281.26	8.50	5.621	82.325
35	289.81	8.85	5.593	81.915
36	298.89	9.70	5.704	83.541
R1	12.90	2.08	-0.010	-0.146
R2	15.08	2.25	-0.043	-0.629
R3	17.58	2.92	-0.004	-0.058
R4	20.99	3.55	0.060	0.879
R5	25.61	5.46	0.106	1.552

TABLE 8.4 (continued)

Run no.	Temp/K	ΔT	Cp	Cp/mole
H6	30.17	4.13	0.164	2.402
H7	34.76	5.27	0.301	4.408
H8	40.58	6.32	0.400	5.858
H9	46.24	5.06	0.511	8.363
H10	51.20	4.87	0.689	10.091
H11	55.79	4.33	0.849	12.434
P1	58.62	5.39	0.878	12.859
P2	64.57	5.91	1.042	15.261
P3	70.31	5.74	1.213	17.766
P4	75.83	5.30	1.399	20.490
P5	81.00	5.02	1.429	20.929
P6	85.84	4.71	1.802	26.392
T1	206.21	9.06	4.439	65.014
T2	215.30	9.12	4.583	67.078
T3	224.59	9.46	4.762	69.744
T4	232.59	8.54	5.037	73.772
T5	241.15	8.58	5.366	78.590

TABLE 8.5 SMOOTHED VALUES OF THE HEAT CAPACITIES OF AMMONIUM, POTASSIUM AND HYDROGEN TUNGSTEN BRONZES

$0^{\circ}C = 273.15K$ HEAT CAPACITY IN JOULES K^{-1} (MOLE BRONZE)$^{-1}$

T/K	$(NH_4)_{0.26}WO_3$	$K_{0.26}WO_3$	$H_{0.40}WO_3$
0	0.000	0.000	0.000
5	0.100	0.101	0.000
10	0.210	0.210	0.025
15	0.535	0.525	0.190
20	1.142	1.110	0.535
25	2.233	2.109	1.355
30	4.070	3.733	2.585
35	6.101	5.605	4.225
40	8.234	7.670	5.905
45	10.49	9.905	7.565
50	12.81	12.18	9.545
55	15.26	16.48	11.53
60	17.66	16.61	13.51
65	19.98	18.62	15.65
70	22.27	20.59	17.68
75	24.54	22.54	19.68
80	26.89	24.56	21.61
85	29.14	26.52	23.56
90	31.33	28.42	25.47
95	33.43	30.24	27.40
100	35.48	32.07	29.40
105	37.49	33.85	31.32
110	39.44	35.59	33.22
115	41.44	37.29	35.22
120	43.12	38.93	37.10
125	44.95	40.64	38.99
130	46.63	42.27	40.85
135	48.31	43.87	42.68
140	49.93	45.45	44.42
145	51.53	46.99	46.13
150	53.11	48.49	47.83
155	54.63	49.96	49.42
160	56.14	51.41	51.00
165	57.63	52.78	52.51
170	59.12	54.10	54.01
175	60.59	55.52	55.45
180	62.10	56.83	56.73
185	63.51	58.23	58.10
190	64.89	59.33	59.58

TABLE 8.5 (continued)

T/K	$(NH_4)_{0.26}WO_3$	$K_{0.26}WO_3$	$H_{0.40}WO_3$
195	66.19	60.49	61.01
200	67.41	61.56	62.41
205	68.60	62.57	63.81
210	69.66	63.53	65.21
215	70.68	64.47	66.61
220	71.64	65.33	68.01
225	72.57	66.13	69.77
230	73.43	67.00	72.13
235	74.29	67.77	75.23
240	75.09	68.51	77.09
245	75.82	69.26	77.95
250	76.55	69.90	78.54
255	77.23	70.64	79.07
260	77.79	71.29	79.41
265	78.48	71.89	79.95
270	79.05	72.47	80.39
273.15	79.22	72.80	80.62
275	79.60	73.01	80.79
280	80.05	73.51	81.21
285	80.50	73.98	81.65
290	80.91	74.41	82.07
295	81.32	74.81	82.49
298.15	81.65	75.06	82.72
300	81.72	75.19	82.89

FIGURE 8.1 HEAT CAPACITIES OF AMMONIUM AND POTASSIUM TUNGSTEN BRONZES.

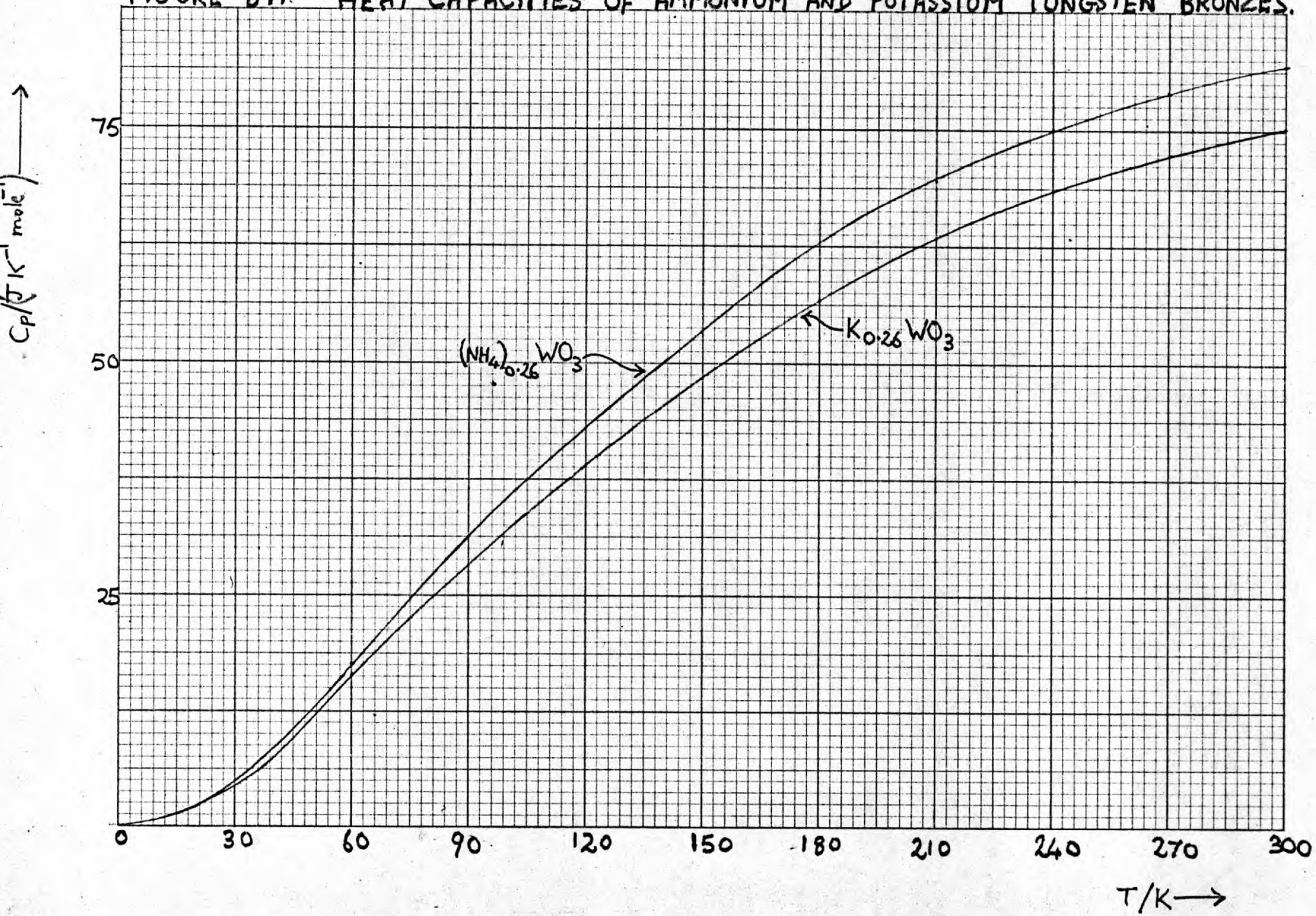


FIGURE 8.2. THE HEAT CAPACITY OF A HYDROGEN TUNGSTEN BRONZE

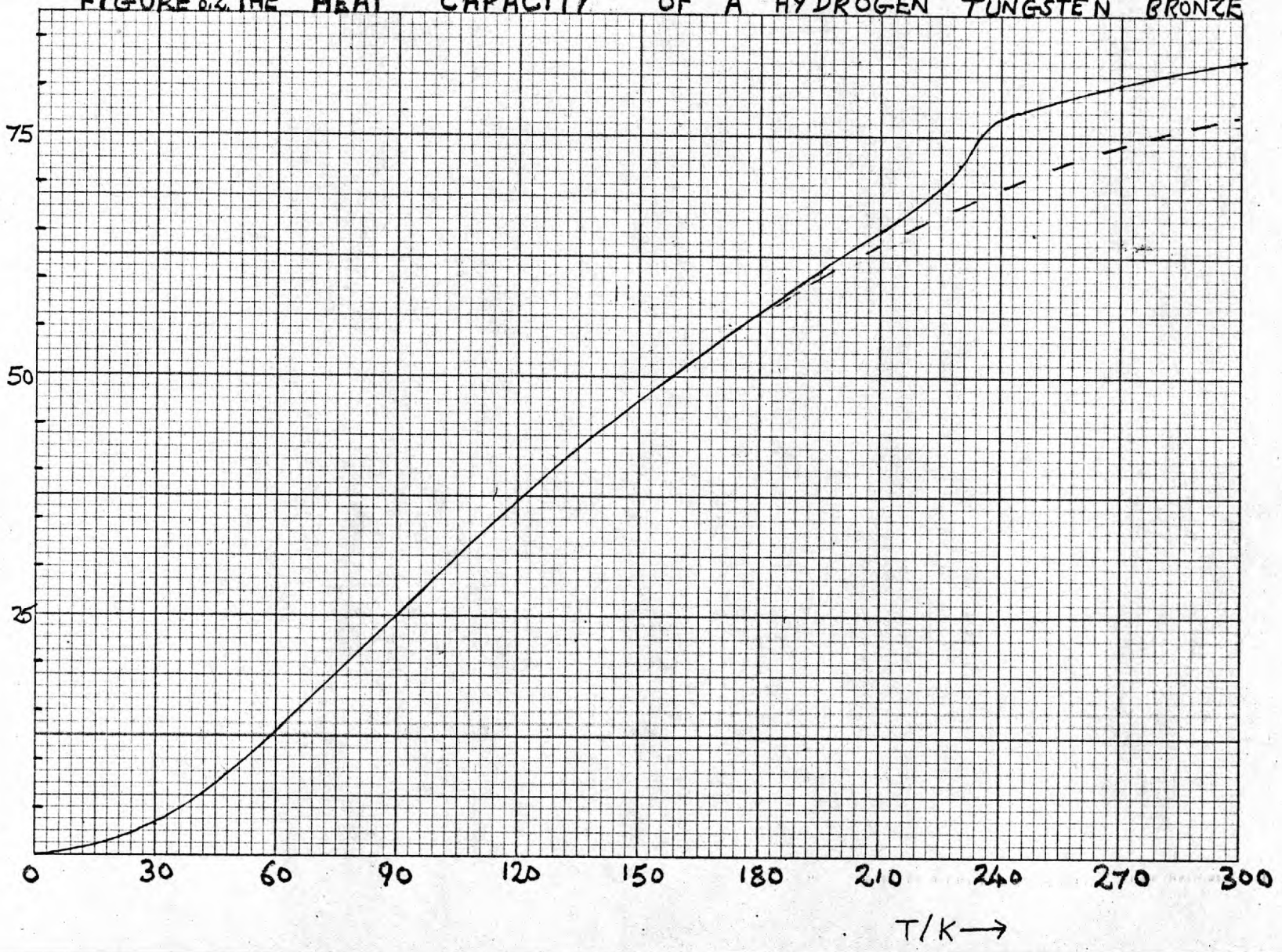


TABLE 8.6 THE ENTROPY (S_T-S_0) OF AMMONIUM, POTASSIUM AND HYDROGEN TUNGSTEN BRONZES IN JOULES $K^{-1}MOLE^{-1}$

$0^oC = 273.15K$

T/K	$(NH_4)_{0.26}WO_3$	$K_{0.26}WO_3$	$H_{0.40}WO_3$
0	0.00	0.00	0.00
10	0.11	0.11	0.01
20	0.48	0.44	0.13
30	1.41	1.34	0.63
40	3.14	2.93	1.85
50	5.48	5.11	3.54
60	8.24	7.72	5.64
70	11.30	10.58	8.04
80	14.58	13.60	10.66
90	18.18	16.71	13.43
100	21.70	19.90	16.32
110	25.26	23.12	19.31
120	28.85	26.37	22.36
130	32.44	29.62	25.48
140	36.02	32.86	28.64
150	39.57	36.10	31.82
160	43.09	39.33	35.01
170	46.58	42.55	38.19
180	50.05	45.72	41.35
190	53.48	48.87	44.59
200	56.88	51.97	47.63
210	60.22	55.08	50.75
220	63.50	58.07	53.85
230	66.72	61.01	56.95
240	69.88	63.89	60.14
250	72.98	66.71	63.32
260	76.01	69.48	66.42
270	78.97	72.19	69.43
273.15	79.88	73.03	70.36
280	81.87	74.85	72.38
290	84.70	77.44	75.25
293.15	86.66	79.51	77.53
300	87.47	79.97	78.05

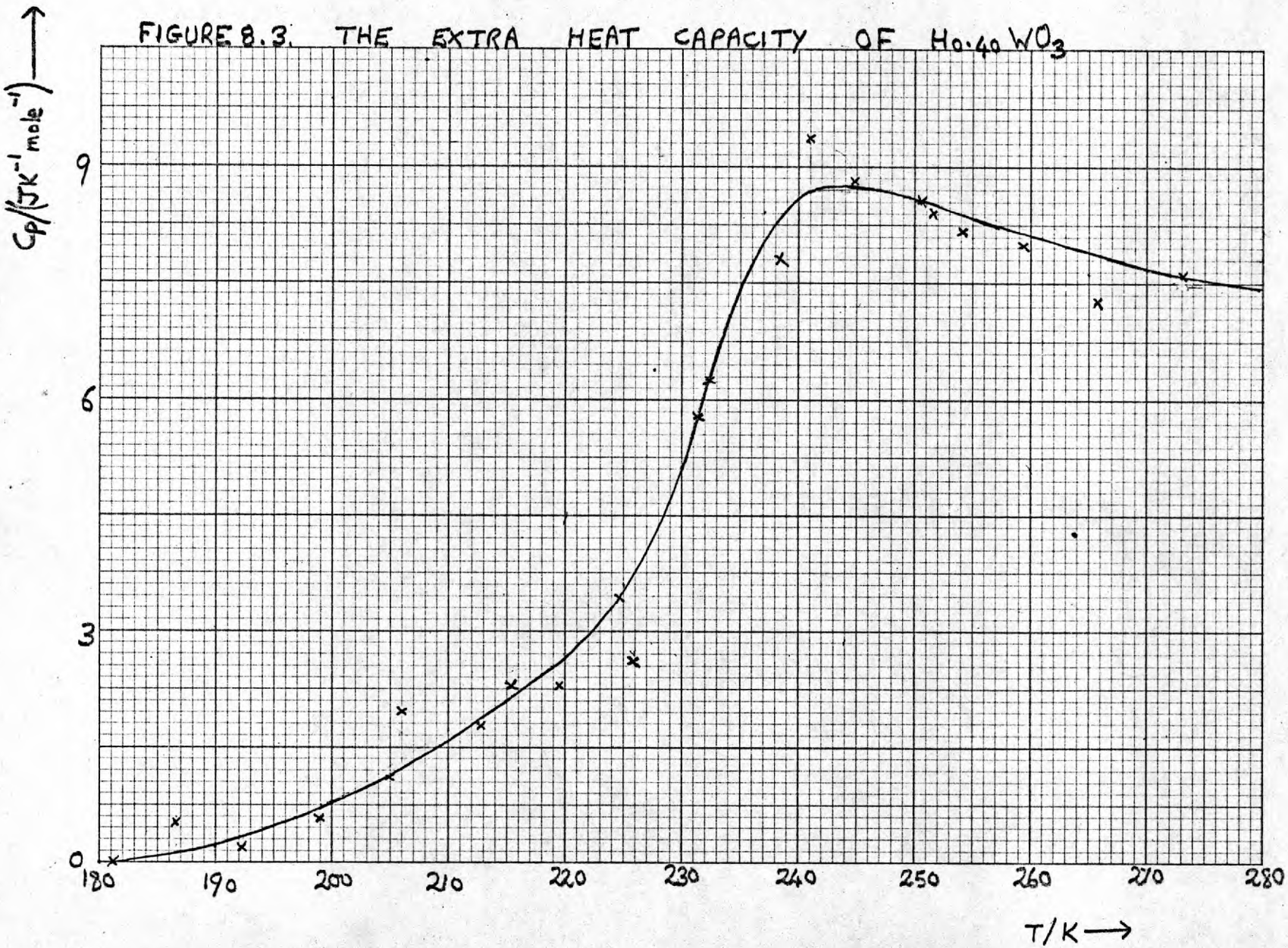
The heat capacity curves of ammonium and potassium tungsten bronzes show a simple sigmoid temperature dependence without any anomalous regions. The hydrogen tungsten bronze heat capacity curve is of a similar form up to 190K, curve 'a', but above this temperature a fairly sharp rise in heat capacity with temperature is observed. Above 240K the heat capacity curve again adopts a similar shape to the ammonium and potassium tungsten bronze curves but is displaced to higher heat capacity values than curve 'a' extrapolated to high temperatures (dotted line in Figure 8.2). This 'extra' heat capacity (difference is heat capacities of dotted line and full curve in Figure 8.2) is shown in Figure 8.3. The extrapolation was made by eye and so will be accurate at best to only $\pm$ 3%. This will lead to an error in the extra heat capacity of about $\pm$ 20%.

Whether the heat capacity of the hydrogen bronze remains displaced from the extrapolation of curve 'a' at temperatures above 300K or returns to this baseline cannot be determined from these heat capacity measurements.

(ii) Discussion of the heat capacities of the tungsten bronzes.

(a) Ammonium and potassium tungsten bronzes

As mentioned in section (i) of this chapter the heat capacity - temperature curves of these two bronzes contain no anomalous regions. The tungsten trioxide lattice in both bronzes is hexagonal and has the following unit cell dimensions:


FIGURE 8.3. THE EXTRA HEAT CAPACITY OF $H_{0.40}WO_3$
$C_p/(JK^{-1}mole^{-1})$ ⟶
0
3
6
9
180
190
200
210
220
230
240
250
260
270
280
T/K ⟶

$K_{0.27}WO_3$ a = 7.40 ± 0.01 c= 7.56 ± 0.01 (Magneli 1953)

$(NH_4)_{0.26}WO_3$ a = 7.39 ± 0.01 c= 7.56 ± 0.01 (Murphy 1969)

Thus as the structures are identical at room temperature, and the absence of heat capacity anomalies precludes the possibility of transitions to other crystal phases at lower temperatures, the higher values of the heat capacity of the ammonium tungsten bronze must be due to a contribution to the heat capacity from the ammonium ions which is greater than that from the potassium ions.

Assuming that the Cp-Cv contribution to the heat capacities of both bronzes is very similar the difference in contributions of the ammonium and potassium ions may be assigned to three molecular processes:

(1) The difference in lattice vibrations of the ammonium and potassium ions in the hexagonal channels.

(2) Internal vibrations of the ammonium ions.

(3) Torsional oscillations of the ammonium ions.

The magnitude of the contribution to the heat capacity from (1) is difficult to estimate. NH_4^+ has a greater ionic radius than K^+ but a lower mass. At high temperatures the heat capacity contribution of vibration of both ions will reach the limiting value of 3R, but the attainment of this value will occur at a higher temperature for NH_4^+ as the lighter ion. Davies and Staveley (1957) and Morfee, Staveley, Walters and Wigley (1960) deduced from comparison of the heat capacities of rubidium and potassium salts of

tetraphenylboron and stannihalides that the lattice vibrations reached their limiting values between 100 and 150K. Westrum and Justice (1969) pointed out similar behaviour for the heat capacity contributions of the cations in $KClO_4$ and $CsClO_4$.

As the internal vibrations of the NH_4^+ make only a very small contribution to heat capacity up to room temperature (2) can be approximated with sufficient accuracy from the frequency assignments of Wagner and Hornig (1950) to the infra-red absorption spectrum of ammonium chloride. The frequencies contributing to the heat capacity and their contribution at -190°C, -78°C, and 28°C are given in Table 8.6.

TABLE 8.6 NH_4^+ INTERNAL VIBRATION MODES CONTRIBUTION TO HEAT CAPACITY (Cp int (NH_4^+))

	-190°C	-78°C	28°C	
Frequency (cm^{-1})	1403	1402	1403	triply degenerate
Frequency (cm^{-1})	1794	1783	1762	doubly degenerate
Total heat capacity contribution/(JK^{-1} (mole NH_4^+)$^{-1}$)	0	0.09	1.63	

The contribution to the heat capacity of the torsional oscillations of the ammonium (3) was determined from the equation

$$\Delta Cp = 1/0.26 \left\{ Cp_{(NH_4)_{0.26}WO_3} - Cp_{K_{0.26}WO_3} \right\} - Cp \text{ int } (NH_4^+)$$

where $Cp_{(NH_4)_{0.26}WO_3}$ etc. are measured heat capacities in $JK^{-1}(mole)^{-1}$. ΔCp versus T shown in Figure 8.4. Below 100K

it must be remembered that ΔC_p is probably less than the heat capacity contribution from the torsional oscillation of the ammonium ions because the difference in lattice vibrations (1) has not been allowed for.

Janik (1964) and others have shown that the ammonium ion does not rotate freely in simple ammonium halides but instead oscillates about one N-H bond. However for ammonium salts with polyatomic anions with low uniformly distributed charge and high crystal symmetry the possibility of free rotation of the NH_4^+ ions is greatly enhanced. Morfee, Staveley, Walters and Wigley (1960) showed that the ammonium ions in ammonium stannichlorides and stannibromides have a heat capacity contribution corresponding to a restricted rotator with a fairly low potential barrier to rotation. Westrum and Justice (1969) found similar behaviour for the ammonium ions in ammonium perchlorate.

The 'anion' in the ammonium tungsten bronze has a very low charge (only - 0.26 per WO_3 unit) and the charge is delocalised into conduction bands over the whole WO_3 lattice. The hexagonal lattice gives a highly symmetrical crystal field. Thus it would be expected that the ammonium ions should behave as restricted rotators with a low potential barrier to rotation.

As the three- dimensional restricted rotator cannot be treated mathematically the rotation of the ammonium ions was considered as divided into three components at right angles,

one direction along the lattice channels and the other two perpendicular to it. The potential function, V, of a restricted rotator in one dimension is given approximately by

$$V = 0.5\ Vo\ (1 - \cos n\phi),$$

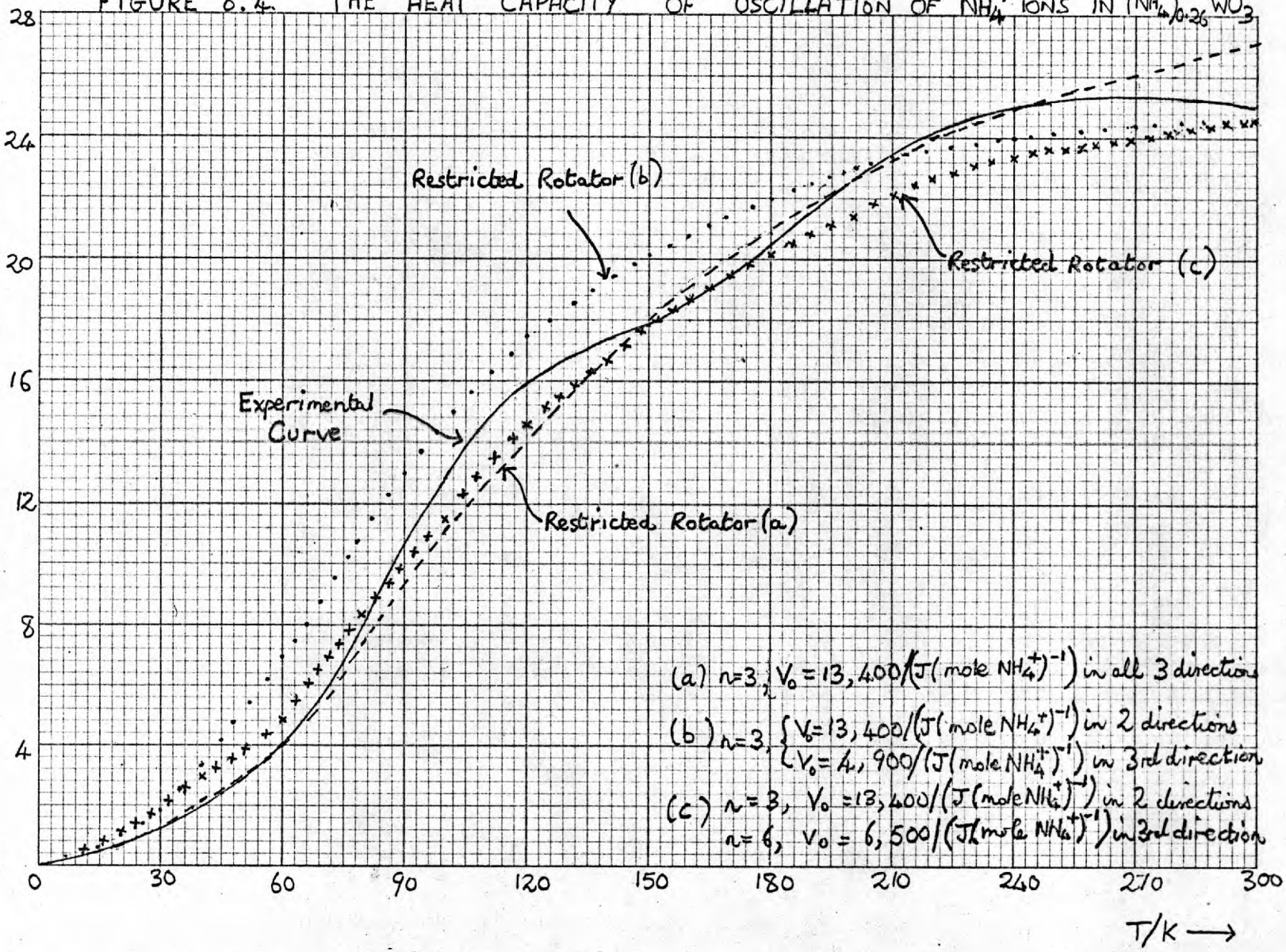
where n is the number of potential minima and Vo is the potential barrier height.

For the ammonium tungsten bronze the number of potential minima for an NH_4^+ ion rotating about an axis along the lattice channels would be six; in the other two directions the number of potential minima will depend on the axis around which the NH_4^+ ions is considered to rotate. If it rotates about a three-fold axis (one N-H bond) n will equal 3. However, if the NH_4^+ ion rotates about a two-fold axis n will equal 4.

Pitzer and Gwinn (1942) have determined the rotational heat capacity of a restricted rotator for various values of n, Vo and temperature. Using a value for the moment of inertia of the ammonium ion of 4.326×10^{-40} g cm^2 (Leung, Taylor and Havens Jr, 1968) the heat capacity for the oscillation of the NH_4^+ ions was calculated employing various values of n and Vo. Three of these calculated curves are compared in Figure 8.6, with the experimental curve.

Although none of the calculated curves completely matches the experimental curve they all exhibit its general features. The curve with $n = 3$ in two directions

FIGURE 8.4 THE HEAT CAPACITY OF OSCILLATION OF NH_4^+ IONS IN $(NH_4)_{0.26}WO_3$



and n = 6 in the other with two different potential barriers best fits the experimental curves as might be expected. Smooth humps in the experimental curve are most probably due to uncertainties in drawing the curves of best fit through the experimental heat capacity points rather than to any physical phenomena.

(b) Hydrogen tungsten bronze

Hydrogen tungsten bronze exhibits a region of anomalously high heat capacity from 190K upwards. This anomaly may primarily be due to a phase transition of the WO_3 lattice or to some change in the ordering or movement of the hydrogen ions. Of course these two processes may not be disconnected: a phase transition in the WO_3 lattice might allow the hydrogen ions greater freedom above 190K and they would then make a greater heat capacity contribution.

Ribnick, Post and Banks (1963) determined the phase diagram of Na_xWO_3 (see Figure 1.6). It may be observed that the crystal symmetry decreases with decreasing sodium content. However for a bronze of fixed sodium content the symmetry may decrease with decreasing temperature. Also regions of the diagram occur in which two crystal phases may coexist.

Similarly it is possible that $H_{0.40}WO_3$ which adopts a cubic structure at room temperature will pass into a lower symmetry phase as the temperature is lowered. In most cases the transition from one crystal phase to another occurs at one temperature and the heat capacity exhibits a discontinuity

at this 'transition' temperature. For the hydrogen tungsten bronze the heat capacity increases anomalously over about 50K. However, the cubic form of $H_{0.40}WO_3$ may pass into another pure phase as the temperature is lowered but the transition may be 'continuous' rather than discontinuous. Ubbelohde (1957) discussed X-ray structural evidence for various compounds showing that change of one phase into another may be continuous and occur not at a single temperature but over a range of temperatures.

The second explanation of the anomaly is that it stems from some change in the order or motion of the hydrogen ions not occasioned by any change in the crystal lattice. Other systems containing H^+ ions or hydrogen molecules 'dissolved' in metallic conductors whose heat capacities have been studied are Pd-H_2 (Nace and Aston, 1957a) and Ta-H_2 (Kelly, 1940).

Palladium black absorbs large quantities of hydrogen gas and forms two phases α and β (both face centred cubic structures). The α phase has a low hydrogen content but the β phase is hydrogen-rich, having the approximate formula Pd_2H. Nace and Aston studied the low temperature heat capacity of this phase and found, in addition to a broad peak at 60K, an anomalous rise in heat capacity at 290K very similar to the hydrogen tungsten bronze heat capacity behaviour. Study of the heat capacity of Pd_2D (Nace and Aston, 1957b) revealed a similar anomaly to the Pd_2H system but commencing at 270K. Kelly studying tantalum containing

small amounts of dissolved hydrogen discovered broad peaks in the heat capacity-temperature curves, the temperature of transition increasing with quantity of hydrogen dissolved.

Nace and Aston (1957b) suggested that the 60K peak was due to rotation of PdH_4 molecules in a PbH_4 Pd lattice and that the 290K anomaly was the contribution from the process

$$PdH_2 + Pd = 2PdH.$$

Kelly showed that the entropies of his peaks were consistent with H^+ ions having three potential energy minima available below the transition and eight minima available above it.

However since the palladium-hydrogen and tantalum-hydrogen systems both contain H^+ ions with similar metallic-conductor environments just as does the hydrogen tungsten bronze, a single molecular process which might explain the heat capacity behaviour of these compounds was sought.

PROTON GAS MODELS

In the calculations described below the H^+ ions in the hydrogen tungsten bronze are considered as a 'proton gas' analogous to the electron gas model of electrons in metallic conductors.

The simplest form of this model is the free electron gas in which valence electrons of the constituent atoms are considered to form a conduction 'gas' the electrons being free to move anywhere within the specimen and experiencing

no interactions with the ion cores. At absolute zero of temperature the electrons will fill up quantum energy levels of increasing energy. The filled levels extend from 0 to E_F, the Fermi energy; levels above E_F are empty.

However as the temperature is raised the kinetic energy of the electron gas increases; some levels are occupied which were vacant at absolute zero, and some levels are vacant which were occupied at absolute zero. The probability that a state at energy E will be occupied in an ideal electron gas in thermal equilibrium is given by the Fermi-Dirac distribution function

$$f(E) = \frac{1}{e^{(E-\mu)/k_B T} + 1} \qquad (1)$$

where K_B is the Boltzmann constant and μ is the chemical potential and is a function of temperature. μ is chosen so that

$$\sum_i f(E_i) = N, \qquad (2)$$

where N is equal to the total number of particles in the system.

The free electron gas model does not take into account the periodic structure of the crystal lattice. Bragg reflection which is a characteristic feature of X-ray and neutron propagation in crystal occurs also for electron waves in crystals and leads to energy gaps. That is to say there exist regions of energy for which real solutions of the Schrödinger equation do not exist.

On the free electron model the allowed energy values

are distributed from zero to infinity with

$$E_k = \frac{\hbar^2}{2m}(kx^2 + ky^2 + kx^2), \qquad (3)$$

provided that the components of the wavevector $\vec{k}$ satisfy

$$kx, ky, kz = 0; \pm \frac{2\pi}{L}; \pm \frac{4\pi}{L}; \ldots\ldots \qquad (4)$$

for periodic boundary conditions over a cube of side L.

$\hbar$ is Planck's constant/2π and m is the electron mass.

We may now consider electrons which are nearly free but with energy gaps. For a linear lattice, lattice constant 'a', the Bragg reflection condition is

$$k = \pm \tfrac{1}{2} G = \pm n\pi/a \qquad (5)$$

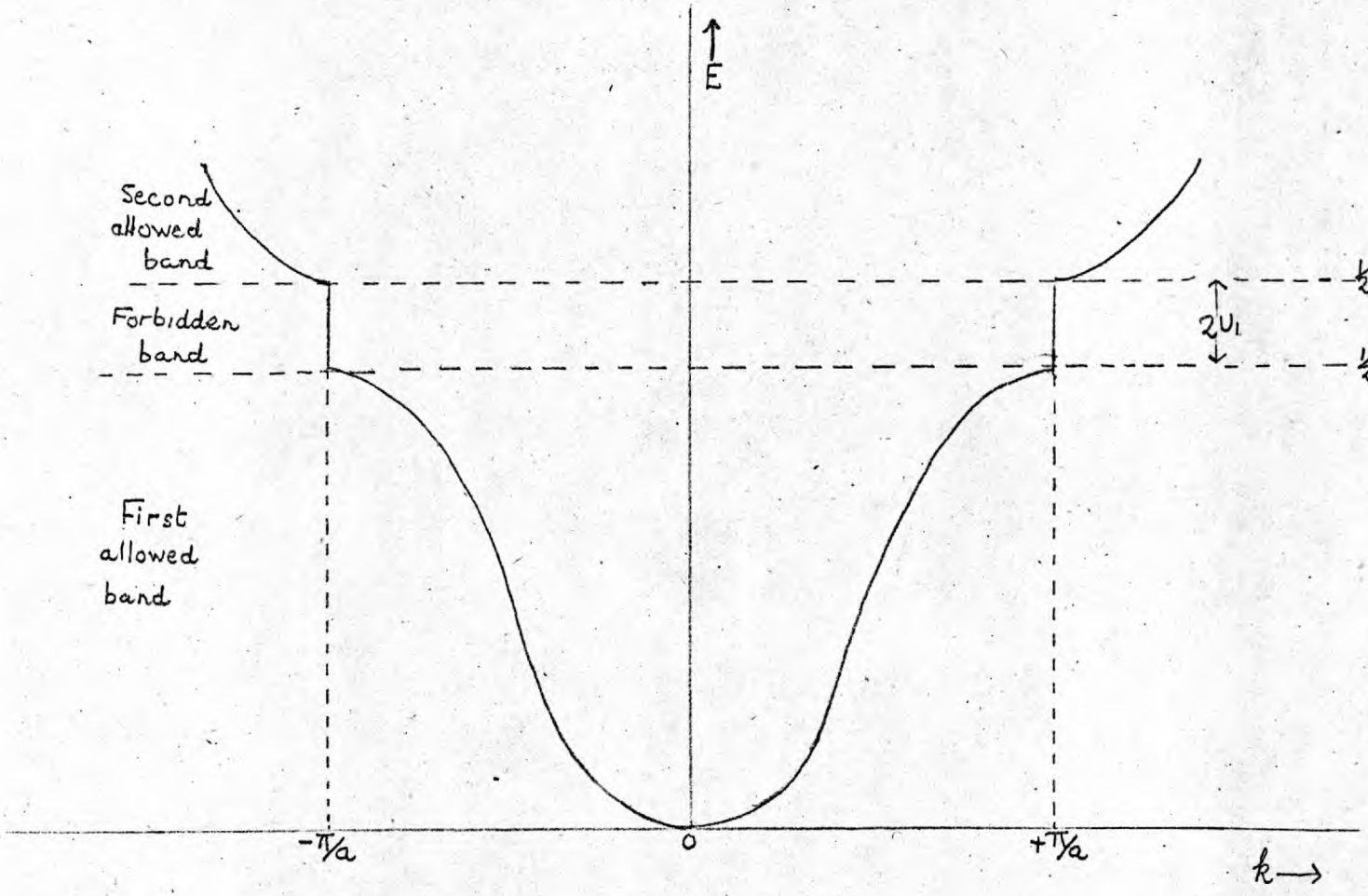
where $G = \pm 2n\pi/a$ is a reciprocal lattice vector and n is an integer. Thus the first reflection and therefore the first energy gap occurs at $k = \pm \pi/a$. An energy versus wavevector plot for this model is shown in Figure 3.5. The region in k space between $-\pi/a$ and $+\pi/a$ is called the first Brillouin zone of this lattice. The allowed values of the electron wavevector k in the first Brillouin zone are given by

$$k = 0; \pm 2\pi/L; \pm 4\pi/L \ldots\ldots N\pi/L \qquad (6)$$

where we have cut the series off at $N\pi/L \cong \pi/a$.

The free electron model has wavefunctions which are travelling waves. But for the energy gap model the solutions of the Schrödinger equation at $k = \pm \pi/a$ are made up equally of waves travelling to the right and to the left: the solutions are standing waves. By expansion of a suitable periodic potential function as a Fourier series summed over all reciprocal lattice vectors the wave equation of an

FIGURE 8.5 PLOT OF ENERGY, E, VERSUS WAVEVECTOR, k, FOR A LINEAR LATTICE, LATTICE CONSTANT, a



electron in a crystal may be determined (Kittel, 1966). From this it may be shown that approximate solutions for the electron energy at the boundaries of the first forbidden zone are

$$E_- = \frac{k^2(G/2)^2}{2m} - U_1 \quad , \quad E_+ = \frac{k^2(G/2)^2}{2m} + U_1$$

where $2U_1$ is the energy gap.

(1) Energy gap model

To see if the electron energy gap model discussed alone might be adapted to H^+ ions in the tungsten bronze structure calculations were carried out to determine that average energy $\langle E \rangle$ and average of the square of the energy $\langle E^2 \rangle$ of a proton gas at a temperature T and hence to determine the proton gas heat capacity.

$$\langle E \rangle = \frac{\int_0^{E_-} E f(E) \cdot \frac{2L}{E_-} \cdot dE + \int_{E_+}^{\infty} E \cdot f(E) \cdot \frac{2L}{E_-} \cdot dE}{\int_0^{E_-} f(E) \cdot \frac{2L}{E_-} \cdot dE + \int_{E_+}^{\infty} f(E) \cdot \frac{2L}{E_-} dE} \qquad (7)$$

where L is Avogadro's Number. The proton mass was taken as 1 and the lattice constant as 1.5 Å. The equation for $\langle E^2 \rangle$ (equation (8)) is obtained by replacing the E's (first terms in the integrands of the numerator) by E^2's.

Before these equations can be solved the chemical potential, μ , in f(E) must be determined. This was effected as suggested in equation (2) by equating the denominator of (7) with the total number of particles in the system. The denominator may be integrated analytically as

follows:

Put $b=1$, $a=e^{-\mu/k_BT}$, $\alpha=1/k_BT$, $x=E-\mu$, $u=ae^{\alpha x}+b$

Then $du = a\alpha e^{\alpha x}dx$

$$\therefore \int \frac{dx}{ae^{\alpha x}+b} = \int \frac{du}{\alpha u(u-b)} = \frac{1}{\alpha b}\left[\ln\left(\frac{u-b}{u}\right)\right]$$

$$\text{Denominator} = \frac{2L k_B T}{E_-}\left\{\left[\ln(1-f(E))\right]_0^{E_-} + \left[\ln(1-f(E))\right]_{E_+}^{\infty}\right\} \qquad (9)$$

= total number of H^+ ions in system.

μ was determined from (9) for various temperatures by trial and error i.e. a computer program was written to determine the value of (9) for many μ's at one temperature. The value of μ for which (9) most nearly equalled the number of H^+ ions was used. This process was then repeated for different temperatures. A μ versus T plot is shown in Figure 8.6. These μ values were were then inserted into equations (7) and (8).

The numerators of (7) and (8) cannot be determined analytically and so they were calculated using Simpson's Rule. A computer program was written to accomplish this with 300 strips for each integral. The heat capacity of the proton gas was determined from the energy fluctuation formula :

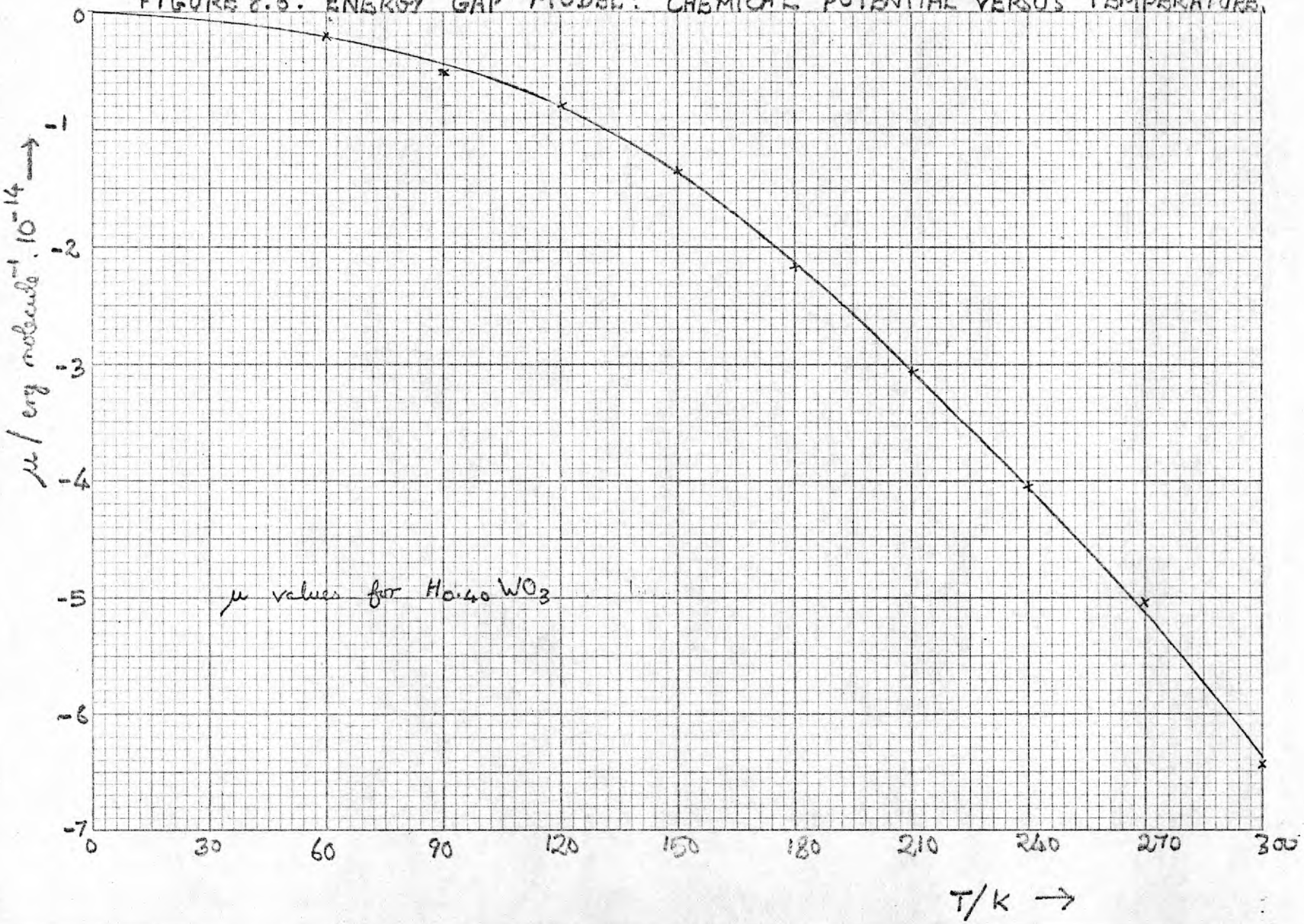
$$\frac{C}{k_B} = \frac{\langle E^2\rangle - \langle E\rangle^2}{(k_BT)^2}, \qquad (10)$$

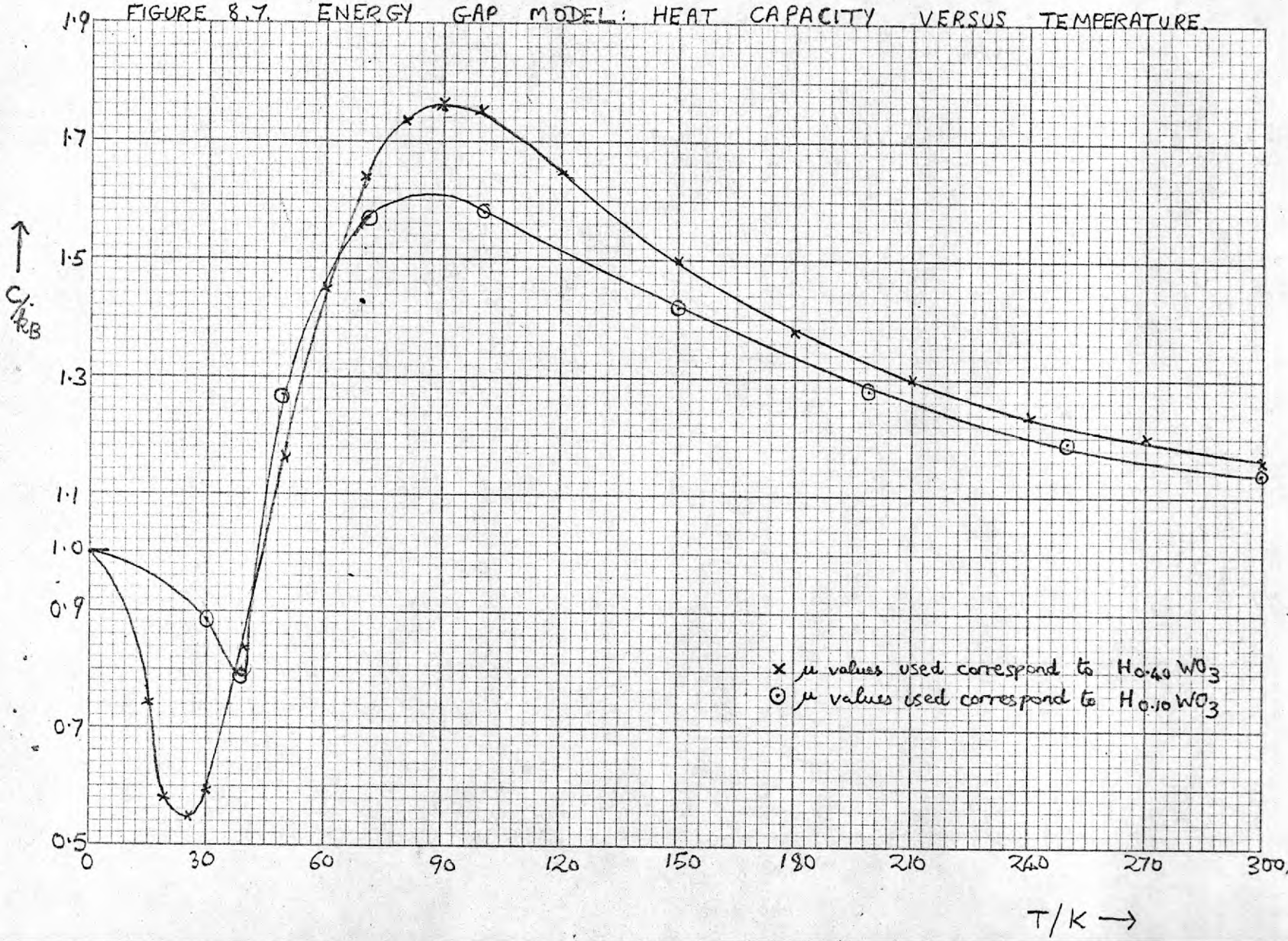
where C is the heat capacity. Plots of C versus T for two different values of are given in Figure 8.7*. Varying μ is equivalent to changing the value of x in H_xWO_3.

The heat capacity of the energy gap model increases over a wider range of temperature and at a much lower

*For independent calculations on the heat capacity of 'Fermi-ions' and employing a similar model see Dash & Bretz(1963).

FIGURE 8.6. ENERGY GAP MODEL: CHEMICAL POTENTIAL VERSUS TEMPERATURE.




FIGURE 8.7. ENERGY GAP MODEL: HEAT CAPACITY VERSUS TEMPERATURE.
C/kB
1·9
1·7
1·5
1·3
1·1
1·0
0·9
0·7
0·5
0
30
60
90
120
150
180
210
240
270
300,
T/K →
× μ values used correspond to H0·40WO3
⊙ μ values used correspond to H0·10WO3

temperature than the anomalous increase in the hydrogen tungsten bronze. However the total increase in heat capacity of the model (multiplied by three to scale up to three dimensions) is $C/R \sim 2$ per mole of H^+ ions which is in good agreement with anomalous heat capacity increase in the hydrogen tungsten bronze. To see if the energy gap model was unsuccessful in its prediction of Cp versus T behaviour because of unjustified approximations (uniform density of energy states and only oneforbidden band) a more realistic model was studied.

(2) The Kronig-Penney Model

This model was devised by Kronig and Penney (1931) to investigate the characteristic features of electron propagation and approximate the periodic potential with a periodic square with potential in one dimension.

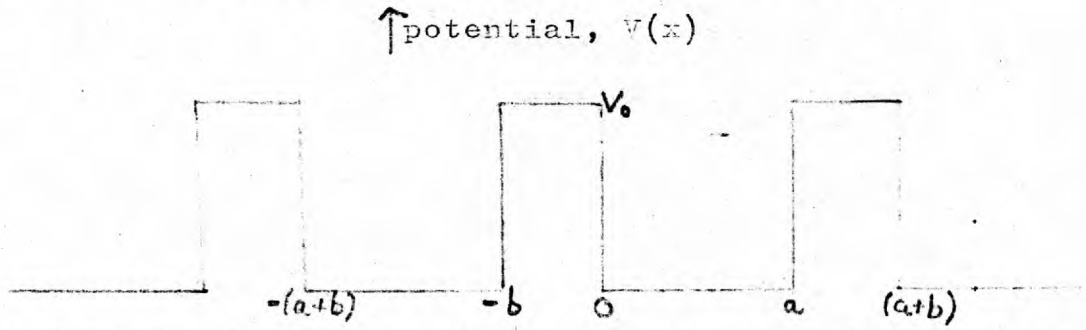


Figure 3.9 Kronig and Penney one-dimension periodic potential

The wave equation of a one dimensional system is given by

$$\frac{d^2\psi}{dx^2} + \frac{2m}{\hbar^2} \cdot (E-V)\psi = 0 \qquad (11)$$

The running wave solutions have the form of a plane wave modulated with the periodicity of the lattice. If we use a Bloch Function to represent the wave function

$$\psi_k = e^{ikx} u_k(x) \qquad (12)$$

where $u_k(x)$ is a periodic function in x with period (a + b) and can be determined by substituting (12) into (11)

$$\frac{d^2u}{dx^2} + 2ik\frac{du}{dx} + \frac{2m}{\hbar^2}(E - E_k - V)u = 0 \qquad (13)$$

where $E_k = \hbar^2k^2/2m$. In the region $0 < x < a$ the equation has the solution

$$u = Ae^{i(\alpha - k)x} + Be^{-i(\alpha + k)x} \qquad (14)$$

with $\alpha = (2mE/\hbar^2)^{\frac{1}{2}}$

In the region $a < x < a + b$ the solution is

$$u = C\,e^{(\beta - ik)x} + D\,e^{-(\beta + ik)x}$$

with $\beta = \left[2m\,(Vo - E)/\hbar^2\right]^{\frac{1}{2}}$

The constants A, B, C and D are chosen so that u and $\frac{du}{dx}$ are continuous at x = 0 and x = a, and by the periodicity required of u(x) the values at x = a must equal those at x = -b, giving the four linear homogeneous equations:

$$\therefore \quad A + B = C + D$$

$$i(\alpha - k)A - i(\alpha + k)B = (\beta - ik)C - (\beta + ik)D$$

$$Ae^{i(\alpha - k)a} + Be^{-i(\alpha + k)a} = Ce^{-(\beta - ik)b} + De^{(\beta + ik)b}$$

$$i(\alpha - k)Ae^{i(\alpha - k)a} - i(\alpha + k)De^{-i(\alpha + k)a} = (\beta - ik)Ce^{-(\beta - ik)b} - (\beta + ik)De^{(\beta + ik)b} \qquad (15)$$

These four equations can be solved only if the determinant of the coefficient vanishes or

$$\frac{\beta^2 - \alpha^2}{2\alpha\beta}\sinh\beta b \cdot \sin\alpha a + \cosh\beta b\cos\alpha a = \cos k(a + b) \qquad (16)$$

The forbidden and allowed energy bands for the model of a proton gas were determined by finding for what ranges of E (16) had solutions. A plot of E versus k(a + b) is shown

in Figure 8.10. Before the values of μ, $\langle E \rangle$ and $\langle E^2 \rangle$ can be determined the density of energy states, $g(E)$, where

$$g(E) = \frac{a + b}{2\pi} \cdot \frac{dk}{dE}$$

must be evaluated for each E and this is accomplished by differentiating (16). $\langle E \rangle$ is then given by

$$\langle E \rangle = \int_0^{E_-} E.g(E)f(E)dE + \int_{E_+}^{E_=} E.g(E)f(E)dE + \int_{E_{\ddagger}}^{E_{\equiv}} E.g(E)f(E)dE + \ldots$$

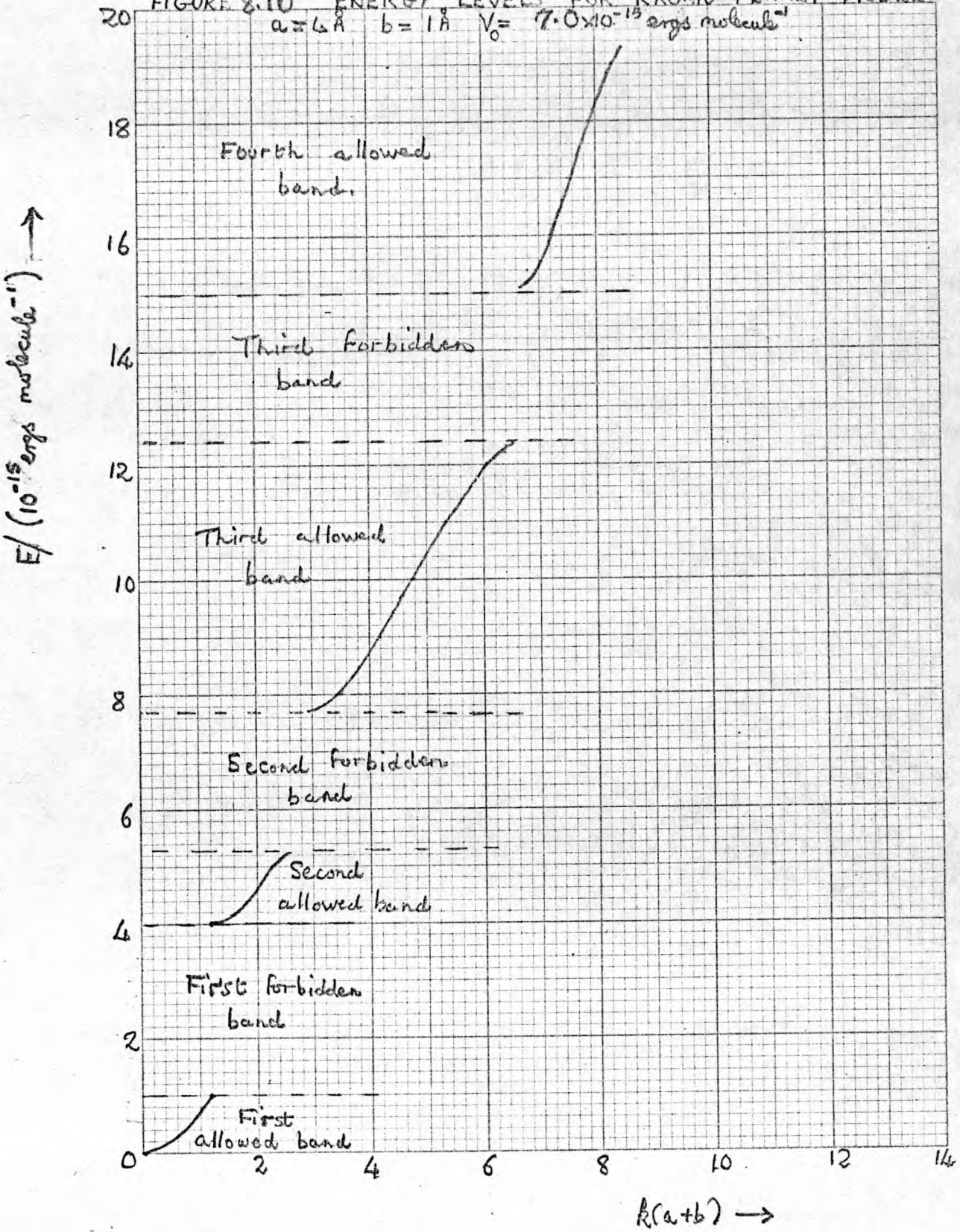
$$\overline{\int_0^{E_-} g(E)f(E)dE + \int_{E_+}^{E_=} g(E)f(E)dE + \int_{E_{\ddagger}}^{E_{\equiv}} g(E)f(E)dE + \ldots} \qquad (17)$$

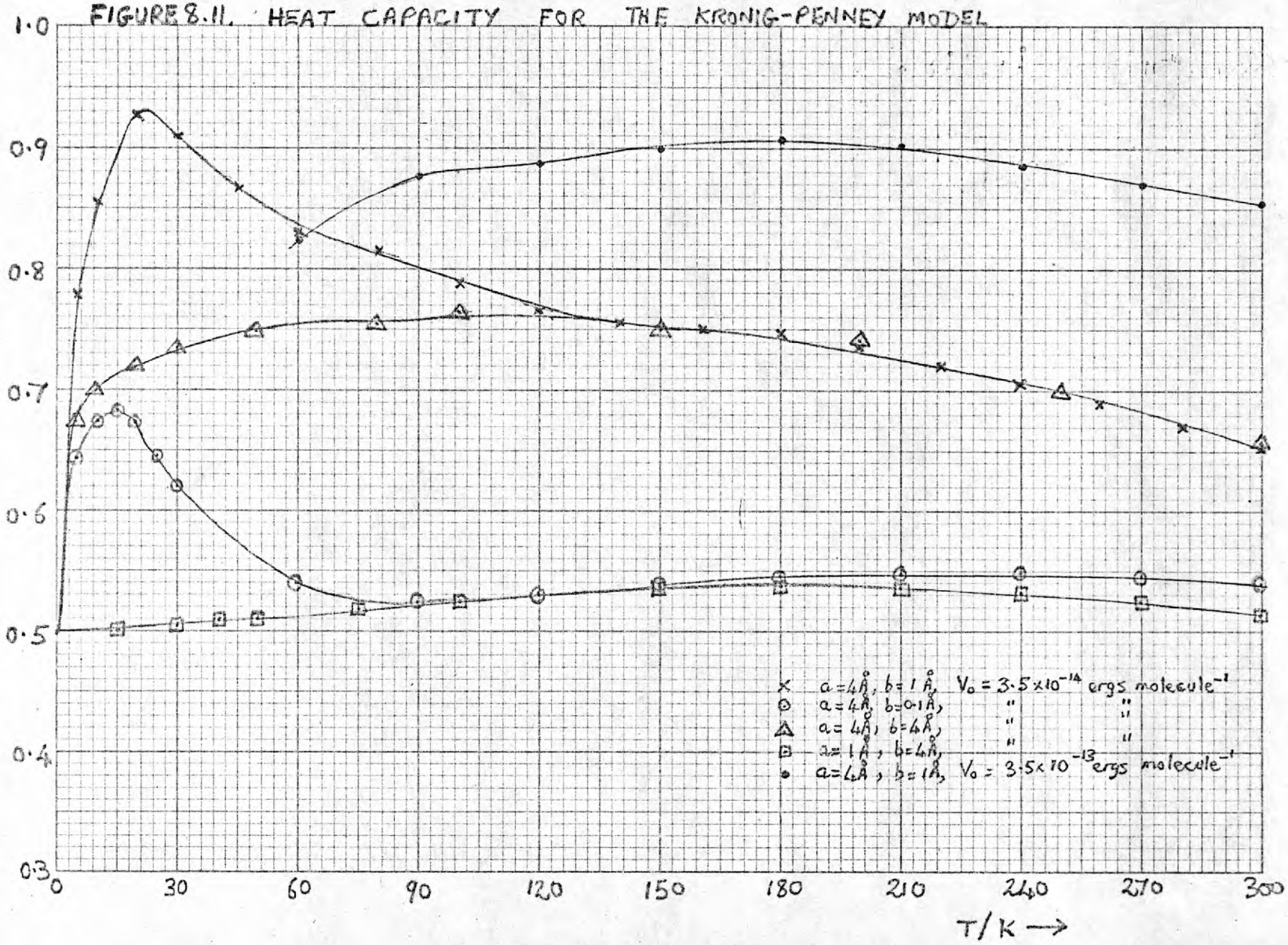
where E_- $E_=$ and $E_{\equiv}$ etc are upper limits of allowed bands and E_+, $E_{\dot{+}}$, $E_{\ddagger}$ are lower limits of allowed bands. Computer programs were written to determine and store $g(E)$ for each E and then determine the chemical potentials and heat capacities of the proton gas for various temperatures. Heat capacity-temperature plots for various values of b, a and Vo are shown in Figure 8.11.

It will be observed that although varying the width of the potential barrier, b, alters the shape of the heat capacity curve it does not increase the temperature at which the heat capacity rises rapidly. Decreasing the value of a (see a = 1Å, b = 4Å curve) increases the temperature at which the heat capacity rises and so does increasing the value of Vo.

The curves all tend to $C/k_B = 0.5$ as T tends to zero. Obviously the heat capacity for rotons moving in a periodic potential should tend to zero at zero degrees Kelvin. The discrepancy is due to the type of potential used in the model-

FIGURE 8.10 ENERGY LEVELS FOR KRONIG-PENNEY MODEL.
$a = 6\,\text{Å}$ $b = 1\,\text{Å}$ $V_0 = 7.0 \times 10^{-15}$ ergs molecule^{-1}




FIGURE 8.11. HEAT CAPACITY FOR THE KRONIG-PENNEY MODEL
1·0
0·9
0·8
0·7
0·6
0·5
0·4
0·3
C/k_B →
0
30
60
90
120
150
180
210
240
270
300
T/K →
× a=4Å, b=1Å, V₀ = 3·5×10⁻¹⁴ ergs molecule⁻¹
⊙ a=4Å, b=0·1Å, " "
△ a=4Å, b=4Å, " "
⊡ a=1Å, b=4Å, " "
• a=4Å, b=1Å, V₀ = 3·5×10⁻¹³ ergs molecule⁻¹

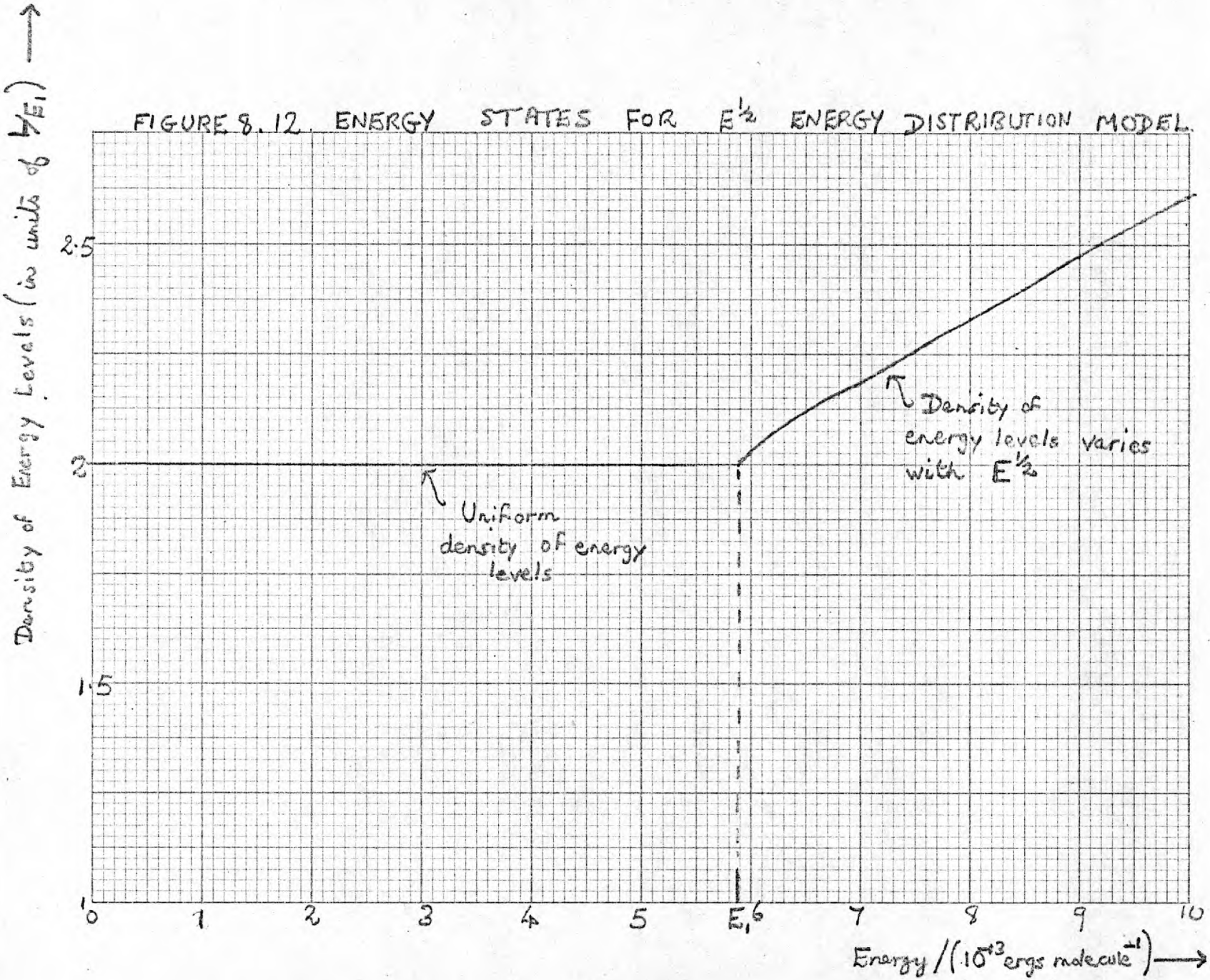
the periodic square well pottential.

The most serious failure of the Kronig-Penney model in this case, however, is that it cannot be made to predict the experimental heat capacity anomaly found for the hydrogen tungsten bronze. By increasing the ratio b:a and increasing Vo it is possible to make the heat capacity for the model increase at higher temperatures but then the increase is very gradual. This absence of a co-operative-type anomaly in the model heat capacity is probably due to one factor ignored in constructing the model. The motion of one hydrogen ion in a periodic potential has been considered but the interaction of the ion with other H^+ ions has not been treated. This interaction may well lead to a co-operative-type anomaly but the mathematics will then be for a many-body problem and may be very difficult to treat.

(3) $E^{\frac{1}{2}}$ energy distribution model

A calculation was also made to see if the hydrogen tungsten bronze heat capacity anomaly might be reproduced by a model containing no energy gaps but a non uniform density of energy states.

Between thevalues E = 0 and $\frac{\hbar^2(G/2)^2}{2m}$ uniform energy distribution was assumedbut above $\frac{\hbar^2(G/2)^2}{2m}(=E_1)$ the distribution was varied with $E^{\frac{1}{2}}$. The energy state distribution is shown in Figure 3.12. With this model the average energy is given by


FIGURE 8.12. ENERGY STATES FOR $E^{1/2}$ ENERGY DISTRIBUTION MODEL.
Density of Energy Levels (in units of γ_{E_1}) ⟶
2·5
2
1·5
1
0
1
2
3
4
5
E_1
6
7
8
9
10
Energy / (10^{-13} ergs molecule^{-1}) ⟶
Uniform density of energy levels
Density of energy levels varies with $E^{1/2}$

$$\langle E \rangle = \frac{\int_0^{E_1} E \cdot \frac{2L}{E_1} f(E)dE + \int_{E_1}^{\infty} E \cdot \frac{2L}{E_1} \frac{E^{\frac{1}{2}}}{E_1^{\frac{1}{2}}} f(E)dE}{\int_0^{E_1} \frac{2L}{E_1} f(E)\,dE + \int_{E_1}^{\infty} \frac{E^{\frac{1}{2}}}{E_1^{\frac{1}{2}}} \cdot \frac{2L}{E_1} f(E)dE} \qquad (18)$$

Here the factor $1/E_1^2$ is included in the integrals from E_1 to infinity to avoid discontinuities in the density of energy states at E_1. The chemical potentials and heat capacities at various temperatures were determined as in the energy gap model except that the second integral in the denominator could no longer be integrated analytically and was evaluated using Simpson's rule with 300 strips. The heat capacity versus temperature plot for this model is shown in Figure 3.13.

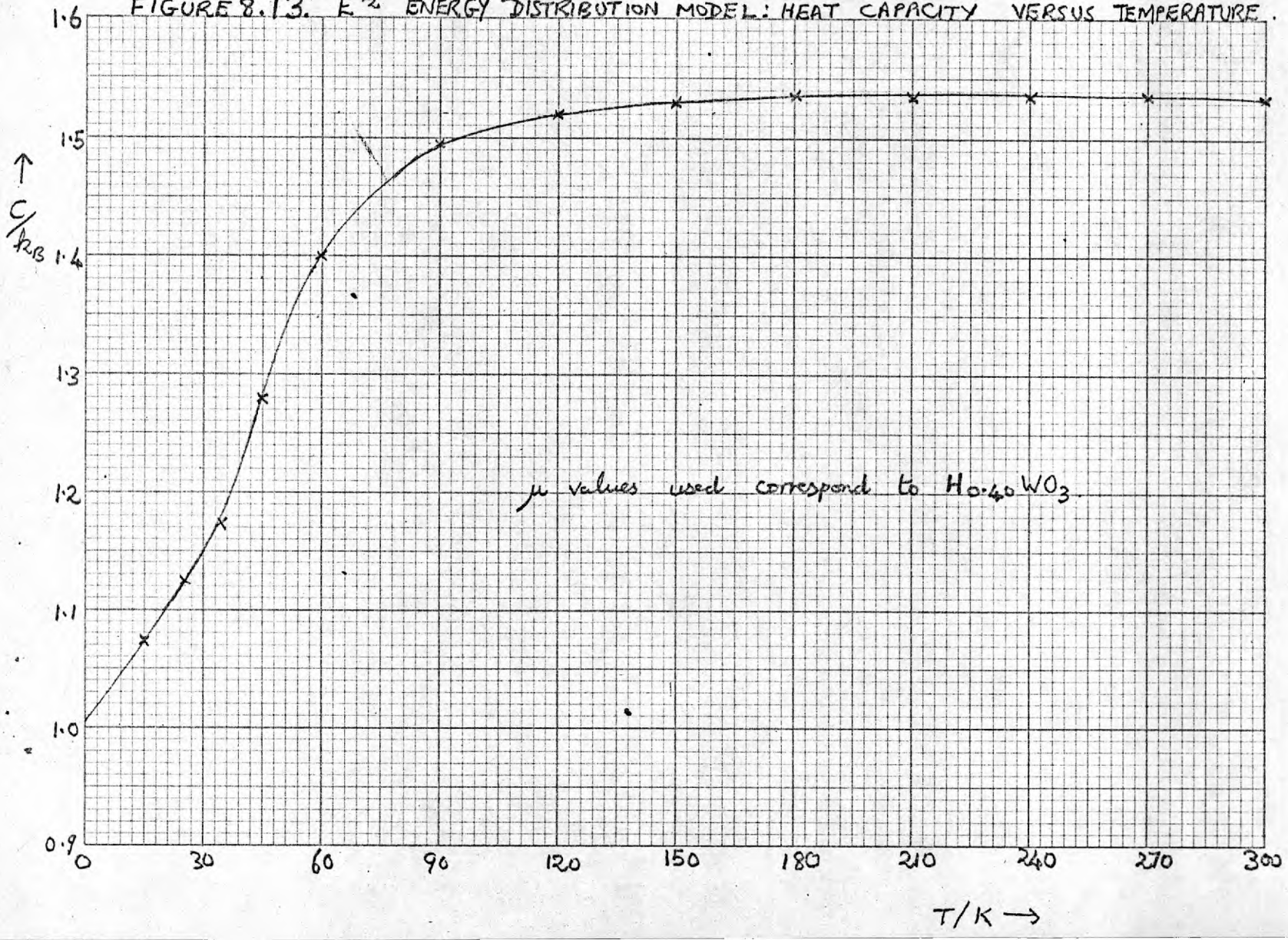
The heat capacity for this model again increases rapidly at very low temperatures and over a temperature range of 100°K. Thus the $E^{\frac{1}{2}}$ dependence model cannot be used to explain the heat capacity anomaly in the hydrogen tungsten bronze.

(iii) Proposals for Further Work

While the heat capacities of the ammonium and potassium tungsten bronzes can be understood by considering the ammonium ions to behave as restricted rotators, more work will be necessary on the hydrogen tungsten bronze system before the nature of the motion of the H^+ ions in the bronze can be understood.

It should be possible in the near future to study the heat capacity of $H_{0.16}WO_3$. However this bronze has a

FIGURE 8.13. $E^{1/2}$ ENERGY DISTRIBUTION MODEL: HEAT CAPACITY VERSUS TEMPERATURE.



tetragonal lattice unlike the cubic $H_{0.40}WO_3$ and any differences noted in the heat capacities of the two bronzes may be due to structural effects rather than to a different concentration of H^+ ions. Better would be to study the heat capacity of the deuterium analogue of $H_{0.40}WO_3$, $D_{0.40}WO_3$.

Further work with the Kronig-Penney model including the proton-proton interactions might be useful if the mathematics proves tractable.

REFERENCES.

Ahlberg J.E., Blanchard E.R. and Lundberg W.O. (1937) J.Chem.Phys. 5,539

Almeningen A,Bastiensen O., Haaland A. and Seip H.M. (1965) Angew. Chem. (International Edition) 4,819

Anderson E.,(1929) International Critical Tables. 5,149

Angla B.,(1947) Compt. Rend. 224,402,1166

Atoji M. and Rundle R.E.,(1960) J.Chem.Phys. 32,627

Barnes R.G., Hultsch R.A. and Jones W.H. (1959) Bull.Amer.Phys.Soc. 4,166

Bell J.D. and Richards R.E.,(1969) Trans.Faraday Soc. 65,2529

Bengen M.F.,(1940) German Patent Appl. O.Z.123438

Bixon M. and Lifson S.,(1967) Tetrahedron 23,769

Born M. and von Kármán T.,(1912) Physik Z. 13,297

Boudard M.,(1970) -to be published in J.Catalysis

Burfoot J.C.,(1967) 'Ferroelectrics-An Introduction to the Physical Principles.' (van Nostrand)

Casey L.M. and Runnels L.K.,(1969) J.Chem.Phys. 51,5070

Chadwell H.M. and Politi F.W.,(1938) J.Amer.Chem.Soc. 60,1291

Chang E. and Westrum E.F.Jr.,(1960) Unpublished Work

Cope A.F.G.,(1967) Ph.D. Thesis,University of London

Cope A.F.G. and Parsonage N.G.,(1969) J.Chem.Thermodynamics 1,99

Cuthill R. and Atkins C.(1937) J.Soc.Chem.Ind. 56,5T

Dash J.G. and Bretz M.,(1968) Phys.Rev. 174,247

Davies T. and Staveley L.A.K.,(1957) Trans. Faraday Soc. 53,19

Debye P.,(1912) Ann.Physik, 39,789

Dickens P.G. and Hurditch R.J.,(1967) Nature 215,1266

Dickens P.G. and Wiseman P.J.,(1970) Unpublished Work

Edwards J.W.,(1959) Ph.D. Thesis,University of London

Einstein A.(1907) Ann.Physik 22,800

Fetterly L.C.,(1947) U.S. Patent 2499820

FinkeH.L.,(1965) Unpublished Work

Finke H.L.,Gross M.D.,Waddington G.and Huffman H.M.,(1954) J.Amer.Chem.Soc. 76,333

Finke H.L.,Scott D.W.,Gross M.D., Messerly J.F., and Waddington G.,(1956) J.Amer.Chem.Soc. 78,5469

Fischer P.H.H. and McDowell C.A.,(1960) Canad J.Chem. 38,137

Gilson D.F.R. and McDowell C.A.,(1959) Nature 183,1183

Gilson D.F.R. and McDowell C.A.,(1961) J.Mol.Phys. 4,125

Ginnings D.C. and West E.D.,(1964) Rev.Sci.Instr. 35,965

Goldsmith G.J. and White J.G. (1959) J.Chem.Phys. 31,1175

Greiner J.D. and Shanks H.R. and Wallace D.C.,(1962) J.Chem.Phys. 36,772

Hägg G. and Magneli A.,(1954) Rev.Pure Appl.Chem. 4,235

Hendrickson J.B.,(1961) J.Amer.Chem.Soc. 83 ,4537

Hendrickson J.B.,(1964) J.Amer.Chem.Soc. 86,4854

Hendrickson J.B.,(1967a) J.Amer.Chem.Soc. 89,7036

Hendrickson J.B.,(1967b) J.Amer.Chem.Soc. 89,7043

Hendrickson J.B.,(1967c) J.Amer.Chem.Soc. 89,7047

Hermann C. and Lenné H.U.,(1952) Naturwiss. 39,234

Janik J.A.,(1964) Proceedings of the 4th Symposium of Inelastic Scattering of Neutrons,Bombay(International Atomic Energy Agency,Vienna- page 243)

Kelly K.K.,(1940) J.Chem.Phys. 8,316

Kington G.L. and Edwards J.W.,(1962) Trans.Faraday Soc. 58,1313

Kittel C.,(1966) 'Introduction to Solid State Physics' 3rd Edition (John Wiley)

Koptzik D.A.,Strukov V.A. and Nevedomskaya I.K.,(1960) Bull.Acad.Sci.U.S.S.R. 24,1233

Kronig R.deL. and Penney W.G.,(1931) Proc.Roy.Soc.(London) A130,499

Kyricau ,(1959) J.Org.Chem. 24,937

Lange F.,(1924) Z.Physik Chem. 110A,343

Lauritsen J.I.,(1958) J.Chem.Phys. 28,118

Laves F.,Nicolaides N.,and Peng K.C.,(1965)
Z.Krist. 121,258

Lenné H.U.,(1954) Acta Cryst. 7,1

Lenné H.U.,(1963a) Z.Krist. 118,439

Lenné H.U.,(1963b) Z.Krist. 118,454

Leung P.S.,Taylor T.I. and Havens W.W.Jr. ,(1963)
J.Chem.Phys. 43,4912

McAdie H.G.,(1962) Canad.J.Chem. 27,2853

McNeill W. and Conroy L.E.,(1962) J.Chem.Phys. 36,87

Magneli A.,(1953) Acta Chem.Scand. 7,315

Meakins R.J.,(1955) Trans Faraday Soc. 51,953

Mecke R. and Kutzelnigg W.,(1959) Z.Anal.Chem. 170,114

Meyers C.H.,(1932) J.Res.Nat.Bur.Standards 9,2983

MorfeeR.G.S.,Staveley L.A.K.,Walters S.T.,Wigley D.L.,(1960)
J.Phys.Chem.Solids 13,132

Murphy D.J.,(1968) Part II Thesis,Oxford University

Nace D.M. and Aston J.G.,(1957a)
J.Amer.Chem.Soc. 79,3623

Nace D.M. and Aston J.G.,(1957b)
J.Amer.Chem.Soc. 79,3627

Parsonage N.G. and Pemberton R.C.,(1967)
Trans.Faraday Soc. 63,1035

Pemberton R.C.,(1966) Ph.D. Thesis,University of London

Pemberton R.C.and Parsonage N.G.,(1965)
Trans.Faraday Soc.61,2112

Pemberton R.C. and Parsonage N.G.,(1966)
Trans.Faraday Soc. 62,553

Pimental and McClellan ,(1960) 'The Hydrogen Bond' (Freeman)

Pitzer K.S. and Gwinn W.D.,(1942) J.Chem.Phys. 10,428

Redlich O.,Gable C.M.,Beason L.R., and Millar R.W.J.,(1950)
J.Amer.Chem.Soc. 72,4161

Redlich O.,Gable C.M.,Dunlop A.K. and Millar R.W.J.,(1950)
J.Amer.Chem.Soc. 72,4153

Ribnick A.S, Post B.,Banks E.,(1963)
Advances in Chemistry Series,No.39,Amer.Chem.Soc.

Ruehrwein R.A. and Huffman H.M.,(1946)
J.Amer.Chem.Soc. 68,1759

Sawyer C.D. and Tower C.H.,(1930) Phys.Rev. 35,269

Schiessler R.W. and Flitter D.W.,(1952)
J.Amer.Chem.Soc. 74,1720

Schlenk W.Jr. ,(1951) Ann.Chem. 573,142

Schlief H.,(1955) J.Prakt.Chem. 2,337

Showell J.S.,Russell J.R., and Swern D.,(1962)
J.Org.Chem. 27,2853

Smith A.D.,(1952) Acta Cryst. 5,224

Solomon A.L.,(1956) Phys.Rev. 104,1191

Southard J.C. and Brickwedde F.G.,(1933)
J.Amer.Chem.Soc. 55,4378

Stroud M.J.F.,(1969) Ph.D. Thesis,University of London

ter Haar D.,(1954) 'Elements of Statistical Mechanics'
(Holt,Rinehart and Wilson) -page 281

Ubbelohde A.R.,(1957) Quart.Rev. 11,246

Umemoto K. and Danyluk S.S.,(1967) J.Phys.Chem. 71,3757

Wagner E.L. and Hornig D.F.,(1950) J.Chem.Phys. 18,296

Westrum D.F.Jr. and Justice B.H.,(1969)
J.Chem.Phys. 50,5083

Westrum D.F.Jr. and McCullough J.P.,(1963) 'Physics and Chemistry of the Organic Solid State' ,Vol 1, Chapter 1
(Interscience)

Wiberg K.B.,(1965) J.Amer.Chem.Soc. 87,1070

Wöhler F.,(1824) Ann.Physik 2,350

Wyckoff R.W.G. and Corey R.B.,(1932a) Z.Krist. 81,102

Wyckoff R.W.G. and Corey R.B.,(1932b0 Z.Krist. 81,386

Zimmerschied W.J.,Dinnerstein R.A.,Weitkamp A.W. and Marschner R.F.,(1950) Ind.Eng.Chem. 42,1300